

CAPITAL UNIVERSITY OF SCIENCE AND
TECHNOLOGY, ISLAMABAD



Scattering Analysis of Acoustic
Waves in Waveguides Containing
Partitioned Wave-Bearing
Cavities

by

Junaid Uzair Satti

A thesis submitted in partial fulfillment for the
degree of Doctor of Philosophy

in the

Faculty of Computing
Department of Mathematics

2021

**Scattering Analysis of Acoustic Waves in
Waveguides Containing Partitioned
Wave-Bearing Cavities**

By

Junaid Uzair Satti
(DMT 151003)

Dr. Martin Bohner, Professor
Missouri University of Science and Technology, Missouri, USA
(Foreign Evaluator 1)

Dr. Won-K wang Park, Professor
Kookmin University, Seoul, South Korea
(Foreign Evaluator 2)

Dr. Muhammad Afzal
(Thesis Supervisor)

Dr. Muhammad Sagheer
(Head, Department of Mathematics)

Dr. Muhammad Abdul Qadir
(Dean, Faculty of Computing)

**DEPARTMENT OF MATHEMATICS
CAPITAL UNIVERSITY OF SCIENCE AND TECHNOLOGY
ISLAMABAD**

2021

Copyright © 2021 by Junaid Uzair Satti

All rights reserved. No part of this thesis may be reproduced, distributed, or transmitted in any form or by any means, including photocopying, recording, or other electronic or mechanical methods, by any information storage and retrieval system without the prior written permission of the author.

DEDICATION

To

My Father (Late)

&

My Mother



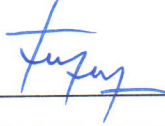
**CAPITAL UNIVERSITY OF SCIENCE & TECHNOLOGY
ISLAMABAD**

Expressway, Kahuta Road, Zone-V, Islamabad
Phone: +92-51-111-555-666 Fax: +92-51-4486705
Email: info@cust.edu.pk Website: <https://www.cust.edu.pk>

CERTIFICATE OF APPROVAL

This is to certify that the research work presented in the thesis, entitled “**Scattering Analysis of Acoustic Waves in Waveguides Containing Partitioned Wave-Bearing Cavities**” was conducted under the supervision of **Dr. Muhammad Afzal**. No part of this thesis has been submitted anywhere else for any other degree. This thesis is submitted to the **Department of Mathematics, Capital University of Science and Technology** in partial fulfillment of the requirements for the degree of Doctor in Philosophy in the field of **Mathematics**. The open defence of the thesis was conducted on **June 04, 2021**.

Student Name : Junaid Uzair Satti (DMT151003)



The Examining Committee unanimously agrees to award PhD degree in the mentioned field.

Examination Committee :

(a) External Examiner 1: Dr. Amjad Hussain
Associate Professor
QAU, Islamabad



(b) External Examiner 2: Dr. Qazi Muhammad Zaigham Zia
Assistant Professor
CUI, Islamabad Campus



(c) Internal Examiner : Dr. Shafqat Hussain
Associate Professor
CUST, Islamabad



Supervisor Name : Dr. Muhammad Afzal
Assistant Professor
CUST, Islamabad



Name of HoD : Dr. Muhammad Sagheer
Professor
CUST, Islamabad



Name of Dean : Dr. Muhammad Abdul Qadir
Professor
CUST, Islamabad



AUTHOR'S DECLARATION

I, **Junaid Uzair Satti (Registration No. DMT-151003)**, hereby state that my PhD thesis entitled, '**Scattering Analysis of Acoustic Waves in Waveguides Containing Partitioned Wave-Bearing Cavities**' is my own work and has not been submitted previously by me for taking any degree from Capital University of Science and Technology, Islamabad or anywhere else in the country/ world.

At any time, if my statement is found to be incorrect even after my graduation, the University has the right to withdraw my PhD Degree.



(**Junaid Uzair Satti**)

Dated: June, 2021

Registration No : DMT-151003

PLAGIARISM UNDERTAKING

I solemnly declare that research work presented in the thesis titled “**Scattering Analysis of Acoustic Waves in Waveguides Containing Partitioned Wave-Bearing Cavities**” is solely my research work with no significant contribution from any other person. Small contribution/ help wherever taken has been duly acknowledged and that complete thesis has been written by me.

I understand the zero tolerance policy of the HEC and Capital University of Science and Technology towards plagiarism. Therefore, I as an author of the above titled thesis declare that no portion of my thesis has been plagiarized and any material used as reference is properly referred/ cited.

I undertake that if I am found guilty of any formal plagiarism in the above titled thesis even after award of PhD Degree, the University reserves the right to withdraw/ revoke my PhD degree and that HEC and the University have the right to publish my name on the HEC/ University Website on which names of students are placed who submitted plagiarized thesis.



(Junaid Uzair Satti)

Dated: June, 2021

Registration No : DMT-151003

List of Publications

It is certified that following publication(s) have been made out of the research work that has been carried out for this thesis:-

1. **J. U. Satti**, M. Afzal, and R. Nawaz, “Scattering analysis of partitioned wave-bearing cavity containing different material properties”, *Physica Scripta*, vol. 94, pp. 115-223, 2019.
2. M. Afzal, **J. U. Satti** and R. Nawaz, “Scattering characteristics of non-planar trifurcated waveguides”, *Meccanica*, vol. 55, pp. 977-988, 2020.
3. M. Afzal and **J. U. Satti**, “The traveling wave formulation of a splitting chamber containing reactive components”, *Archive of Applied Mechanics*, vol. 91(5), pp. 1959-1980, 2021.

Junaid Uzair Satti

(DMT 151003)

Acknowledgement

“All praise to ALLAH alone, most beneficent and merciful. He is the first, He is the last, He is hidden and He knows about everything. He brings the night into day and brings day into night and he knows the thoughts of the heart” (AL-QURAN). I have the pearl of my eyes to admire countless blessing of ALLAH ALMIGHTY because the world is bound, knowledge is limited and time of life is too short to express his dignity. It is one of His infinite benedictions that He bestowed upon me with the potential and ability to complete the present research program.

I wish to express my sincere appreciations to my respectable supervisor Dr. Muhammad Afzal, Assistant Professor in Capital University of Science and Technology, Islamabad for his many valuable suggestions, constant support and encouragement. His excellent knowledge and motivation helped me to make my research experience worthwhile.

I would like to thank Capital University of Science and Technology, Islamabad, Pakistan, for providing suitable environment for research purpose. I express my thankful feelings to all the faculty members especially Dr. Muhammad Sagheer Head of Department Mathematics for their kind support and constructive suggestion during my research work. I am especially thankful to Dr. Rab Nawaz for their kind support and valuable suggestions to enhance my knowledge. I am also thankful to my research fellows, Sajid Shafique, Touqeer Nawaz and Hazrat Bilal who supported me during my research work.

Of course, at this stage I cannot forget my whole family especially my great beloved mother, my brother, my sister and my wife for their prayers, continuous support and love. Their prayers have lightened up my spirit to finish this thesis.

Abstract

The present thesis addresses a class of boundary value problems arising in the modelling of scattering of acoustic waves in ducts or channels comprising partitioning of guiding structure along with abrupt geometric changes and material contrast. The mathematical formulation of such problems includes Helmholtz's type governing equation and involves Dirichlet, Neumann, Robin type, and/or higher order boundary conditions. The envisaged problems are solved by using the mode-matching (MM) scheme. This approach relies on the eigenfunction expansions of propagating modes of duct regions, the orthogonal characteristics of eigenfunctions and the matching conditions at interfaces. The eigenvalue problems with higher order boundary conditions, the eigen-sub-systems are of and non-Sturm Liouville category whereby the use of generalized orthogonal characteristics is indispensable. Such eigenfunction characteristics are incorporated in the process of conversion of differential systems into linear algebraic systems and ensure the convergence of the systems. Moreover, the low frequency approximation solution is developed for some cases and is compared with MM. For each physical problem, the solution schemes are validated through opposite mathematical and physical argument. To analyze the physical consequences of each model problem as a noise control measure, the transmission loss and/or scattering powers in different regimes are discussed numerically.

Contents

Author's Declaration	v
Plagiarism Undertaking	vi
List of Publications	vii
Acknowledgement	viii
Abstract	ix
List of Figures	xii
List of Tables	xvi
Abbreviations	xvii
Symbols	xviii
1 Introduction	1
1.1 Background and Literature Survey	3
1.2 Thesis Structure	8
2 Preliminaries	11
2.1 Acoustic Setting	12
2.1.1 Acoustic Impedance	15
2.1.2 Elastic Membrane	16
2.2 Non-Dimensional Setting	17
2.2.1 Governing Equation and Boundary Conditions	18
2.3 Development of Orthogonality Relations (OR)	19
2.3.1 Impedance Impedance Case	20
2.3.2 Rigid Membrane Case	22
2.3.3 Rigid Membrane Rigid Case	24
2.3.4 Rigid Porous Case	26
2.4 Mathematical Techniques for Waveguide Problems	29
2.4.1 Mode-Matching (MM) Technique	29

2.4.2	Low Frequency Approximation (LFA)	30
2.5	Energy Flux	31
3	Scattering Characteristics of Non-Planar Trifurcated Waveguides	32
3.1	Mathematical Formulation	33
3.2	Mode-Matching (MM) Solution	35
3.3	Energy Balance	41
3.4	Numerical Results and Discussion	43
4	Scattering Analysis of a Partitioned Wave-Bearing Cavity Con- taining Different Material Properties	52
4.1	Mathematical Formulation	53
4.1.1	Wave Propagation in the Inlet Duct	55
4.1.2	Wave Propagation in the Expansion Chamber	56
4.1.3	Wave Propagation in the Outlet Duct	58
4.2	Mode-Matching (MM) Solution	58
4.3	A Low Frequency Approximation (LFA)	63
4.4	Numerical Results and Discussion	66
5	The Traveling Wave Formulation of a Splitting Chamber Con- taining Reactive Components	82
5.1	Mathematical Formulation	83
5.2	Mode-Matching (MM) Solution	89
5.3	A Low Frequency Approximation (LFA)	92
5.4	Numerical Results and Discussion	95
6	Scattering Characteristics of Splitting Chamber Loaded by Elas- tic Components with Material Contrast	109
6.1	Problem Formulation	110
6.1.1	Inlet and Outlet	111
6.1.2	Expansion Chamber	112
6.1.2.1	Upper and Lower Regions	112
6.1.2.2	Central Region	116
6.2	Mode-Matching (MM) Solution	119
6.2.1	Porous Wall	119
6.2.2	Metallic Fairing	124
6.3	Numerical Results and Discussion	128
6.3.1	Scheme Validation	129
6.3.2	Transmission Loss (TL) Analysis	133
7	Conclusion	136
	Bibliography	140

List of Figures

2.1	The geometry of physical problem.	20
2.2	Duct geometry for a general problem.	23
2.3	The geometrical configuration of physical problem.	24
2.4	The duct configuration for a general problem.	27
3.1	The geometry of physical problem.	33
3.2	The scattering energies plotted against non-dimensional height a for discontinuous structure where $\bar{h} = 5 \times \bar{a}, \bar{b} = 3 \times \bar{a}$ and $N = 30$ terms.	44
3.3	The scattering energies plotted against non-dimensional height a for continuous structure where $\bar{h} = \bar{b} = 3 \times \bar{a}$ and $N = 30$ terms.	44
3.4	The energy flux against non-dimensional height b for discontinuous structure where $\bar{h} = 3 \times \bar{b}, \bar{a} = 0.05\text{m}, f = 250\text{Hz}$ and $N = 30$ terms.	45
3.5	The scattering energies plotted against non-dimensional height b for continuous structure where $\bar{h} = \bar{b}, \bar{a} = 0.05\text{m}, f = 250\text{Hz}$ and $N = 30$ terms.	45
3.6	The scattering energies plotted against discontinuous height h where $\bar{a} = 0.05\text{m}, \bar{b} = 0.1\text{m}, f = 250\text{Hz}$ and $N = 30$ terms.	46
3.7	The scattering energies verses frequency for different values of Tension for discontinuous structure where $\bar{h} = 0.15\text{m}$ and $N = 30$ terms.	47
3.8	The scattering energies verses frequency for different values of Tension for continuous structure where $\bar{h} = 0.1\text{m}$ and $N = 30$ terms.	47
3.9	The scattering energies plotted against number of terms N for discontinuous structure where $\bar{h} = 0.15\text{m}, f = 250\text{Hz}$ and $T = 350\text{N}$	49
3.10	The scattering energies plotted against number of terms N for planar structure where $\bar{h} = 0.1\text{m}, f = 250\text{Hz}$ and $T = 350\text{N}$	49
3.11	The real part of normal velocities verses height in non-dimensional form at interface, where, $\bar{h} = 0.15\text{m}, f = 250\text{Hz}$ and $N = 120$ terms.	50
3.12	The imaginary part of normal velocities verses height in non-dimensional form at interface, where $\bar{h} = 0.15\text{m}, f = 250\text{Hz}$ and $N = 120$ terms.	50
3.13	The real part of pressures verses height in non-dimensional form at interface, where, $\bar{h} = 0.15\text{m}, f = 250\text{Hz}$ and $N = 120$ terms.	51
3.14	The imaginary part of pressures verses height in non-dimensional form at interface, where, $\bar{h} = 0.15\text{m}, f = 250\text{Hz}$ and $N = 120$ terms.	51

4.1	The geometry of physical problem.	54
4.2	Transmission loss against frequency with fibrous sheet along with vertical step-discontinuities for: a) $\eta = -0.5$, b) $\eta = 0$, where, $\bar{a} = 0.15\text{m}$, $\bar{b} = 0.3\text{m}$, $\bar{L} = 0.25\text{m}$ and $N = 20$ terms.	68
4.3	Transmission loss against frequency with perforated sheet along with vertical step-discontinuities for: a) $\eta = -0.5$, b) $\eta = 0$, where, $\bar{a} = 0.15\text{m}$, $\bar{b} = 0.3\text{m}$, $\bar{L} = 0.25\text{m}$ and $N = 20$ terms.	69
4.4	Transmission loss against frequency with fibrous sheet and planar expansion chamber for: a) $\eta = -0.5$, b) $\eta = 0$, where, $\bar{a} = \bar{b} = 0.15\text{m}$, $\bar{L} = 0.25\text{m}$ and $N = 20$ terms.	72
4.5	Transmission loss against frequency with perforated sheet and planar expansion chamber for: a) $\eta = -0.5$, b) $\eta = 0$, where, $\bar{a} = \bar{b} = 0.15\text{m}$, $\bar{L} = 0.25\text{m}$ and $N = 20$ terms.	73
4.6	Transmission loss against frequency with vertical step-discontinuities involving expansion chamber while the central region comprises; a) rigid walls, b) soft walls, where, $\bar{a} = 0.15\text{m}$, $\bar{b} = 0.3\text{m}$, $\bar{L} = 0.25\text{m}$, $T=350\text{N}$ and $N = 20$ terms.	74
4.7	Transmission loss against frequency with vertical step-discontinuities involving expansion chamber while the central region comprises: a) rigid walls, b) soft walls, where, $\bar{a} = 0.15\text{m}$, $\bar{b} = 0.3\text{m}$, $\bar{L} = 0.25\text{m}$, $T=7500\text{N}$ and $N = 20$ terms.	75
4.8	Transmission loss against frequency with planar expansion chamber while the central region comprises: a) rigid b) soft, where, $\bar{a} = \bar{b} = 0.15\text{m}$, $\bar{L} = 0.25\text{m}$, $T=350\text{N}$ and $N = 20$ terms.	76
4.9	Transmission loss against frequency with planar expansion chamber while the central region comprises: a) rigid b) soft, where, $\bar{a} = \bar{b} = 0.15\text{m}$, $\bar{L} = 0.25\text{m}$, $T=7500\text{N}$ and $N = 20$ terms.	77
4.10	Discontinuous expansion chamber comprises: a) rigid b) soft c) perforated d) fibrous, where, $\bar{a} = 0.15\text{m}$, $\bar{b} = 0.3\text{m}$, $\bar{h} = 0.1\text{m}$, $\bar{L} = 0.25\text{m}$, $T=350\text{N}$ and $f = 581\text{Hz}$	79
4.11	Planar expansion chamber comprises: a) rigid b) soft c) perforated d) fibrous, where, $\bar{a} = \bar{b} = 0.15\text{m}$, $\bar{h} = 0.1\text{m}$, $\bar{L} = 0.25\text{m}$, $T=350\text{N}$ and $f = 581\text{Hz}$	80
4.12	The real and imaginary parts of pressures against duct height at $x = \pm L$ and $N = 20$ terms.	81
4.13	The real and imaginary parts of velocities against duct height at $x = \pm L$ and $N = 20$ terms.	81
5.1	The geometry of physical problem.	84
5.2	The plot of first few wave numbers in $s - plane$, where $\eta = 0.5$, $\bar{a} = 0.15\text{m}$, $\bar{d} = 0.1\text{m}$, $\bar{h} = 0.2\text{m}$, $\bar{b} = 0.3\text{m}$, $\bar{L} = 0.25\text{m}$ and $T = 3250\text{N}$	86
5.3	The plot of first few roots in $\gamma - plane$, where $\eta = 0.5$, $\bar{a} = 0.15\text{m}$, $\bar{d} = 0.1\text{m}$, $\bar{h} = 0.2\text{m}$, $\bar{b} = 0.3\text{m}$, $\bar{L} = 0.25\text{m}$ and $T = 3250\text{N}$: (a) Coupled modes and (b) Uncoupled modes.	87

5.4	For fibrous coating and the elastic components pinned inside the cavities ($\bar{h} > \bar{a}$), the Transmission loss against frequency, where, (a) $\eta = 0.5$ and (b) $\eta = 0$, for $N = 25$ terms.	96
5.5	For perforated coating and the elastic components pinned inside the cavities ($\bar{h} > \bar{a}$), the Transmission loss against frequency, where, (a) $\eta = 0.5$ and (b) $\eta = 0$, for $N = 25$ terms.	97
5.6	For fibrous coating and elastic components attached at apertures of cavities ($\bar{h} = \bar{a}$), the Transmission loss against frequency, where, (a) $\eta = 0.5$ and (b) $\eta = 0$, for $N = 25$ terms.	98
5.7	For perforated coating and elastic components attached at apertures of cavities ($\bar{h} = \bar{a}$), the Transmission loss against frequency, where, (a) $\eta = 0.5$ and (b) $\eta = 0$, for $N = 25$ terms.	99
5.8	TL against the position of membrane h in cavities for; a) fibrous coating and b) perforated coating, where, $\bar{a} = 0.15m$, $\bar{d} = 0.1m$, $\bar{b} = 0.3m$, $\bar{L} = 0.25m$, $T=350N$, $f = 586Hz$ and $N = 20$ terms.	101
5.9	TL against tension when elastic components are pinned inside the cavities ($\bar{h} > \bar{a}$) for; a) fibrous case, and b) perforated case, where, $\bar{a} = 0.15m$, $\bar{h} = 0.2m$, $\bar{d} = 0.1m$, $\bar{b} = 0.3m$, $\bar{L} = 0.25m$, $f = 250Hz$ and $N = 20$ terms.	102
5.10	TL against tension when elastic components are attached at the aperture of the the cavities for; a) fibrous case and b) perforated case, where, $\bar{a} = \bar{h} = 0.15m$, $\bar{d} = 0.1m$, $\bar{b} = 0.3m$, $\bar{L} = 0.25m$, $f = 250Hz$ and $N = 20$ terms.	103
5.11	Energy flux against truncation number N when the elastic components are pinned inside the cavities for; ($\bar{h} > \bar{a}$) a) fibrous case and b) perforated case, where, $\bar{a} = 0.15m$, $\bar{b} = 0.3m$, $\bar{h} = 0.2m$, $\bar{d} = 0.1m$, $\bar{L} = 0.25m$, $T=350N$ and $f = 500Hz$	106
5.12	Energy flux against truncation number N when the elastic components are attached at the apertures of cavities ($\bar{h} = \bar{a}$) for; a) fibrous case b) perforated case, where, $\bar{a} = \bar{h} = 0.2m$, $\bar{b} = 0.3m$, $\bar{d} = 0.1m$, $\bar{L} = 0.25m$, $T=350N$ and $f = 500 Hz$	106
5.13	The real and imaginary parts of pressures against duct height at $x = \pm L$ and $N = 20$ terms.	107
5.14	The real and imaginary parts of velocities against duct height at $x = \pm L$ and $N = 20$ terms.	108
6.1	The geometry of physical problem.	110
6.2	Configuration of the central region of the expansion chamber.	117
6.3	Reflected (ε_1) power and transmitted power (ε_2) versus truncation parameter (N) with $\bar{a} = 0.06m$, $\bar{d} = 0.1m$, $\bar{h} = 0.15m$, $\bar{b} = 0.3m$, $\bar{L} = 0.25m$, $T = 350Nm^{-2}$, and $f = 500Hz$	130
6.4	Real and imaginary parts of pressure vs. duct height (y) for metallic fairing with $N = 50$, $\bar{a} = 0.06m$, $\bar{d} = 0.15m$, $\bar{h} = 0.24m$, $\bar{b} = 0.33m$, and $\bar{L} = 0.25m$	131

6.5	Real and imaginary parts of velocity vs. duct height (y) for porous wall with $N = 50$, $\bar{a} = 0.06m$, $\bar{d} = 0.1m$, $\bar{h} = 0.25m$, $\bar{b} = 0.45m$, and $\bar{L} = 0.25m$	132
6.6	Transmission loss (Db) vs. frequency (Hz) with $\bar{a} = 0.06m$, $\bar{d} = 0.1m$, $\bar{h} = 0.15m$, $\bar{b} = 0.3m$, $\bar{L} = 0.25m$, and $N = 20$ terms.	133
6.7	Transmission loss (Db) vs. frequency (Hz) for different choices of height \bar{a} (top) and \bar{b} (bottom) with $\bar{d} = 0.1m$, $\bar{h} = 0.15m$, $\bar{L} = 0.25m$, and $N = 20$ terms.	134
6.8	Transmission loss (Db) vs. frequency (Hz) for different choices of tention T with $\bar{a} = 0.02m$, $\bar{b} = 0.3m$, $\bar{d} = 0.1m$, $\bar{h} = 0.15m$, $\bar{L} = 0.25m$, and $N = 20$ terms.	135

List of Tables

3.1	The scattering energies against truncation parameter N , where $\bar{a} = 0.05\text{m}$, $T=350\text{N}$, $f = 250\text{Hz}$	48
4.1	Propagating modes in discontinuous waveguide.	70
4.2	Propagating modes in planar waveguide.	71
4.3	Discontinuous expansion chamber, where, $\bar{a} = 0.15\text{m}$, $\bar{b} = 0.3\text{m}$, $\bar{h} = 0.1\text{m}$, $\bar{L} = 0.25\text{m}$, $T = 350\text{N}$, $f = 581\text{Hz}$	78
4.4	Planar expansion chamber, where, $\bar{a} = 0.15\text{m}$, $\bar{b} = 0.15\text{m}$, $\bar{h} = 0.1\text{m}$, $\bar{L} = 0.25\text{m}$, $T = 350\text{N}$, $f = 581\text{Hz}$	78
5.1	Cut-on mode frequencies when the elastic components are pinned inside of the cavities ($\bar{a} < \bar{h}$).	100
5.2	Cut-on mode frequencies when the elastic components attached at apertures of cavities ($\bar{h} = \bar{a}$).	100
5.3	The case when elastic membranes pinned inside of the cavities, where, $\bar{a} = 0.15\text{m}$, $\bar{b} = 0.3\text{m}$, $\bar{d} = 0.1\text{m}$, $\bar{h} = 0.2\text{m}$, $\bar{L} = 0.25\text{m}$, $T=350\text{N}$, $f = 500\text{Hz}$	104
5.4	The case when elastic membranes are attached at aperture of cavities, where, $\bar{a} = \bar{h} = 0.2\text{m}$, $\bar{b} = 0.3\text{m}$, $\bar{d} = 0.1\text{m}$, $\bar{L} = 0.25\text{m}$, $T=350\text{N}$, $f = 500\text{Hz}$	105
6.1	Parameters a_1, \dots, a_8 related to the bulk acoustic properties of considered absorbent materials.	129
6.2	Discontinuous expansion chamber: $\bar{a} = 0.06\text{m}$, $\bar{d} = 0.1\text{m}$, $\bar{h} = 0.15\text{m}$, $\bar{b} = 0.3\text{m}$, $\bar{L} = 0.25\text{m}$, $T=350\text{N}$, $f = 500\text{Hz}$	130

Abbreviations

MM	Mode-Matching
LFA	Low-Frequency Approximation
WH	Wiener-Hopf
SL	Sturm Liouville
TL	Transmission-Loss
OR	Orthogonality Relation
HVAC	Heating Ventilation and Air-Conditioning

Symbols

p	Acoustic pressure
ρ_0	Density in equilibrium state
\mathbf{u}	Velocity vector
f	Frequency
ω	Angular frequency
c	Speed of sound
k	Wave number
δ_{mn}	Kronecker delta
N	Truncation number
$\bar{W}(\bar{x}, \bar{y}, \bar{t})$	Membrane displacement
c_m	Speed of sound on membrane
T	Tension
ρ_m	Mass density
μ	Membrane wavenumber in <i>vacuo</i>
α	Membrane fluid loading parameter
∇	Gradient
t	Time
$e^{-i\omega\bar{t}}$	Harmonic time dependence
i	iota
\mathbf{n}	normal vector
Γ	Propagation constant for porous material
γ	Gamma
ϵ	Epsilon

Φ	Scalar fluid potential
β	Specific acoustic admittance
ξ_1	Frequency of porous material
ε	Varepsilon
ζ	Zeta
η	Eta
θ	Theta
ϑ	Vartheta
κ	Kappa
λ	Lambda
ν	Nu
ξ	Axi
π	Pi
ϖ	Varpi
ϱ	Varrho
τ	Tau
υ	Upsilon
φ	Varphi
χ	Chi
ψ	Psi
Σ	Sigma
σ	Flow resistivity
Re	Real
$*$	Complex conjugate
Ω	Domain of duct region
β_1	Normalized complex density for porous material
P_{trans}	Power transmitted
P_{ref}	Power reflected
P_{abs}	Power absorbed
ς	Specific impedance

Chapter 1

Introduction

Today the noise pollution has become the most common problem. Frequent sources of unwanted sound such as Heating Ventilation and Air Conditioning (HVAC) system, exhaust system of motor vehicles and aero-engines contribute a lot in environmental nuisance. This motivates the scholars and engineers to develop models and design objects that are useful in the reduction of structural vibrations and associated noises. Numerous theoretical models and engineering structures have been proposed so far to attenuate the vibrations of different frequency. The most common example is a silencer design of automobiles, which includes various geometrical configurations and sound absorbent materials to minimize the noise of exhaust engines. Accordingly, the duct like components are generally found in HVAC systems and aero-engines, whose purpose may vary depending upon the aim of application. However many times such ducts prove the source of transformation of unwanted noise. These noises are usually generated from the tonal fans, for instance “buzz-saw” and chimney stacks of power stations. To minimize such noises passive and active devices are employed.

In passive devices, relatively simple structures include expansion chamber silencers along with the abrupt cross-sectional variations or Helmholtz resonators. The use of sound insulation materials to get broadband attenuation of noise has been recognized as the most practical noise abatement technique [1–5]. Two types of such materials are commonly used; fibrous materials and perforated materials. Fibrous

materials are normally composed of a set of continuous filaments and contain tiny air passageways that allow air to move through it. When sound energy strikes the fibers, frictional drag between the moving air and the fiber filaments force the air molecule to vibrate causing the loss in its energy. Simultaneously, most fibrous materials absorb energy by scattering energy from the fibers followed by vibration of the individual particle. Whereas, the perforated materials are sheets or screens of metals, plastic or other material containing pattern of holes, slots or decorative shapes [6, 7]. Studies have shown that the perforated materials attenuate significantly the sound levels and have limited effects on humans health [8].

But a major issue with porous lining is that it is ineffective to reduce the low frequency range of noises. On the other hand, the active control measures or Helmholtz resonators, which aim at internal reflection of radiated waves with geometric variations or material properties, work well to mitigate the low frequency noise, albeit prohibited largely due to constraints on spacing with installation of bulky devices and sudden drop of pressure with geometric variations, for instance see [9–11]. The low frequency noise control is thus technically a challenging issue. In contrast, the reactive methods which rely on the partitioning of silencing object accompanied with flexible components and/or absorbent linings cope well the low and mid frequency range of vibrations as well as avoids sudden pressure drop with various geometric changes, for instance see [12–15].

The present thesis concerns with the acoustic wave propagation in waveguides or ducts. The study is important mainly because of extensive applications of scattering phenomena in structural design and ducting system of buildings and aircrafts. The study become more interesting while incorporating the wave-bearing boundaries together with parallel partitioning. The material properties along the partitioning walls may be assumed different. The study in general incorporates the dissipative effects as well as the geometric design principles. The later becomes more interesting while dealing with the analysis of splitting expansion chamber loaded by absorbent linings and sandwiched elastic components backed by rigid cavities. Already, the effects of splitter fairing and porous wall on silencer performance have been investigated in literature, for instance see [16–18]. These splitters

may contain bulk reacting porous material separated from the airway by a thin perforated sheet. These perforated sheets are joined to metallic fairing and porous wall at either end of the splitter, lowering the static air pressure across the silencer. Also there are many cases wherein the ducts or channels involve discontinuities in geometries and/or the change of material properties. The sudden changes in geometry and/or material properties greatly affect the performance of reactive device.

The aforementioned physical problems are governed by Helmholtz or Laplace type equation and contain Dirichlet, Neumann and Robin or higher order boundary conditions. Numerous analytical and numerical methods have been proposed so far to solve the envisaged boundary value problems. Each technique encompasses strength and limitations depending upon the governing problem and aims of investigation. For instance, to discuss the effects of absorbing lining, asymptotic method [19, 20], finite element method [21], point collocation method [22] and multimodal methods [23] are useful. However, if the problem including higher order boundary conditions mode-matching (MM) technique advanced recently [24–28] is employed. Likewise to encounter the contributions of modes the low frequency approximation (LFA) method [29–31] is used. In present thesis LFA have been devised to deal the scattering effects through different channel having various geometric and material properties.

1.1 Background and Literature Survey

Acoustics has become a broad interdisciplinary field encompassing the academic disciplines of physics, engineering, psychology, speech, audiology, music, architecture, physiology, neuroscience, and others. Among the branches of acoustics are architectural acoustics, physical acoustics, musical acoustics, psychoacoustics, electroacoustics, noise control, shock and vibration, underwater acoustics, speech, physiological acoustics, etc. Sound can be produced by a number of different processes, which include vibrating bodies, changing airflow, time-dependent heat

sources and supersonic flow. The term acoustics comes from the Greek word akouein, meaning to hear. Sauveur, in 1701, first time used the term acoustics for the science of sound.

Pythagoras, who during 600 BC developed mathematics in Greek culture, studied vibrating strings and musical sound. He found that by splitting the length of a vibrating string into simple ratios, consonant musical intervals are formed. A great deal of early acoustical study was closely related to musical acoustics. The relationship of the pitch of a string to its vibrating duration was reviewed by Galileo and he related the amount of vibrations per unit time to the pitch. Sauveur made comprehensive studies of frequency in relation to pitch. The English mathematician Taylor offered a dynamic solution for a vibrating string frequency based on the supposed curve of the string form when vibrating in its simple mode. For the vibrating string, Bernoulli set up a partial differential equation and obtained solutions that d'Alembert interpreted as waves moving along the string in both directions[32].

Apparently, the first solution to the problem of vibrating membranes was proposed by Poisson's and Clebsch viewed the circular membrane. There are somewhat more complex vibrating plates than vibrating membranes. Chladni outlined his way of using sand sprayed on vibrating plates in 1787 to show nodal lines. He noted that the addition of one nodal circle increased the frequency of a circular plate by about the same amount as the addition of two nodal diameters, a relationship which Rayleigh called the law of Chladni. To explain plate vibrations, Sophie Germain wrote a fourth-order equation and thus won a prize given by the French Emperor Napoleon, while Kirchhoff later gave a more precise treatment of the boundary conditions. Rayleigh, in his celebrated book "Theory of Sound" considered both membrane and plates [33].

In the 19th century, acoustics really flourished. We will try to provide a skeleton, at least, by mentioning the work of a few scientists. Tyndall observed that longitudinal vibration was produced by rubbing a rod. He also formulated the effects of fog and water in various weather conditions on the transmission of sound. Helmholtz improved the work of Tyndall by working over the quality of musical

sound and invented a vibrational microscope. Stokes presented a three-dimensional equation of motion of a viscous fluid which was known as Navier-Stokes equation. Bell invented a microphone. Edison recorded first time human voice for posterity. Scheibler formed tonometer for controlling the frequency in small steps. Koenig formed a tonometer which controlled frequency ranging from 16Hz to 21845Hz and made cylindrical and spherical Helmholtz resonators of different kinds.

The study of acoustics may be presented in several ways in the 20th century. Sabine, father of architectural acoustics, measured quantity of sound in the room and made acoustical theaters. Rayleigh found a way to measure the intensity of a sound source. Knudsen and Harris improved the work of Sabine by investigating the effects of molecular relaxation phenomena in gases and liquid. Bolt with the help of Beranek and Newman worked over the acoustical building, halls, musical sheds and centers for performing art. Lighthill studied about non-linear acoustics in fluid. Hamilton, Blackstock and Beyer investigated the propagation of sound through liquids, gases or solids.

There are many interesting and challenging problems in the field of acoustic, elasticity, electromagnetic wave theory and water wave theory etc that involve propagation and scattering of waves in parallel plate waveguide [34–39]. One of the first study involving acoustic scattering in a rigid cylindrical duct was presented by Miles [40]. The British Broadcasting Corporation (BBC) was among the pioneers to use membrane absorbers for their studios on large scale. BBC predicted that a 5 percent perforated membrane gives peak performance in the frequency range of 300-400 Hz. The earlier models impermeable membrane are used to the Helmholtz integral formulation, later on these models were extended to permeable membranes see [41]. The attenuation of sound inside a duct is an essential subject of practical concern. The continued interest is often motivated by the necessity to design objects in which structural vibration and the noise associated with it is to be lessened. The problem of noise attenuation has been extensively studied over the last few decades. Abom [42] discussed an expansion chamber including extensions from inlet and outlet duct regions to make it a structure of concentric ducts. He considered uniform and reactive linings at the ends of the chamber and

conferred about the acoustic performance of a device. Selamat et al [43] compared the results of different approaches with experimental measurements, for a likewise circular expansion chamber silencer to discuss the acoustic attenuation performance. Huang [12] modeled a drum-like silencer by using elastic membrane in the expansion chamber to attenuate the low frequency noise. Later, he extended his work with side-branch cavities covered by flexible plates, which give rise to noise attenuation through wave reflection towards the upstream [14]. Lawrie and Guled [13] considered a generalization of reactive silencer discussed by Huang [12, 14, 44]. They concentrated on the performance of device at low-frequency regime in which dissipative silencers are typically less efficient. Furthermore, Wang et al. [45] comprehensively analyzed the effect of sandwich plates in expansion chamber to facilitate practical implementations. The effect and optimization of additional vertical partitions inside the expansion chamber, which leads to an increase of transmission loss (TL) and a simultaneous enhancement of flow performance, is discussed by Lee and Kim [10]. Cummings [17] discussed the attenuation of sound in ducts lined on two opposite walls with porous material with some applications to splitter. Later Astley and Cummings [46] used finite element scheme for attenuation in duct lined with porous material. Lawrie and Kirby [22] discussed a point collocation approach to modelling large dissipative silencers. The influence of baffle fairing on the acoustic performance at rectangular splitter silencers is discussed by Kirby [18]. Afzal et al. [47] discussed dissipation of waves in discontinuous flexible waveguide. Nawaz et al. [30] analyzed acoustic propagation in two-dimensional waveguide for membrane bounded duct. The attenuation of noise in infinite closed ducts by means of acoustically absorbing liners has been reported extensively in literature, for instance, see [48–51].

Rawlins and Hassan [50] constitute a trifurcated waveguide problem with Robin type boundary conditions and absorbent lining to study the attenuation of sound in semi-infinite waveguide. Rawlins [49] showed that unwanted noise within a waveguide can be reduced by using acoustically absorbent lining. He proved that acoustic performance of duct can be increased by lining its walls with an acoustically absorbent material. Bykaksoy and Polat [39] discussed acoustic scattering in

a bifurcated waveguide with rigid/soft boundary conditions by applying Wiener-Hopf (WH) approach immersed with the MM scheme. Ayub et al. [15] used WH approach to study that how effectively the unwanted noise can be reduced in a trifurcated waveguide by proper selection of different parameters with soft/Robin type boundary conditions. They observed that soft surfaces show good noise reduction effects on the noise transmitted through the waveguide as compared with hard surfaces.

However, there are many cases where the ducts or channels involve discontinuities in geometries or change in material properties. When a sound wave travels along a channel, a sudden change in geometry greatly effect the scattering energy for example, in the cavity resonance mechanism, a silencer cavity is used to reduce the noise produced in car exhaust system. In such situations where the problems contain geometric discontinuities and more complex bounding properties the use of WH technique is not appropriate. Thus, there is a need to explore an alternative way that may handle more complicated physical situations together with mathematical ease. The MM scheme or eigenfunction expansion method is exactly such a simple method has been adopted to elucidate relatively more complex geometries and substantial medium properties. In this method, eigenmodes of each region are found first and matched at each junction discontinuity to satisfy the appropriate boundary conditions. The method only requires a geometry in which separation of variables can be applied. Hassan [52] used matched eigenfunction expansion method for trifurcated waveguide and analyze that this method does not involve complicated functions which arise from WH technique. By taking motivation from trifurcated waveguide, Hassan et al. [53] used MM scheme to a more complicated pentafurcated waveguide. Afzal et al. [28] used MM scheme for solution of scattering problem in flexible waveguide with abrupt geometric changes.

Note that in case of rigid/soft and impedance type bounding surfaces the pressure or normal velocity modes are orthogonal and thus lead to Sturm-Liouville (SL) systems and thereby usual orthogonal properties yield the accurate solution of the problem. However, in case of flexible bounding surfaces like membrane or elastic plate the pressures or normal velocities modes are non-orthogonal and

thus lead to non-SL systems where usual orthogonal properties is inadequate, and thus, the recently developed generalized orthogonal properties, are until indispensable. The eigenvalues in these cases are the roots of the dispersion relation and are found numerically. Lawrie and Abraham [54] discussed about the generalized orthogonal properties of boundary value problems including higher order boundary conditions. They applied the proposed scheme on prototype problems to explain acoustic scattering in membrane bounded ducts. Warren et al. [55] applied MM scheme to analyze the acoustic scattering from step-discontinuity in the membrane bounded waveguides. Without step-discontinuity (planar waveguide) they compared the MM and WH results, and found a good agreement in both the results. Lawrie [24] proved that the eigenfunctions associated with the elastic membrane or plate type boundaries are linearly dependent and encompass generalized orthogonal characteristics. Afterwards, many authors have applied the MM scheme to discuss different physical problems [26, 28, 30, 31, 47, 56, 57]. The aim of current study is to analyze the acoustic scattering problems in flexible duct involving trifurcated waveguides, partitions wave bearing cavity containing different material properties and sandwiched elastic components and reacting linings bounded by porous wall and metallic fairing.

1.2 Thesis Structure

The thesis is organized in the following order.

In Chapter 2, we discuss acoustic setting of wave equation including the role of boundary conditions and their non-dimensional setting. The procedure to develop orthogonality relation (OR) for a duct bounded by different materials are also discussed. In addition, a brief study about different mathematical techniques is presented, as well.

In Chapter 3, we discuss the MM scheme to analyze the reflection and transmission of acoustic waves in a trifurcated waveguide with multiple bounding properties.

Here the emphasis is made on the study of trifurcated waveguide involving dynamic flexible boundaries. The related pressure or normal velocity modes are non-orthogonal and thus yield a non-SL system. The orthogonal and non-orthogonal modes are matched across the regions at interface to recast the differential system into the linear algebraic system of equations, which are then solved numerically. These investigations are published in the journal **Meccanica** (2020), **Vol. 55**, **pp. 977-988**.

Chapter 4 deals with an expansion chamber silencer that contains membrane bounded cavities and horizontal partitioning inside it. The surfaces of partitioning walls are assumed as rigid, soft, impedance or sound absorbing material. The study is general in the sense that it may incorporate the dissipative effects along with the geometric design principles; wherein the sound is attenuated by reflection and/or absorption of acoustic energy within the element. The MM scheme has been used to obtain the solution of modeled problem. The approach is different from the scheme adopted by Huang [12]. He represented the fields in various duct regions in terms of Fourier integrals and then found the involving coefficients from the membrane conditions. This approach works well if the membranes are in line with the inlet/outlet duct regions. However, has limitation if the membranes are above or below the inlet/outlet sections. Moreover, the considered physical problem is solved by using the LFA to compare the results in low frequency regime. The LFA used in [30, 31] assumes only the limited number of modes which are subjected to the imposed conditions. Therefore, solution obtained via this approximation is expected to work in low frequency regime only wherein the planar modes of duct regions take part to propagate energy. The key findings of this chapter has been published in the journal **Physica Scripta** (2019), **Vol. 94**, **pp. 115-223**.

Chapter 5 investigates the scattering through a splitting expansion chamber radiated by the incident duct mode. The segments of the expansion chamber contain absorbent linings and sandwiched elastic membranes backed by rigid cavities. Lee and Kim [10] showed that the internal partitioning of the muffler expansion chamber significantly effects the transmission characteristics of device at some specific

values of frequency. The current work anticipates a mathematical frame work of the physical model that incorporates the silencing objects capable of noise attenuation at low, mid and high range of frequencies. The MM solution is developed to analyze the physical problem. The adopted scheme is different from the approach discussed by Huang [12], wherein the elastic membranes are present in line with the inlet and outlet duct walls, and the sound field is specified by means of Fourier integrals. Whereas, the coefficients of Fourier integrals are determined through the substitution of sound field into the membrane conditions. But the case considered here is somehow general with reference to the position of elastic components, and contain elastic components that may or may not be in line with the inlet and outlet duct walls, which undoubtedly leads to discontinuity in geometry. Moreover, the considered physical problem is solved by using the LFA to compare the results in low frequency regime. The key findings of this chapter has been published in the journal **Archive of Applied Mechanics** (2021), **Vol.** 91(5), **pp.** 1959-1980.

In Chapter 6, a generalization of silencer investigated by Lawrie and Guled is considered. The device comprises a two dimensional silencer in which expansion chamber is splitted. The segment of expansion chamber contain sandwich elastic membrane and two splitters in its central region. These splitters contain bulk reacting porous material separated from the airway by a thin, perforated sheet. These perforated sheets are joined to metallic fairing and porous wall at either end of the splitter, lowering the static air pressure loss across the silencer. The aim of this article is to investigate the effect of splitter fairing and porous wall on silencer performance. The MM solution is used to analyze the physical problem.

Chapter 7, is about the conclusion of this thesis.

Chapter 2

Preliminaries

In this Chapter, we discuss acoustic setting of wave equation including the role of boundary conditions and their non-dimensional setting. The boundary conditions are considered to be: rigid, soft, absorbent lining, and elastic membrane. The physical problems are governed by Helmholtz or Laplace equation and having boundary conditions rigid, soft or impedance type underlie SL category, thereby appearance of eigenfunctions are linearly independent and satisfy the standard orthogonality conditions (for more details, see for instance [79]). The orthogonality conditions help to recast the differential system to linear algebraic system during the matching analysis which is discussed in ongoing chapters of the thesis. On the other hand if the problem is governed by Helmholtz's or Laplace equation and involve higher order boundary conditions such as membrane, the governing linearly dependent eigenfunctions do not satisfy standard orthogonality conditions, and thus the generalized orthogonality conditions are employed. In more general form the development of such orthogonality conditions is explained in [24].

This chapter is organized as: Section 2.1 is dedicated to the acoustic setting of wave equation and boundary conditions. Non-dimensional setting is illustrated in Section 2.2. Development of orthogonality relations (OR) are presented in Section 2.3. Mathematical techniques for waveguide problems are discussed in Section 2.4 and lastly Section 2.5 depicts the energy flux.

2.1 Acoustic Setting

Acoustic waves are the pressure fluctuations in a material medium which transfer energy from one point to another point of medium. The medium can be solid, liquid and gases. The equation of motion responsible for the propagation of acoustic waves in such a medium can be derived by considering the conservation laws and thermodynamic properties of the medium. For inviscid stationary compressible fluid the conservation laws can be stated as:

Conservation of mass: The conservation of mass equation is defined as:

$$\frac{\partial \rho'}{\partial t} + \nabla \cdot (\rho' \mathbf{u}') = 0. \quad (2.1)$$

Conservation of momentum: The conservation of momentum equation without any body force is defined as:

$$\rho' \left(\frac{\partial \mathbf{u}'}{\partial t} + \mathbf{u}' \cdot \nabla \mathbf{u}' \right) + \nabla p' = 0, \quad (2.2)$$

where $p'(r, t)$ denotes fluid pressure having mass density $\rho'(r, t)$ with mass velocity $\mathbf{u}'(\mathbf{r}, t)$ and t is time. When the fluid is at rest, these quantities have the constant values, $\rho' = \rho_0$, $\mathbf{u}' = 0$ and $p' = p_0$, (say). The waves propagate through a medium by means of compression and rarefaction. In compression wave particles are closest together whereas in rarefaction wave particles are farthest apart. In inviscid medium, the small perturbations can be defined through linear approximation:

$$\begin{aligned} \rho' &= \rho_0 + \rho + \dots, & \rho &\ll \rho_0 \\ p' &= p_0 + p + \dots, & p &\ll p_0 \\ \mathbf{u}' &= \mathbf{u} + \dots, \end{aligned} \quad (2.3)$$

where $\rho = \rho' - \rho_0$, $p = p' - p_0$ and $\mathbf{u} = \mathbf{u}'$ are density, pressure and velocity fluctuations respectively. As these fluctuations are small so their second and higher order terms can be neglected. We use (2.3) to linearize (2.1) and (2.2), yielding

$$\frac{\partial \rho}{\partial t} + \nabla \cdot (\rho_0 \mathbf{u}) = 0, \quad (2.4)$$

$$\rho_0 \frac{\partial \mathbf{u}}{\partial t} + \nabla p = 0. \quad (2.5)$$

We combine the governing equations by the relationship $\frac{\partial}{\partial t}$ (2.4) - $\nabla \cdot$ (2.5) to obtain

$$\frac{\partial^2 \rho}{\partial t^2} - \nabla^2 p = 0. \quad (2.6)$$

On assuming the fluid media to be barotropic, (i.e. the pressure is a function of density only i.e $p' = p'(\rho')$). The Taylor series expansion about ρ_0 may apply to get:

$$p' = p_0 + \left(\frac{\partial p'}{\partial \rho'} \right)_{\rho'=\rho_0} (\rho' - \rho_0) + O((\rho' - \rho_0)^2). \quad (2.7)$$

By neglecting the second and higher order terms we obtain:

$$p = c^2 \rho, \quad (2.8)$$

where $c = \left(\frac{\partial p'}{\partial \rho'}(\rho_0) \right)^{\frac{1}{2}}$ is the speed of sound in compressible fluid.

By using (2.8) into (2.6) we get the linear acoustic wave equation

$$\nabla^2 p = \frac{1}{c^2} \frac{\partial^2 p}{\partial t^2}. \quad (2.9)$$

Notice that, acoustic density and acoustic velocity also satisfy (2.9), that are:

$$\nabla^2 \rho = \frac{1}{c^2} \frac{\partial^2 \rho}{\partial t^2} \quad (2.10)$$

and

$$\nabla^2 \mathbf{u} = \frac{1}{c^2} \frac{\partial^2 \mathbf{u}}{\partial t^2}. \quad (2.11)$$

The acoustic excitation involves irrotational flow of an inviscid fluid therefore:

$$\nabla \times \mathbf{u} = 0 \quad (2.12)$$

implying

$$\mathbf{u} = \nabla\Phi, \quad (2.13)$$

where Φ is scalar fluid potential.

By using (2.13) into (2.5), the acoustic pressure can be written as:

$$p = -\rho_0 \frac{\partial\Phi}{\partial t}. \quad (2.14)$$

Accordingly, the acoustic wave equation takes the form:

$$\nabla^2\Phi = \frac{1}{c^2} \frac{\partial^2\Phi}{\partial t^2}. \quad (2.15)$$

In dimensional setting, (2.15) satisfy the dimensional fluid potential $\Phi(\bar{x}, \bar{y}, \bar{t})$ as:

$$\frac{\partial^2\bar{\Phi}}{\partial\bar{x}^2} + \frac{\partial^2\bar{\Phi}}{\partial\bar{y}^2} = \frac{1}{c^2} \frac{\partial^2\bar{\Phi}}{\partial\bar{t}^2}, \quad (2.16)$$

where (\bar{x}, \bar{y}) and \bar{t} are dimensional spatial and time variables respectively. In this thesis we have assumed the harmonic time dependence of $e^{-i\omega\bar{t}}$, where ω is the radian frequency, thus we can write $\Phi(\bar{x}, \bar{y}, \bar{t})$ as:

$$\bar{\Phi}(\bar{x}, \bar{y}, \bar{t}) = \bar{\phi}(\bar{x}, \bar{y}) e^{-i\omega\bar{t}}, \quad (2.17)$$

where $\bar{\phi}(\bar{x}, \bar{y})$ is the time-independent dimensional fluid potential.

By using (2.17) into (2.15), we get two-dimensional Helmholtz equation that is:

$$\left\{ \frac{\partial^2}{\partial\bar{x}^2} + \frac{\partial^2}{\partial\bar{y}^2} + k^2 \right\} \bar{\phi}(\bar{x}, \bar{y}) = 0, \quad (2.18)$$

where $k = \omega/c$ is the wave number.

Here analysis of acoustic waveguide based on the variation of medium and bounding properties is presented. The medium properties have been discussed in the present section. The bounding properties are assumed impedance, rigid, soft or flexible.

2.1.1 Acoustic Impedance

The ratio between pressure and normal fluid velocity at a point on the surface is called acoustic impedance of the surface [65]:

$$Z = \frac{p}{\mathbf{u} \cdot \mathbf{n}}, \quad (2.19)$$

where \mathbf{n} is the normal vector directed into the surface. It yields the boundary condition for absorbent linings (impedance's type) as:

$$\left\{ \mathbf{n} \cdot \text{grad} + \rho Z^{-1} \frac{\partial}{\partial t} \right\} \Phi = 0. \quad (2.20)$$

In dimensional setting (2.20) satisfy the dimensional boundary condition for absorbent linings (impedance's type) as:

$$\left\{ \bar{\mathbf{n}} \cdot \bar{\text{grad}} + \rho c \bar{Z}^{-1} \frac{\partial}{\partial t} \right\} \bar{\Phi} = 0. \quad (2.21)$$

By using (2.17) into (2.21) we get

$$\left\{ \bar{\mathbf{n}} \cdot \bar{\text{grad}} + \rho c \bar{Z}^{-1} k \right\} \bar{\phi} = 0 \quad (2.22)$$

or

$$\left\{ \bar{\mathbf{n}} \cdot \bar{\text{grad}} + \bar{\beta} k \right\} \bar{\phi} = 0, \quad (2.23)$$

where $\bar{\beta} = \rho c \bar{Z}^{-1}$ is specific acoustic admittance.

Here (2.23) is Robin type boundary condition specifies a linear combination of a function and its directional derivative along the outward normal to the boundary [81].

- **Rigid conditions:** The boundary surface is usually fairly rigid when normal component of velocity is equal to zero [65], which is obtained by considering specific acoustic admittance $\bar{\beta} = 0$ in (2.23) i.e.

$$\bar{\nabla} \bar{\phi} \cdot \bar{\mathbf{n}} = 0. \quad (2.24)$$

Here (2.24) is Neumann type boundary condition specifies a directional derivative of a function along the outward normal to the boundary [81].

- **Soft conditions:** The boundary surface is moderately soft if the magnitude of its specific acoustic admittance is large [65], that is considering $\bar{\beta} = \infty$ in (2.23) we get:

$$\bar{\phi}(\bar{x}, \bar{y}) = 0. \quad (2.25)$$

Here (2.25) is Dirichlet type boundary condition specifies the value that the function needs to take on along the boundary of the domain [81].

2.1.2 Elastic Membrane

An elastic membrane is a plate or lamina containing negligible bending resisting when it is subjected to tension; for example drum head. Membranes are deformable like a sheet of rubber and that contain wave behavior similar to the waves on assemblage of flexible strings. Therefore, the tensile stress of the membrane can be referred as tension (T). The derivation of equation of vibrating membrane can be seen in many text see for example [82]. The two dimensional wave equation when external force is zero can be expressed as:

$$\left\{ \frac{\partial^2}{\partial x^2} + \frac{\partial^2}{\partial y^2} \right\} W = \frac{1}{c_m^2} \frac{\partial^2 W}{\partial t^2}. \quad (2.26)$$

In dimensional setting, (2.26) can be written as:

$$\left\{ \frac{\partial^2}{\partial \bar{x}^2} + \frac{\partial^2}{\partial \bar{y}^2} \right\} \bar{W} = \frac{1}{c_m^2} \frac{\partial^2 \bar{W}}{\partial \bar{t}^2}. \quad (2.27)$$

As there is an elastic membrane lying parallel to x -axis so the dimensional membrane displacement $\bar{W}(\bar{x}, \bar{y}, \bar{t})$ satisfies the dimensional equation of motion as:

$$\left\{ \frac{\partial^2}{\partial \bar{x}^2} - \frac{1}{c_m^2} \frac{\partial^2}{\partial \bar{t}^2} \right\} \bar{W} = \frac{1}{T} [\bar{p}]^+ \quad (2.28)$$

and

$$\bar{W}(\bar{x}, \bar{t}) = \bar{w}(\bar{x}) e^{-i\omega\bar{t}}, \quad (2.29)$$

where $c_m = \sqrt{T/\rho_m}$ represents the sound's speed on membrane having density ρ_m and tension T . The quantity $[\bar{p}]_-^+$ on the right hand side of (2.28) denotes the difference of fluid pressure across the side regions of the membrane while dimensional displacement is $\bar{W} = \partial\bar{\Phi}/\partial\bar{y}$. By using (2.17) and (2.29) into (2.28) we get

$$\left\{ \frac{\partial^2}{\partial\bar{x}^2} + \frac{\omega^2}{c_m^2} \right\} \bar{w} = \frac{i\omega\rho}{T} [\bar{\phi}]_-^+. \quad (2.30)$$

However, since

$$\bar{w} = \frac{i}{\omega} \frac{\partial\bar{\phi}(\bar{x}, \bar{y})}{\partial\bar{y}}. \quad (2.31)$$

Thus (2.31) becomes:

$$\left\{ \frac{\partial^2}{\partial\bar{x}^2} + \frac{\omega^2}{c_m^2} \right\} \frac{\partial\bar{\phi}}{\partial\bar{y}} = \frac{\omega^2\rho}{T} [\bar{\phi}]_-^+. \quad (2.32)$$

When elastic membrane is connected physically to other surfaces it may be fixed or free to deflect. Here only fixed edges are discussed.

- If the membrane is fixed at any point than the displacement of membrane is assumed to be zero, and hence

$$\frac{\partial\bar{\phi}(\bar{x}, \bar{y})}{\partial\bar{y}} = 0. \quad (2.33)$$

- If the membrane is free to deflect than the gradient is assumed to be zero, that is

$$\frac{\partial^2\bar{\phi}(\bar{x}, \bar{y})}{\partial\bar{x}\bar{y}} = 0. \quad (2.34)$$

2.2 Non-Dimensional Setting

Acoustic wave equation and boundary conditions are non-dimensionalized by taking the typical length $\frac{1}{k}$ and time scale $\frac{1}{\omega}$ under the transformation $\bar{x} = \frac{x}{k}$, $\bar{y} = \frac{y}{k}$

and $\bar{t} = \frac{t}{\omega}$ where, $k = \frac{\omega}{c} = L^{-1}$. With the aid of these transformation, it is convenient to write

$$\bar{\phi}(\bar{x}, \bar{y}) = \phi\left(\frac{x}{k}, \frac{y}{k}\right), \quad (2.35)$$

or

$$\bar{\phi}(\bar{x}, \bar{y}) = \frac{1}{k^2} \phi(x, y) \quad (2.36)$$

and

$$\frac{\partial^2}{\partial \bar{x}^2} = k^2 \frac{\partial^2}{\partial x^2}, \quad \frac{\partial^2}{\partial \bar{y}^2} = k^2 \frac{\partial^2}{\partial y^2}, \quad (2.37)$$

where $\phi(x, y)$ be the dimensionless fluid potential.

2.2.1 Governing Equation and Boundary Conditions

Thus, the dimensionless form of governing equation is Helmholtz equation

$$\left\{ \frac{\partial^2}{\partial x^2} + \frac{\partial^2}{\partial y^2} + \tilde{\Gamma} \right\} \phi(x, y) = 0. \quad (2.38)$$

where

$$\tilde{\Gamma} := \begin{cases} 1, & \text{if the inside region contains a compressible fluid,} \\ \Gamma, & \text{if the inside region contains a porous material.} \end{cases}$$

The quantity Γ is the dimensionless propagation constant for the porous material (under the assumption that $\phi \propto e^{-\Gamma x}$ within the material).

- **Impedance Boundary Conditions:** The non-dimensional general form of impedance boundary condition for lower and upper region of waveguide is defined as:

$$\phi(x, y) - i\varsigma \frac{\partial \phi(x, y)}{\partial y} = 0, \quad (2.39)$$

$$\phi(x, y) + i\varsigma \frac{\partial \phi(x, y)}{\partial y} = 0, \quad (2.40)$$

where $\varsigma = \beta^{-1}$, $\beta = \rho c Z^{-1}$, the non-dimensional specific acoustic admittance.

- **Rigid and Soft Boundary Conditions:** The rigid and soft boundary conditions in non-dimensional form can be written as

$$\frac{\partial\phi(x, y)}{\partial n} = 0 \quad (2.41)$$

and

$$\phi(x, y) = 0. \quad (2.42)$$

- **Elastic Membrane Boundary Conditions:** The non-dimensional general form of membrane boundary conditions for lower and upper regions is defined as:

$$\left(\frac{\partial^2}{\partial x^2} + \mu^2\right)\frac{\partial\phi}{\partial y} \mp [\phi]_{\pm}^+ = 0. \quad (2.43)$$

The quantities $\mu = c/c_m$ and $\alpha = \omega^2\rho/(Tk^3)$ are respectively the non-dimensional membrane wave number and the fluid loading parameter in *vacuo*, see [55].

2.3 Development of Orthogonality Relations (OR)

In order to derive OR we first determine an eigenfunction expansion for the fluid potential ϕ from (2.38) by using separation of variable technique defined as:

$$\phi(x, y) = \sum_{n=0}^{\infty} B_n Y_n(y) e^{\pm i s_n x}, \quad (2.44)$$

where $Y_n(y)$, s_n and B_n represent the eigenfunctions, wave numbers and modal coefficients respectively. Now we discuss the OR satisfied by eigenfunctions for ducts having different boundaries.

2.3.1 Impedance Impedance Case

In this case lower and upper surface of waveguide have absorbing lining. The separation of variable reduces (2.38) to give

$$Y_n''(y) - \kappa_n^2 Y_n(y) = 0, \quad n = 0, 1, 2, \dots \quad (2.45)$$

$$\alpha_1 Y_n(h) + \alpha_2 Y_n'(h) = 0, \quad (2.46)$$

$$\alpha_1 Y_n(-h) - \alpha_2 Y_n'(-h) = 0, \quad (2.47)$$

where $s_n = \sqrt{1 - \kappa_n^2}$ and κ_n , $n = 0, 1, \dots$ are the eigenvalues. Note that the parameters α_1 and α_2 are arbitrary chosen here to consider the boundary walls to be acoustically rigid, soft or absorbing lining [65]. For instance, to consider the absorbing lining we may set $\alpha_1 = 1$ and $\alpha_2 = i\zeta$.



FIGURE 2.1: The geometry of physical problem.

Let us show that the admissible eigenfunctions $Y_n(y)$ satisfy usual OR over the interval $[-h, h]$ for this we multiply (2.45) by $Y_m(y)$ and integrate from $-h$ to h gives:

$$\int_{-h}^h Y_m(y) Y_n''(y) dy = \kappa_n^2 \int_{-h}^h Y_n(y) Y_m(y) dy. \quad (2.48)$$

Integrating left hand side of (2.48) by parts yields:

$$\begin{aligned}
\int_{-h}^h Y_m(y) Y_n''(y) dy &= [Y_m(y) Y_n'(y)]_{-h}^h - [Y_m'(y) Y_n(y)]_{-h}^h + \int_{-h}^h Y_n(y) Y_m''(y) dy \\
&= \frac{-\alpha_1}{\alpha_2} [Y_m(h) Y_n(h) + Y_m(-h) Y_n(-h) - Y_m(h) Y_n(h) \\
&\quad - Y_m(-h) Y_n(-h)] + \kappa_m^2 \int_{-h}^h Y_n(y) Y_m(y) dy \\
&= \kappa_m^2 \int_{-h}^h Y_n(y) Y_m(y) dy.
\end{aligned} \tag{2.49}$$

Substituting (2.49) into (2.48) gives:

$$(\kappa_n^2 - \kappa_m^2) \int_{-h}^h Y_n(y) Y_m(y) dy = 0. \tag{2.50}$$

Now if $m \neq n$ then the above equation implies that

$$\int_{-h}^h Y_n(y) Y_m(y) dy = 0. \tag{2.51}$$

However, $m = n$ implies that

$$J_m = \int_{-h}^h Y_m^2(y) dy. \tag{2.52}$$

Combining (2.51) and (2.52) we get:

$$\int_{-h}^h Y_n(y) Y_m(y) dy = J_m \delta_{mn}, \tag{2.53}$$

where, δ_{mn} is Kronecker delta

$$\delta_{mn} = \begin{cases} 1 & m = n, \\ 0 & m \neq n. \end{cases}$$

- **Rigid Rigid Case:** In this case lower and upper surface of waveguide are bounded by rigid plates and by fixing the values of parameter as $\alpha_1 = 0$ and $\alpha_2 = 1$ bounding properties of waveguide can be taken as rigid. The OR for

rigid rigid case is written as:

$$\int_{-h}^h Y_n(y)Y_m(y)dy = h\delta_{mn}\epsilon_m. \quad (2.54)$$

$$\epsilon_m = \begin{cases} 2 & m = 0, \\ 1 & m \neq 0. \end{cases}$$

- **Soft Soft Case:** In this case lower and upper surface of waveguide are bounded by soft plates and by fixing the values of parameter as $\alpha_1 = 1$ and $\alpha_2 = 0$ bounding properties of waveguide can be taken as soft. The OR for soft soft case is written as:

$$\int_{-h}^h Y_n(y)Y_m(y)dy = h\delta_{mn}. \quad (2.55)$$

2.3.2 Rigid Membrane Case

In this case lower surface of wavguide is bounded by rigid plate while its upper surface is bounded by elastic membrane over the interval $[h, b]$. Here $s_n = \sqrt{1 + \kappa_n^2}$; κ_n , $n = 0, 1, \dots$ are the eigenvalues that satisfy the dispersion relation:

$$(\kappa_n^2 + 1 - \mu^2) Y_n'(b) - \alpha Y_n(b) = 0, \quad (2.56)$$

$$Y_n'(h) = 0. \quad (2.57)$$

Let us show that the admissible eigenfunctions $Y_n(y)$, are orthogonal and satisfy generalized OR over the interval $[h, b]$ for this we multiplying (2.45) by $Y_m(y)$ and integrating from h to b gives:

$$\int_h^b Y_m(y) Y_n''(y) dy = \kappa_n^2 \int_h^b Y_n(y) Y_m(y) dy. \quad (2.58)$$

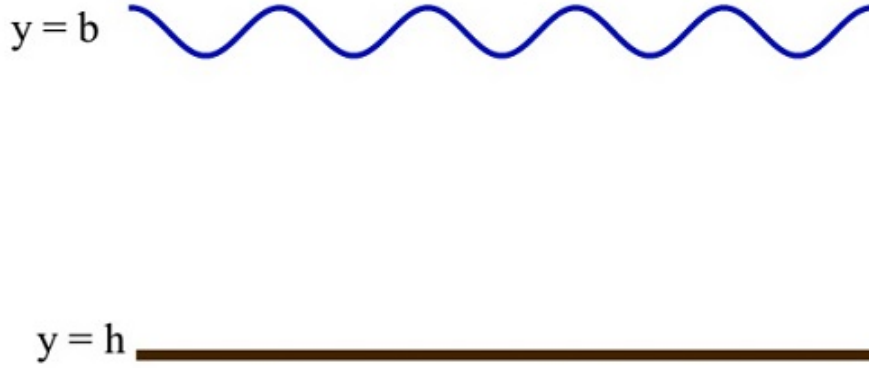


FIGURE 2.2: Duct geometry for a general problem.

Integrating left hand side of (2.58) by parts yields:

$$\begin{aligned}
 \int_h^b Y_m(y) Y_n''(y) dy &= [Y_m(y) Y_n'(y)]_h^b - [Y_m'(y) Y_n(y)]_h^b + \int_h^b Y_n(y) Y_m''(y) dy \\
 &= Y_m(b) Y_n'(b) - Y_m'(b) Y_n(b) + \int_h^b Y_n(y) Y_m''(y) dy \\
 &= \frac{Y_m'(b) Y_n'(b)}{\alpha} (\kappa_m^2 - \kappa_n^2) + \kappa_m^2 \int_h^b Y_n(y) Y_m(y) dy. \quad (2.59)
 \end{aligned}$$

Substituting (2.59) into (2.58) gives:

$$(\kappa_n^2 - \kappa_m^2) Y_n'(b) Y_m'(b) + \alpha (\kappa_n^2 - \kappa_m^2) \int_h^b Y_n(y) Y_m(y) dy = 0. \quad (2.60)$$

Now if $m \neq n$ then the above equation implies that

$$Y_n'(b) Y_m'(b) + \alpha \int_h^b Y_n(y) Y_m(y) dy = 0. \quad (2.61)$$

However, $m = n$ implies that

$$D_n = [Y_n'(b)]^2 + \alpha \int_h^b Y_n^2(y) dy. \quad (2.62)$$

Combining (2.61) and (2.62) we get:

$$Y_n'(b) Y_m'(b) + \alpha \int_h^b Y_n(y) Y_m(y) dy = \delta_{mn} D_n. \quad (2.63)$$

2.3.3 Rigid Membrane Rigid Case

In this case elastic membrane is sandwiched at $y = h$ between two rigid plates at upper and lower surface of wavguide over the interval $[d, b]$. Here the eigenvalues $\kappa_n = \sqrt{s_n^2 - 1}$, $n = 0, 1, \dots$ satisfy the dispersion relation:

$$(\kappa_n^2 + 1 - \mu^2) Y_n'(h) - \alpha [Y_n(y)]_{h^+}^{h^-} = 0, \quad (2.64)$$

$$Y_n'(d) = 0, \quad (2.65)$$

$$Y_n'(b) = 0, \quad (2.66)$$

$$Y_n'(h^-) = Y_n'(h^+). \quad (2.67)$$

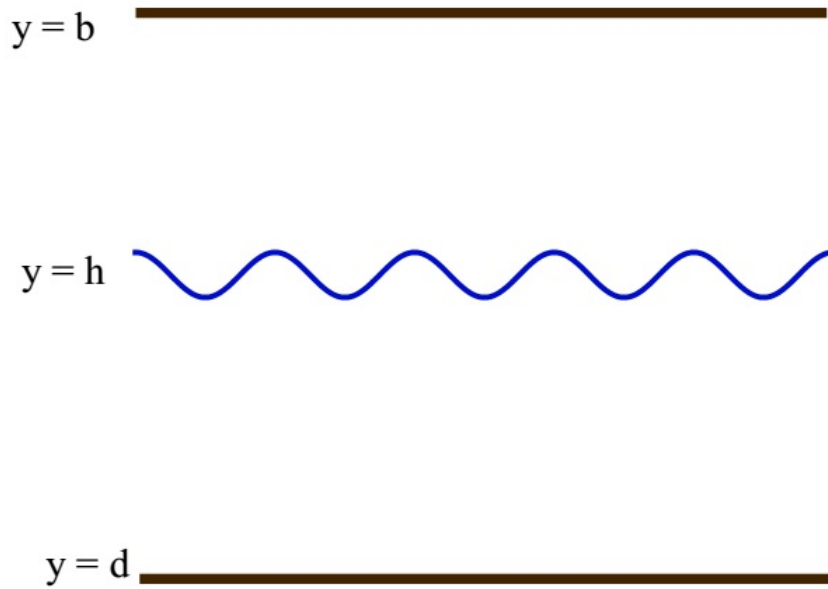


FIGURE 2.3: The geometrical configuration of physical problem.

Let us show that the admissible eigenfunctions $Y_n(y)$, are orthogonal and satisfy generalized OR over the interval $[d, b]$ for this we multiply (2.45) by $Y_m(y)$ and integrating from d to b gives:

$$\int_d^b Y_m(y) Y_n''(y) dy = \kappa_n^2 \int_d^b Y_n(y) Y_m(y) dy. \quad (2.68)$$

Integrating left hand side of (2.68) by parts yields:

$$\begin{aligned}
\int_d^b Y_m(y) Y_n''(y) dy &= \int_d^{h^-} Y_m(y) Y_n''(y) dy + \int_{h^+}^b Y_m(y) Y_n''(y) dy \\
&= [Y_m(y) Y_n'(y)]_d^{h^-} - [Y_m'(y) Y_n(y)]_d^{h^-} + \int_d^{h^-} Y_n(y) Y_m''(y) dy \\
&\quad + [Y_m(y) Y_n'(y)]_{h^+}^b - [Y_m'(y) Y_n(y)]_{h^+}^b + \int_{h^+}^b Y_n(y) Y_m''(y) dy \\
&= Y_m(h^-) Y_n'(h^-) - Y_m'(h^-) Y_n(h^-) + \int_d^{h^-} Y_n(y) Y_m''(y) dy \\
&\quad - Y_m(h^+) Y_n'(h^+) + Y_m'(h^+) Y_n(h^+) + \int_{h^+}^b Y_n(y) Y_m''(y) dy \\
&= Y_n'(h) [Y_m(y)]_{h^+}^{h^-} - Y_m'(h) [Y_n(y)]_{h^+}^{h^-} + \int_d^b Y_n(y) Y_m''(y) dy \\
&= \frac{Y_m'(h) Y_n'(h)}{\alpha} (\kappa_m^2 - \kappa_n^2) + \kappa_m^2 \int_d^b Y_n(y) Y_m(y) dy. \quad (2.69)
\end{aligned}$$

Substituting (2.69) into (2.68) gives:

$$(\kappa_n^2 - \kappa_m^2) Y_n'(h) Y_m'(h) + \alpha (\kappa_n^2 - \kappa_m^2) \int_d^b Y_n(y) Y_m(y) dy = 0. \quad (2.70)$$

Now if $m \neq n$ then the above equation implies that

$$Y_n'(h) Y_m'(h) + \alpha \int_d^b Y_n(y) Y_m(y) dy = 0. \quad (2.71)$$

However, $m = n$ implies that

$$M_n = [Y_n'(h)]^2 + \alpha \int_d^b Y_n^2(y) dy. \quad (2.72)$$

Combining (2.71) and (2.72) we get:

$$Y_n'(h) Y_m'(h) + \alpha \int_d^b Y_n(y) Y_m(y) dy = \delta_{mn} M_n. \quad (2.73)$$

2.3.4 Rigid Porous Case

In this case there are three regions of waveguide R_1 , R_2 and R_3 over the interval $[-d, d]$. Regions R_1 and R_3 are loaded with a porous material and are separated from the air containing region R_2 by means of porous linings at $y = \pm a$. Here $s_n = \sqrt{\kappa_n^2 + \Gamma_n^2}$ and $s_n = \sqrt{\kappa_n^2 + 1}$ $n = 0, 1, 2, \dots$, where quantity Γ is the dimensionless propagation constant for the porous material that is given by

$$\Gamma = 1 + ia_1\xi_1^{a_2} + a_3\xi_1^{a_4}. \quad (2.74)$$

The quantity $\xi_1 = \frac{f\rho}{\sigma}$ is the dimensionless frequency, defined in terms of the flow resistivity σ (Rayls. m^{-1}). Here a_1, a_2, a_3 and a_4 are parameters related to the bulk acoustic properties of the porous material [83].

The eigenfunctions of regions R_1 , R_2 and R_3 can be written as:

$$Y_n(y) := \begin{cases} Y_{1n}, & -d < y < -a, \\ Y_{2n}, & -a < y < a, \\ Y_{3n}, & a < y < d. \end{cases}$$

These functions satisfy the transverse boundary and continuity conditions

$$Y'_{1n}(-d^+) = 0, \quad (2.75)$$

$$Y'_{3n}(d^-) = 0, \quad (2.76)$$

$$Y'_{2n}(-a) = Y'_{1n}(-a), \quad (2.77)$$

$$Y_{2n}(-a) = \beta_1 Y_{1n}(-a), \quad (2.78)$$

$$Y_{2n}(a) = \beta_1 Y_{3n}(a) \quad (2.79)$$

and

$$Y'_{2n}(a) = Y'_{3n}(a), \quad (2.80)$$

where, $\beta_1 = \frac{\rho(\omega)}{\rho}$ is the corresponding normalized complex density in which $\rho(\omega)$ is the equivalent complex density for porous material [77] is defined by.

$$\beta_1 = \Gamma(1 + a_5 \xi_1^{a_6} - ia_7 \xi_1^{a_8}). \quad (2.81)$$

Here a_5, a_6, a_7 and a_8 are parameters related to the bulk acoustic properties of the porous material [83] and Γ is defined in (2.74).

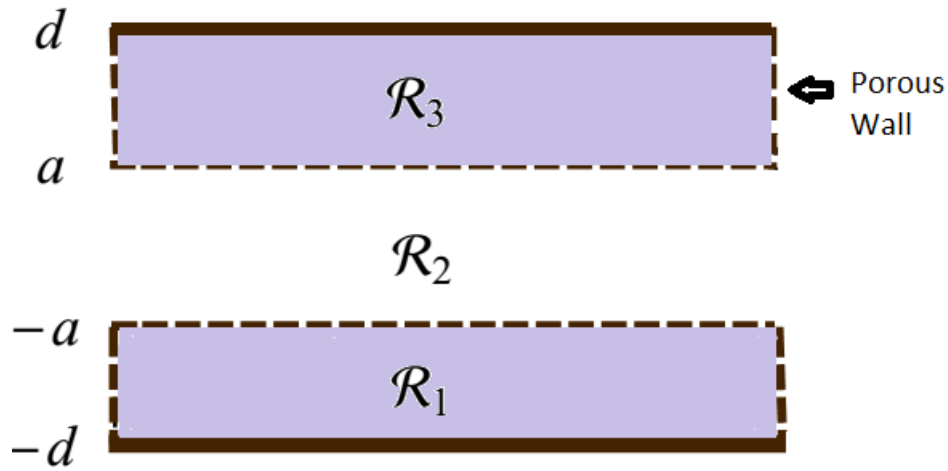


FIGURE 2.4: The duct configuration for a general problem.

Let us show that the admissible eigenfunctions $Y_n(y)$, $n = 0, 1, 2, \dots$, are orthogonal and satisfy OR over the interval $[-d, d]$ for this we multiply (2.45) by $Y_m(y)$ and integrating from $-d$ to d gives:

$$\int_{-d}^d Y_m(y) Y_n''(y) dy = \kappa_n^2 \int_{-d}^d Y_n(y) Y_m(y) dy. \quad (2.82)$$

$$\begin{aligned} & \int_{-d}^{-a} Y_{1m}(y) Y_{1n}''(y) dy + \int_{-a}^a Y_{2m}(y) Y_{2n}''(y) dy + \int_a^d Y_{3m}(y) Y_{3n}''(y) dy \\ &= \kappa_n^2 \left[\int_{-d}^{-a} Y_{1m}(y) Y_{1n}(y) dy + \int_{-a}^a Y_{2m}(y) Y_{2n}(y) dy + \int_a^d Y_{3m}(y) Y_{3n}(y) dy \right]. \end{aligned} \quad (2.83)$$

As there is porous wall over the interval $-d$ to $-a$ and a to d so we replace $Y_{1m}(y)$ by $\beta_1 Y_{1m}(y)$ and $Y_{3m}(y)$ by $\beta_1 Y_{3m}(y)$ so (2.83) can be written as:

$$\begin{aligned} & \beta_1 \int_{-d}^{-a} Y_{1m}(y) Y_{1n}''(y) dy + \int_{-a}^a Y_{2m}(y) Y_{2n}''(y) dy + \beta_1 \int_a^d Y_{3m}(y) Y_{3n}''(y) dy \\ &= \kappa_n^2 \left[\beta_1 \int_{-d}^{-a} Y_{1m}(y) Y_{1n}(y) dy + \int_{-a}^a Y_{2m}(y) Y_{2n}(y) dy + \beta_1 \int_a^d Y_{3m}(y) Y_{3n}(y) dy \right]. \end{aligned} \quad (2.84)$$

Integrating left hand side of (2.84) by parts yields:

$$\begin{aligned} & \beta_1 \int_{-d}^{-a} Y_{1m}(y) Y_{1n}''(y) dy + \int_{-a}^a Y_{2m}(y) Y_{2n}''(y) dy + \beta_1 \int_a^d Y_{3m}(y) Y_{3n}''(y) dy \\ &= [\beta_1 Y_{1m}(y) Y_{1n}'(y)]_{-d}^{-a} - [\beta_1 Y_{1m}'(y) Y_{1n}(y)]_{-d}^{-a} + \beta_1 \int_{-d}^{-a} Y_{1n}(y) Y_{1m}''(y) dy \\ &+ [Y_{2m}(y) Y_{2n}'(y)]_{-a}^a - [Y_{2m}'(y) Y_{2n}(y)]_{-a}^a + \int_{-a}^a Y_{1n}(y) Y_{1m}''(y) dy \\ &+ [\beta_1 Y_{3m}(y) Y_{3n}'(y)]_a^d - [\beta_1 Y_{3m}'(y) Y_{3n}(y)]_a^d + \beta_1 \int_a^d Y_{3n}(y) Y_{3m}''(y) dy \\ &= \beta_1 Y_{1m}(-a) Y_{1n}'(-a) - \beta_1 Y_{1m}'(-a) Y_{1n}(-a) + \beta_1 \int_{-d}^{-a} Y_{1n}(y) Y_{1m}''(y) dy \\ &+ Y_{2m}(a) Y_{2n}'(a) - Y_{2m}(-a) Y_{2n}'(-a) - Y_{2m}'(a) Y_{2n}(a) + Y_{2m}'(-a) Y_{2n}(-a) \\ &+ \int_{-a}^a Y_{2n}(y) Y_{2m}''(y) dy - \beta_1 Y_{3m}(a) Y_{3n}'(a) + \beta_1 Y_{3m}'(a) Y_{3n}(a) \\ &+ \beta_1 \int_a^d Y_{3n}(y) Y_{3m}''(y) dy \\ &= Y_{2m}(-a) Y_{2n}'(-a) - Y_{2m}'(-a) Y_{2n}(-a) + \beta_1 \int_{-d}^{-a} Y_{1n}(y) Y_{1m}''(y) dy \\ &+ Y_{2m}(a) Y_{2n}'(a) - Y_{2m}(-a) Y_{2n}'(-a) - Y_{2m}'(a) Y_{2n}(a) + Y_{2m}'(-a) Y_{2n}(-a) \\ &+ \int_{-a}^a Y_{2n}(y) Y_{2m}''(y) dy - Y_{2m}(a) Y_{2n}'(a) + Y_{2m}'(a) Y_{2n}(a) + \beta_1 \int_a^d Y_{3n}(y) Y_{3m}''(y) dy \\ &= \beta_1 \int_{-d}^{-a} Y_{1n}(y) Y_{1m}''(y) dy + \int_{-a}^a Y_{2n}(y) Y_{2m}''(y) dy + \beta_1 \int_a^d Y_{3n}(y) Y_{3m}''(y) dy \\ &= \kappa_m^2 \left[\beta_1 \int_{-d}^{-a} Y_{1n}(y) Y_{1m}(y) dy + \int_{-a}^a Y_{2n}(y) Y_{2m}(y) dy + \beta_1 \int_a^d Y_{3n}(y) Y_{3m}(y) dy \right]. \end{aligned} \quad (2.85)$$

Substituting (2.85) into (2.84) gives:

$$\begin{aligned} & (\kappa_n^2 - \kappa_m^2) [\beta_1 \int_{-d}^{-a} Y_{1n}(y) Y_{1m}(y) dy + \int_{-a}^a Y_{2n}(y) Y_{2m}(y) dy \\ & + \beta_1 \int_a^d Y_{3n}(y) Y_{3m}(y) dy] = 0. \end{aligned} \quad (2.86)$$

Now if $m \neq n$ then the above equation implies that

$$\beta_1 \int_{-d}^{-a} Y_{1n}(y) Y_{1m}(y) dy + \int_{-a}^a Y_{2n}(y) Y_{2m}(y) dy + \beta_1 \int_a^d Y_{3n}(y) Y_{3m}(y) dy = 0. \quad (2.87)$$

However, $m = n$ implies that

$$J_n = \beta_1 \int_{-d}^{-a} Y_{1n}^2(y) dy + \int_{-a}^a Y_{2n}^2(y) dy + \beta_1 \int_a^d Y_{3n}^2(y) dy. \quad (2.88)$$

Combining (2.87) and (2.88) we get:

$$\beta_1 \int_{-d}^{-a} Y_{1n}(y) Y_{1m}(y) dy + \int_{-a}^a Y_{2n}(y) Y_{2m}(y) dy + \beta_1 \int_a^d Y_{3n}(y) Y_{3m}(y) dy = \delta_{mn} J_n. \quad (2.89)$$

2.4 Mathematical Techniques for Waveguide Problems

A variety of analytical techniques are used for the solution of boundary value problem arising from the propagation or scattering of waves in waveguides. A brief description of some frequently used techniques are provided in the following lines.

2.4.1 Mode-Matching (MM) Technique

Mode-matching (MM) scheme relies on the matching of velocity and pressure modes at interface. Refer to the articles Evans and Linton [78] and Lebedev et

al. [79], MM scheme has been designed to solve the problems having complicated geometries and involving propagation in ducts or channels with higher order boundary conditions. The original aim of introducing this method is to solve the canonical problems regulated by Laplace or Helmholtz equations along with the duct boundaries of Dirichlet, Neumann or Robin type. Therefore, the reflection and transmission of waves in ducts/channels are mostly analysed by matching the modes across the interface between two sections of the waveguide. Such a problems have been discussed by Drazin and Reid [80].

The MM, a recently developed and effective technique, is capable to solve boundary value problem defined on geometries with vertical discontinuities. Initially this technique was devised for canonical problems of Sturm-Liouville (SL) nature but with the passage of time the use of this technique was extended to more complicated problems of non-SL type. As a first step, the velocity potentials are calculated in terms of the unknown scattering coefficients. The unknown coefficients are recovered by employing a generalized OR. Finally, the method results in a system of infinite linear algebraic equations. These infinite systems of equations are truncated to extract the unknown scattering coefficients. Warren et al. [55] employed the MM scheme to acoustic scattering problem in a membrane bounded waveguide with structural discontinuities. Afzal et al. [28] used this technique to find the solution of scattering problem in flexible waveguide with abrupt geometric changes. Nawaz and Lawrie [31] kept one side of a flange to be soft while the other side to be rigid and then MM scheme is used to get the solution of scattering problem.

2.4.2 Low Frequency Approximation (LFA)

A LFA may not be suitable for higher order mode forcing. It matches the integral quantities like mean pressure and velocity potential at the interface. The total number of modes to be considered for this approximation can simply be determined by the number of physical condition employed on the structure of the waveguide at the interface. Unlike, MM scheme, LFA does not require any OR

it matches the mean values which are independent of the wavenumber. However, this approximation plays a vital role in testing the MM solution in low frequency regime. Nawaz and Lawrie [31] have also used this approximation to compare its results with that of MM scheme. Similarly, Lawrie and Guled [13] have used this approximation while solving a problem related to the variation of the position of an internal membrane in a silencer.

2.5 Energy Flux

The accuracy of approximate solution is measured through energy flux. The presented solution must obey the Conservation Law i.e when power is fed into a system it must be equal to sum of reflected and transmitted powers. The expressions of energy flux for fluid and elastic membrane are different [55].

For Fluid:

$$\frac{\partial \mathcal{E}}{\partial t} = Re \left\{ i \int_{\Omega} \phi \left(\frac{\partial \phi}{\partial x} \right)^* dy \right\}. \quad (2.90)$$

For Elastic Membrane:

$$\frac{\partial \mathcal{E}}{\partial t} = Re \left\{ \frac{i}{\alpha} \left(\frac{\partial \phi}{\partial y} \right) \left(\frac{\partial^2 \phi}{\partial x \partial y} \right)^* \right\}, \quad (2.91)$$

where, the superposed asterisk (*) stands for the complex conjugate and Ω is the domain of different duct regions.

Chapter 3

Scattering Characteristics of Non-Planar Trifurcated Waveguides

In this Chapter, the study of reflection and transmission of acoustic waves in a trifurcated waveguide with multiple bounding properties is discussed. Note that in case of rigid or soft type bounding surfaces the duct modes are orthogonal and, thus leads to Sturm-Liouville (SL) systems and thereby the use of usual orthogonal properties yield the accurate solution of the problem. But the cases wherein the boundaries involve higher order derivatives such as membranes boundaries the eigen systems are non-SL. Nevertheless, the systems satisfy the generalized orthogonal properties [24, 28, 47, 54]. The orthogonal and non-orthogonal modes are matched across the regions at interface to recast the differential system into the linear algebraic system of equations which are then solved numerically. The study is sorted in the following sections. The boundary value problem is formulated in Section 3.1. The mode-matching (MM) solution is found in Section 3.2. The formulation of energy flux and mathematical validation for the associated structure are provided in Section 3.3. The numerical simulations and the discussion of the obtained results are provided in Section 3.4.

3.1 Mathematical Formulation

Here we formulate the boundary value problem to discuss the reflection and transmission of fundamental duct mode incident in trifurcated waveguide at interface. In dimensional setting of coordinates (\bar{x}, \bar{y}) , the waveguide is stretched infinitely along x -direction containing two semi-infinite duct sections of different heights. The duct section along with $\bar{x} < 0$ is bounded by rigid plates whilst the section along $\bar{x} > 0$ includes trifurcation which is made by using the symmetrically located rigid horizontal plates at $\bar{y} = \pm\bar{a}$ and the elastic membranes at $\bar{y} = \pm\bar{h}$. At interface $\bar{x} = 0$, these two semi-infinite duct sections are joined by rigid vertical walls. A compressible fluid of density ρ and sound speed c is filled inside the waveguide, whereas, the outer region of it is contained in *vacou*. The geometry of the physical problem is shown in Figure 3.1.

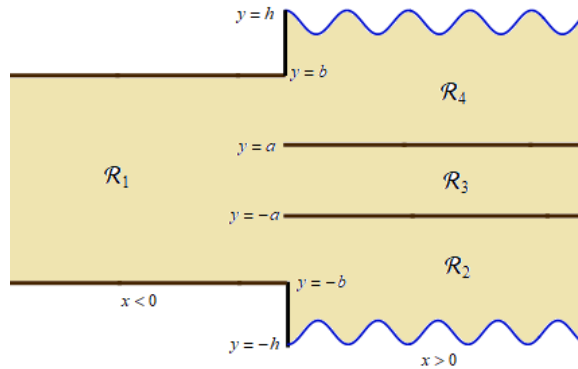


FIGURE 3.1: The geometry of physical problem.

The dimensional field potential in duct regions can be given by

$$\bar{\psi}(\bar{x}, \bar{y}) = \begin{cases} \bar{\psi}_1(\bar{x}, \bar{y}), & -\bar{b} \leq \bar{y} \leq \bar{b}, \bar{x} \leq 0, \\ \bar{\psi}_2(\bar{x}, \bar{y}), & -\bar{h} \leq \bar{y} \leq -\bar{a}, \bar{x} \geq 0, \\ \bar{\psi}_3(\bar{x}, \bar{y}), & -\bar{a} \leq \bar{y} \leq \bar{a}, \bar{x} \geq 0, \\ \bar{\psi}_4(\bar{x}, \bar{y}), & \bar{a} \leq \bar{y} \leq \bar{h}, \bar{x} \geq 0. \end{cases} \quad (3.1)$$

The boundary value problem is reduced to time-independent by assuming a harmonic time dependence of $e^{-i\omega\bar{t}}$ and made dimensionless by taking scales and

transformations defined in Chapter 2. Therefore dimensionless form of governing equation is Helmholtz equation

$$(\nabla^2 + 1)\psi(x, y) = 0, \quad (3.2)$$

where $\psi(x, y)$ is the dimensionless fluid velocity potential. Whereas, the dimensionless form of boundary conditions are:

$$\frac{\partial\psi_1}{\partial y} = 0, \quad y = \pm b, \quad -\infty < x < 0, \quad (3.3)$$

$$\left(\frac{\partial^2}{\partial x^2} + \mu^2\right) \frac{\partial\psi_2}{\partial y} - \alpha\psi_2 = 0, \quad y = -h, \quad x > 0, \quad (3.4)$$

$$\frac{\partial\psi_j}{\partial y} = 0, \quad y = \pm a^\pm, \quad x > 0, \quad j = 2, 3, 4, \quad (3.5)$$

$$\left(\frac{\partial^2}{\partial x^2} + \mu^2\right) \frac{\partial\psi_4}{\partial y} + \alpha\psi_4 = 0, \quad y = h, \quad x > 0, \quad (3.6)$$

$$\frac{\partial\psi_2}{\partial x} = 0, \quad x = 0, \quad -h \leq y \leq -b \quad (3.7)$$

and

$$\frac{\partial\psi_4}{\partial x} = 0, \quad x = 0, \quad b \leq y \leq h. \quad (3.8)$$

Here ψ_j are the fluid velocity potentials in regions R_j for $j = 1, 2, 3, 4$. In order to describe the behavior of membrane at semi-infinite edges, two edge conditions are imposed. These conditions also ensure the uniqueness of the solution [82]. At semi-infinite edges the selection of zero displacement conditions yield

$$\frac{\partial\psi_2}{\partial y} = 0, \quad x = 0, \quad y = -h, \quad (3.9)$$

$$\frac{\partial\psi_4}{\partial y} = 0, \quad x = 0, \quad y = h. \quad (3.10)$$

At the matching interface, the normal component of velocities and the fluid pressures can be matched by using continuity conditions of scattering modes across

the regions. That are:

$$\frac{\partial \psi_2}{\partial x} = \begin{cases} 0 & x = 0, & -h \leq y \leq -b, \\ \frac{\partial \psi_1}{\partial x} & x = 0, & -b \leq y \leq -a, \end{cases} \quad (3.11)$$

$$\frac{\partial \psi_3}{\partial x} = \frac{\partial \psi_1}{\partial x} \quad x = 0, \quad -a \leq y \leq a, \quad (3.12)$$

$$\frac{\partial \psi_4}{\partial x} = \begin{cases} \frac{\partial \psi_1}{\partial x} & x = 0, & a \leq y \leq b, \\ 0 & x = 0, & b \leq y \leq h, \end{cases} \quad (3.13)$$

$$\psi_1 = \begin{cases} \psi_2 & x = 0, & -b \leq y \leq -a, \\ \psi_3 & x = 0, & -a \leq y \leq a, \\ \psi_4 & x = 0, & a \leq y \leq b. \end{cases} \quad (3.14)$$

In the next section MM solution is developed for the boundary value problem of the present section.

3.2 Mode-Matching (MM) Solution

To formulate the MM solution, we first find the eigenfunction expansion forms and related orthogonality relations (OR) of propagating and scattering modes in the various duct regions. These are explained in accompanying subsections.

- Region $\mathcal{R}_1 := \{x < 0, -b \leq y \leq b\}$

On using the separation of variable technique, (3.2) and (3.3) lead to the eigenfunction expansion form of fluid potential as:

$$\psi_1(x, y) = e^{ix} + \sum_{n=0}^{\infty} A_n \cos [\xi_n(y + b)] e^{-i\eta_n x}, \quad (3.15)$$

where, wave numbers $\eta_n = \sqrt{1 - \xi_n^2}$; $n = 0, 1, 2, \dots$ can be defined in terms of the eigenvalues ξ_n wherein the eigenvalues satisfy the dispersion relation

$$\sin(2b\xi_n) = 0. \quad (3.16)$$

The admissible eigenfunctions $\cos[\xi_n(y + b)]$ for $n = 0, 1, 2, \dots$ satisfy the usual form of OR, that is:

$$\int_{-b}^b \cos[\xi_n(y + b)] \cos[\xi_m(y + b)] dy = b\epsilon_m \delta_{mn}, \quad (3.17)$$

where, δ_{mn} is Kronecker delta and

$$\epsilon_m = \begin{cases} 2 & m = 0, \\ 1 & m \neq 0. \end{cases}$$

Note that A_n , is the amplitude of the n^{th} reflected mode. These amplitudes will be found later through matching conditions.

- Region $\mathcal{R}_2 : \{x > 0, -h \leq y \leq -a\}$

In this region, (3.2), (3.4) and (3.5) lead to the eigenfunction expansion form of transmitted field as:

$$\psi_2(x, y) = \sum_{n=0}^{\infty} B_n \cosh[\gamma_n(y + a)] e^{i\nu_n x}, \quad (3.18)$$

where, wave numbers $\nu_n = \sqrt{1 + \gamma_n^2}$; $n = 0, 1, 2, \dots$ can be defined in terms of the eigenvalues γ_n wherein the eigenvalues satisfy the dispersion relation:

$$(\gamma_n^2 + 1 - \mu^2)\gamma_n \sinh[\gamma_n(h - a)] - \alpha \cosh[\gamma_n(h - a)] = 0. \quad (3.19)$$

The roots of (3.19) can be found numerically and contain following properties:

- i) There is one real root $\gamma_0 > 0$ and infinite number of imaginary roots.

ii) For each root γ_n , there is another root $-\gamma_n$, $n = 1, 2, 3, \dots$

These are organized by employing the convention that the real roots appear first and than the positive imaginary roots which are sorted sequentially in an ascending order. However, the negative imaginary roots are omitted. Consequently, the appearing eigen-sub-system is non-SL but contains well defined generalize orthogonal properties, see [24]. The admissible eigenfunctions $\cosh[\gamma_n(y + a)]$, for $n = 0, 1, 2, \dots$ satisfy the generalized OR:

$$\begin{aligned} \alpha \int_{-h}^{-a} \cosh[\gamma_m(y + a)] \cosh[\gamma_n(y + a)] dy \\ = E_m \delta_{mn} - \gamma_m \gamma_n \sinh[\gamma_m(h - a)] \sinh[\gamma_n(h - a)], \end{aligned} \quad (3.20)$$

where

$$E_m = \frac{(h - a)\alpha}{2} + \left\{ \gamma_m^2 + \frac{1 + \gamma_m^2 - \mu^2}{2} \right\} \sinh^2[\gamma_m(h - a)]. \quad (3.21)$$

Note that the coefficients B_n , $n = 0, 1, 2, \dots$ in (3.18) are the amplitudes of transmitted modes and are unknowns. These can be written in term of reflected modes by matching the normal velocity modes across the inlet region \mathcal{R}_1 and lower region \mathcal{R}_2 at interface. For this on using (3.15)-(3.18) into (3.11), we get

$$\sum_{n=0}^{\infty} B_n \nu_n \cosh[\gamma_n(y + a)] = \begin{cases} 0, & -h \leq y \leq -b, \\ 1 - \sum_{n=0}^{\infty} A_n \eta_n \cos[\xi_n(y + b)], & -b \leq y \leq -a. \end{cases} \quad (3.22)$$

On multiplying equation (3.22) with $\alpha \cosh[\gamma_m(y + a)]$, integrating from $-h$ to $-a$ and then by using the generalized OR (3.20), we get:

$$B_m = \frac{\gamma_m \sinh[\gamma_m(h - a)]}{\nu_m E_m} e_1 + \frac{\alpha}{\nu_m E_m} \left\{ Q_{m0} - \sum_{n=0}^{\infty} A_n \eta_n Q_{mn} \right\}, \quad (3.23)$$

where,

$$e_1 = i\psi_{2xy}(0, -h) \quad (3.24)$$

and

$$Q_{mn} = \frac{2b}{n^2\pi^2 + 4b^2\gamma_m^2} \left\{ n\pi \sin\left[\frac{(b-a)n\pi}{2b}\right] + 2b\gamma_m \sinh[(b-a)\gamma_m] \right\}. \quad (3.25)$$

Here the constant e_1 is unknown which describes the behavior of membrane at finite edge $(x, y) = (0, -h)$. To determine the value of this constant e_1 , we substitute (3.23) into (3.18) and then the use of zero displacement edge condition (3.9) reveals:

$$e_1 = \frac{\alpha}{S} \sum_{m=0}^{\infty} \frac{\gamma_m \sinh[\gamma_m(h-a)]}{\nu_m E_m} \left[\sum_{m=0}^{\infty} Q_{m0} - \sum_{n=0}^{\infty} A_n \eta_n Q_{mn} \right], \quad (3.26)$$

where

$$S = \sum_{m=0}^{\infty} \frac{\gamma_m^2 \sinh^2[\gamma_m(h-a)]}{\nu_m E_m}. \quad (3.27)$$

- Region \mathcal{R}_3 : $\{x > 0, -a \leq y \leq a\}$

For this region, (3.2) and (3.5) lead to the eigenfunction expansion form of transmitted field as:

$$\psi_3(x, y) = \sum_{n=0}^{\infty} C_n \cos[\tau_n(y+a)] e^{i\lambda_n x}, \quad (3.28)$$

where, wave numbers $\lambda_n = \sqrt{1 - \tau_n^2}$; $n = 0, 1, 2, \dots$ can be defined in terms of the eigenvalues τ_n wherein the eigenvalues satisfy the dispersion relation:

$$\sin(2a\tau_n) = 0. \quad (3.29)$$

The admissible eigenfunctions $\cos[\tau_n(y+a)]$ for $n = 0, 1, 2, \dots$ satisfy the usual OR:

$$\int_{-a}^a \cos[\tau_m(y+a)] \cos[\tau_n(y+a)] dy = a\delta_{mn}\epsilon_n. \quad (3.30)$$

Note that in (3.28) the transmitted mode coefficients $C_n, n = 0, 1, 2, \dots$ are unknowns. These can be written in term of reflected modes by matching the normal velocity modes across the inlet region \mathcal{R}_1 and central region \mathcal{R}_3 at interface. For

this, we use (3.15) and (3.28) into (3.12) to get:

$$\sum_{n=0}^{\infty} C_n \lambda_n \cos[\tau_n(y+a)] = 1 - \sum_{n=0}^{\infty} A_n \eta_n \cos[\xi_n(y+b)], \quad -a \leq y \leq a. \quad (3.31)$$

On multiplying (3.31) by $\cos[\tau_m(y+a)]$, integrating from $-a$ to a and then using the usual OR (3.30), it is found that:

$$C_m = \frac{1}{a\lambda_m\epsilon_m} \left\{ R_{m0} - \sum_{n=0}^{\infty} A_n \eta_n R_{mn} \right\}, \quad (3.32)$$

where,

$$R_{mn} = \begin{cases} 2a & m = n = 0, \\ L_{mn} & m \neq n, \\ M_m & m = n. \end{cases} \quad (3.33)$$

in which

$$L_{mn} = \frac{-2a^2nb}{(b^2m^2 - a^2n^2)\pi} \left(\sin\left[(a+b)\frac{n\pi}{2b}\right] \cos[m\pi] + \sin\left[(a-b)\frac{n\pi}{2b}\right] \right) \quad (3.34)$$

and

$$M_m = \frac{a^2b}{(a^2 - b^2)m\pi} \left(3 \sin\left[(a-b)\frac{m\pi}{2b}\right] + \sin\left[(a+3b)\frac{m\pi}{2b}\right] \right). \quad (3.35)$$

- Region $\mathcal{R}_4 : \{x > 0, a \leq y \leq h\}$

In this region the (3.2), (3.5) and (3.6) yield the eigenfunction expansion form of transmitted field as:

$$\psi_4(x, y) = \sum_{n=0}^{\infty} D_n \cosh[\gamma_n(y-a)] e^{i\nu_n x}, \quad (3.36)$$

where, wave numbers $\nu_n = \sqrt{1 + \gamma_n^2}$; $n = 0, 1, 2, \dots$ can be defined in terms of the eigenvalues γ_n wherein these eigenvalues are the roots of the dispersion relation (3.19) and contain properties stated for lower region \mathcal{R}_2 . The admissible eigenfunctions $\cosh[\gamma_n(y - a)]$ for $n = 0, 1, 2, \dots$ satisfy the generalized OR

$$\begin{aligned} \alpha \int_a^h \cosh[\gamma_m(y - a)] \cosh[\gamma_n(y - a)] dy \\ = E_m \delta_{mn} - \gamma_m \gamma_n \sinh[\gamma_m(h - a)] \sinh[\gamma_n(h - a)], \end{aligned} \quad (3.37)$$

where E_m is defined in (3.21) and $D_n, n = 0, 1, 2, \dots$ are the amplitudes of transmitted modes and are unknowns. These can be written in term of reflected modes by matching the normal velocity modes across the inlet regions \mathcal{R}_1 and upper region \mathcal{R}_4 at interface. For this, we invoke, (3.15) and (3.36) into (3.13) to get

$$\sum_{n=0}^{\infty} D_n \nu_n \cosh[\gamma_n(y - a)] = \begin{cases} 1 - \sum_{n=0}^{\infty} A_n \eta_n \cos[\xi_n(y + b)] & a \leq y \leq b, \\ 0, & b \leq y \leq h. \end{cases} \quad (3.38)$$

On multiplying (3.38) with $\alpha \cosh[\gamma_m(y - a)]$, integrating from a to h and then using generalized OR (3.37), we found

$$D_m = \frac{\gamma_m \sinh[\gamma_m(h - a)]}{\nu_m E_m} e_2 + \frac{\alpha}{E_m \nu_m} \left\{ P_{m0} - \sum_{n=0}^{\infty} A_n \eta_n P_{mn} \right\}, \quad (3.39)$$

where

$$P_{mn} = \frac{-2b}{n^2 \pi^2 + 4b^2 \gamma_m^2} \left\{ n\pi \sin\left[\frac{(a+b)n\pi}{2b}\right] + 2b\gamma_m \cos[n\pi] \sinh[(a-b)\gamma_m] \right\} \quad (3.40)$$

and

$$e_2 = -i\psi_{4xy}(0, h). \quad (3.41)$$

Here the constant e_2 is unknown which describe the behavior of membrane at finite edge $(x, y) = (0, h)$. For zero displacement edge condition (3.9), it is found that:

$$e_2 = -\frac{\alpha}{S} \sum_{m=0}^{\infty} \frac{\gamma_m \sinh[\gamma_m(h - a)]}{\nu_m E_m} \left\{ P_{m0} - \sum_{n=0}^{\infty} A_n \eta_n P_{mn} \right\}. \quad (3.42)$$

Finally we use the continuity condition of pressure at interface and determine the reflected modes coefficients explicitly in terms of transmitted mode coefficients. Thus, on using (3.15), (3.18), (3.28) and (3.36) into (3.14), it is straightforward to obtain

$$1 + \sum_{n=0}^{\infty} A_n \cos [\xi_n(y + b)] = \begin{cases} \sum_{n=0}^{\infty} B_n \cosh[\gamma_n(y + a)], & -b \leq y \leq -a, \\ \sum_{n=0}^{\infty} C_n \cos[\tau_n(y + a)], & -a \leq y \leq a, \\ \sum_{n=0}^{\infty} D_n \cosh[\gamma_n(y - a)], & a \leq y \leq b. \end{cases} \quad (3.43)$$

On multiplying with $\cos [\xi_m(y + b)]$, integrating from $-b$ to b and then using the usual OR (3.17), we found

$$A_m = -\delta_{m0} + \frac{1}{b\epsilon_m} \left\{ \sum_{n=0}^{\infty} B_n Q_{nm} + \sum_{n=0}^{\infty} C_n R_{nm} + \sum_{n=0}^{\infty} D_n P_{nm} \right\}. \quad (3.44)$$

Note that the above equation relates the reflected mode coefficients of region R_1 with the transmitted mode coefficients of regions $R_j, j = 2, 3, 4$. However, by substituting (3.23), (3.32) and (3.39) into (3.44), a system of infinite linear algebraic equations containing unknowns $A_n, n = 0, 1, 2, \dots$ is achieved. This system is truncated upto N terms and then is solved numerically for unknown coefficients.

3.3 Energy Balance

Here we determine the expressions for energy/power flux in various duct regions R_j for $j = 1, 2, 3, 4$. The non-dimensional form of power/energy flux propagating through fluid per unit length in z-direction can be written as [55]

$$\frac{\partial \mathcal{E}}{\partial t} = Re \left\{ i \int_{\Omega} \psi \left(\frac{\partial \psi}{\partial x} \right)^* dy \right\}, \quad (3.45)$$

where, the superposed asterisk (*) stands for the complex conjugate and Ω is the domain of different duct regions. However, the dimensionless form of energy flux

propagating along the membrane boundaries is given as [55]

$$\frac{\partial \mathcal{E}}{\partial t} = Re \left\{ \frac{i}{\alpha} \left(\frac{\partial \psi}{\partial y} \right) \left(\frac{\partial^2 \psi}{\partial x \partial y} \right)^* \right\}_{y=\pm h}. \quad (3.46)$$

Now by substituting the incident field $\exp(ix)$ into (3.45), the incident power is found to be $2b$. When this power is fed into the system it will be equal to the sum of reflected and transmitted powers of duct regions. This is conservation law. The mathematical forms of the scattering powers are found by using the field potentials of duct regions into (3.45) and (3.46), that are

$$\mathcal{E}_1 = \frac{1}{2} Re \left\{ \sum_{n=0}^{\infty} |A_n|^2 \eta_n^* \epsilon_n \right\}, \quad (3.47)$$

$$\mathcal{E}_2 = \frac{1}{2b\alpha} Re \left\{ \sum_{n=0}^{\infty} |B_n|^2 \nu_n^* E_n \right\}, \quad (3.48)$$

$$\mathcal{E}_3 = \frac{a}{2b} Re \left\{ \sum_{n=0}^{\infty} |C_n|^2 \lambda_n^* \epsilon_n \right\}, \quad (3.49)$$

$$\mathcal{E}_4 = \frac{1}{2b\alpha} Re \left\{ \sum_{n=0}^{\infty} |D_n|^2 \nu_n^* E_n \right\}. \quad (3.50)$$

Here \mathcal{E}_1 represents the power reflected in region R_1 and $\mathcal{E}_j, j = 2, 3, 4$ show transmitted powers in duct regions R_j for $j = 2, 3, 4$ where, the incident power is being scaled at unity. Whereas, the conserved power identity is

$$\mathcal{E}_1 + \mathcal{E}_2 + \mathcal{E}_3 + \mathcal{E}_4 = 1. \quad (3.51)$$

Note that the MM solution found in previous section preserve the conserve power identity (3.51). In fact, on multiplying with $\sum_{m=0}^{\infty} A_m^* \eta_m^* \epsilon_m b$, (3.44) yields

$$\begin{aligned} \sum_{m=0}^{\infty} |A_m|^2 \eta_m^* \epsilon_m b &= -2A_0^* b + \sum_{n=0}^{\infty} \left\{ B_n \sum_{m=0}^{\infty} A_m^* \eta_m^* Q_{nm} + C_n \sum_{m=0}^{\infty} A_m^* \eta_m^* R_{nm} \right. \\ &\quad \left. + D_n \sum_{m=0}^{\infty} A_m^* \eta_m^* P_{nm} \right\}. \end{aligned} \quad (3.52)$$

But from (3.23), (3.32) and (3.39), we can write:

$$\sum_{m=0}^{\infty} A_m^* \eta_m^* Q_{nm} = Q_{n0} + \frac{1}{\alpha} \{ \gamma_n^* \sinh^* [\gamma_n (h - a)] e_1^* - B_n^* \nu_n^* E_n \}, \quad (3.53)$$

$$\sum_{m=0}^{\infty} A_m^* \eta_m^* R_{nm} = R_{n0} - C_n^* \lambda_n^* \epsilon_n a, \quad (3.54)$$

$$\sum_{m=0}^{\infty} A_m^* \eta_m^* P_{nm} = P_{n0} + \frac{1}{\alpha} \{ \gamma_n^* \sinh^* [\gamma_n (h - a)] e_2^* - D_n^* \nu_n^* E_n \}. \quad (3.55)$$

By invoking (3.53)-(3.55) into (3.52), and then simplifying the resulting equation with the aid of (3.9)-(3.10) and (3.44), we conclude that

$$\sum_{j=1}^4 \mathcal{E}_j = \mathcal{E}_T = 1, \quad (3.56)$$

which is exactly the conserved power identity (3.51).

3.4 Numerical Results and Discussion

In this section, the wave scattering in the waveguide of infinite length and finite height together with discontinuities located at $x = 0$ is studied by analyzing the reflection and transmission of energy flux in different regions of the channel. The system of equations defined by (3.23), (3.32), (3.39) and (3.44) is truncated first upto $n = m = 0, 1, 2, \dots, N$ terms and then is solved numerically. In the numerical results, $c = 343 \text{ms}^{-1}$, $\rho = 1.2043 \text{kgm}^{-3}$ and $\rho_m = 0.1715 \text{kgm}^{-3}$, remain fixed [13]. The scattering powers \mathcal{E}_j for $j = 1, 2, 3, 4$ are referred as the reflection and transmission of energy flux in duct regions. In our discussion $k = 2\pi f/c$ and $y = k \times \bar{y}$ are referred as the wave number and dimensionless height.

In Figures 3.2 and 3.3, the reflected energy \mathcal{E}_1 and transmitted energies \mathcal{E}_2 , \mathcal{E}_3 and \mathcal{E}_4 versus the non-dimensional size of central region a at fixed frequency $f = 250 \text{Hz}$ and tension $T = 350 \text{N}$ are plotted for structure discontinuities involving channel and planner channel. It is seen that as the duct size increases, the transmission in rigid walls bounded region increases while the transmission in membrane bounded

sections decreases. But when the new cuts-on appear the transmission in the membrane bounded regions start increasing. It is important to notice that the cut-on duct modes for the discontinuous case occur at $a \approx 1.05$ and $a \approx 1.82$ (see Figure 3.2) while for the continuous case these appear at $a \approx 0.51$, $a \approx 1.05$ and $a \approx 2.08$ (see Figure 3.3). Moreover, relatively more reflection for planar waveguide than discontinuous waveguide is observed. However, the energy relation (3.56) remains valid in whole regime.

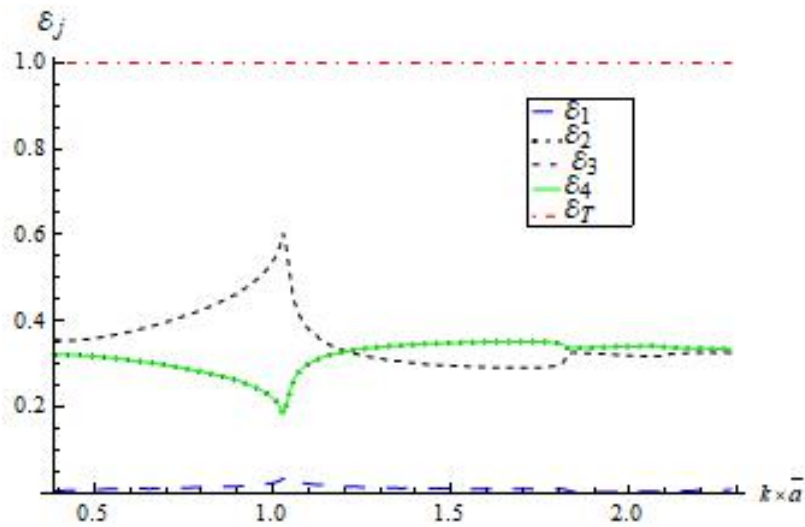


FIGURE 3.2: The scattering energies plotted against non-dimensional height a for discontinuous structure where $\bar{h} = 5 \times \bar{a}$, $\bar{b} = 3 \times \bar{a}$ and $N = 30$ terms.

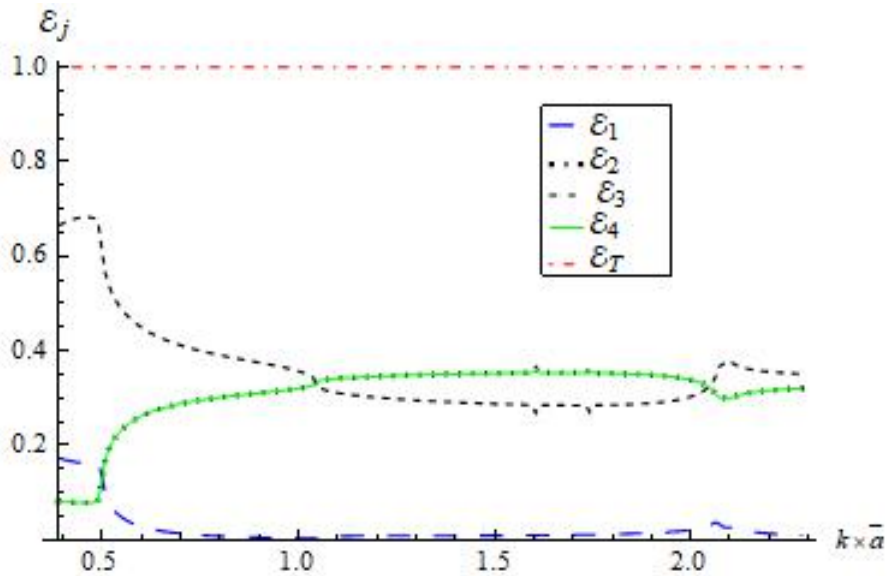


FIGURE 3.3: The scattering energies plotted against non-dimensional height a for continuous structure where $\bar{h} = \bar{b} = 3 \times \bar{a}$ and $N = 30$ terms.

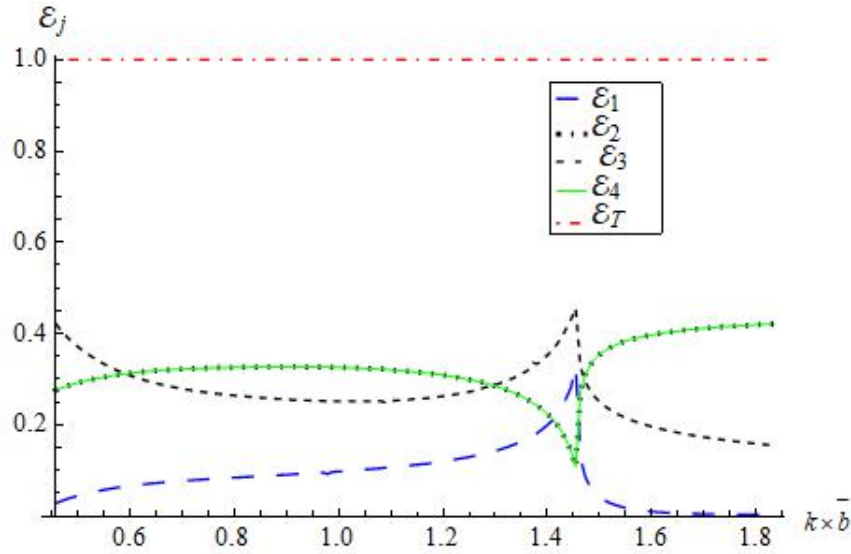


FIGURE 3.4: The energy flux against non-dimensional height b for discontinuous structure where $\bar{h} = 3 \times \bar{b}$, $\bar{a} = 0.05\text{m}$, $f = 250\text{Hz}$ and $N = 30$ terms.

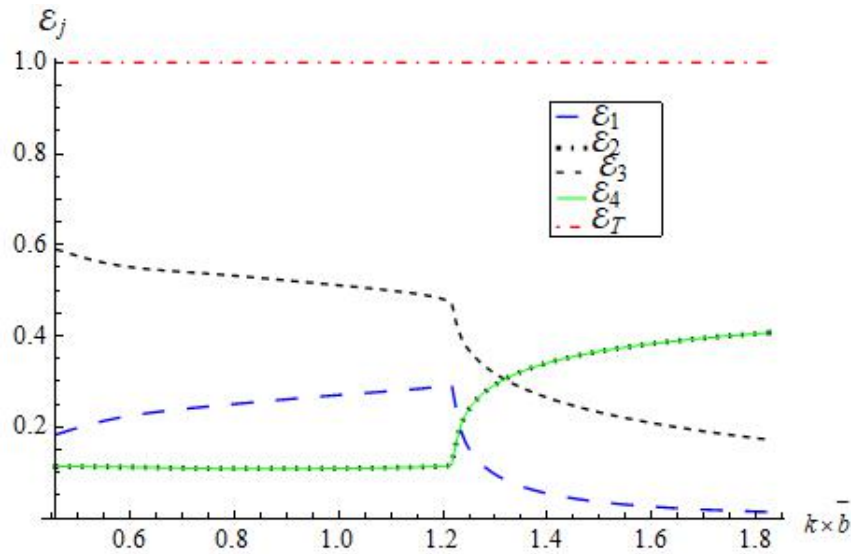


FIGURE 3.5: The scattering energies plotted against non-dimensional height b for continuous structure where $\bar{h} = \bar{b}$, $\bar{a} = 0.05\text{m}$, $f = 250\text{Hz}$ and $N = 30$ terms.

Figures 3.4 and 3.5 show the scattering energy against the size of inlet duct while the size of central region R_3 is fixed at $\bar{a} = 0.05\text{m}$. Now by varying the size of inlet duct that patently varies the size of lower region R_2 and upper region R_4 ($\bar{h} = 3 \times \bar{b}$), the reflection in inlet region R_1 and transmission in central region R_3 increase, whilst the transmissions in lower region R_2 and upper region R_4 are decreased. But when new ducts modes become cut-on the scattering behaves inversely. Note

that these cut-on modes appear at $b = k \times \bar{b} \approx 1.46$ for configuration involving discontinuities (see Figure 3.4) and appear at $b = k \times \bar{b} \approx 1.23$ with planar structure (see Figure 3.5), whereas, $0.1\text{m} \leq \bar{b} \leq 0.4\text{m}$, $f = 250\text{Hz}$ and tension $T = 350\text{N}$. The comparison of Figures 3.4 and 3.5 depicts that relatively greater amount of acoustic energy is transmitted through the central region against the size of inlet duct region in the case of structurally continuous setting.

The alteration in symmetric height discontinuities greatly effect the scattering energies as shown in Figure 3.6. The dimensionless height discontinuities $h = k \times \bar{h}$ are changed symmetrically from $\bar{h} = 0.1\text{m}$ to $\bar{h} = 0.4\text{m}$ by keeping remaining parameters fixed. The cut-on duct modes occur at $k \times \bar{h} \approx 1.23$. From Figure 3.6 it is interesting to note that the variation in height discontinuities greatly affect the scattering energies.

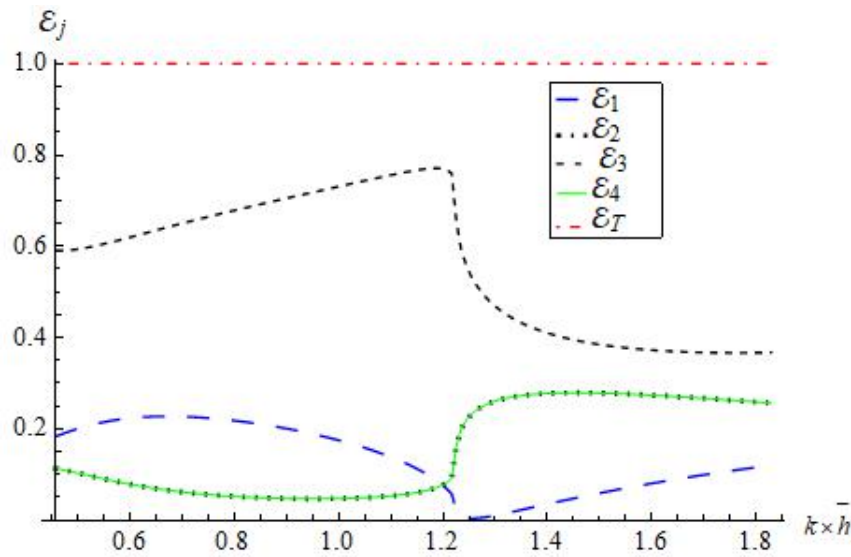


FIGURE 3.6: The scattering energies plotted against discontinuous height h where $\bar{a} = 0.05\text{m}$, $\bar{b} = 0.1\text{m}$, $f = 250\text{Hz}$ and $N = 30$ terms.

In Figures 3.7 and 3.8, the scattering energy components are shown against frequency for the different values of membrane tension whereas the vertical height dimensions remain unchanged. The tension T is directly related to the elastic modulus. The variations of tension change the speed of wave on membrane $c_m = T/\rho_m$ which alters the membrane wave number $\mu = c/c_m$. Likewise the fluid loading parameter $\alpha = \omega^2 \rho / (T k^3)$ is also varied by changing the tension of membrane.

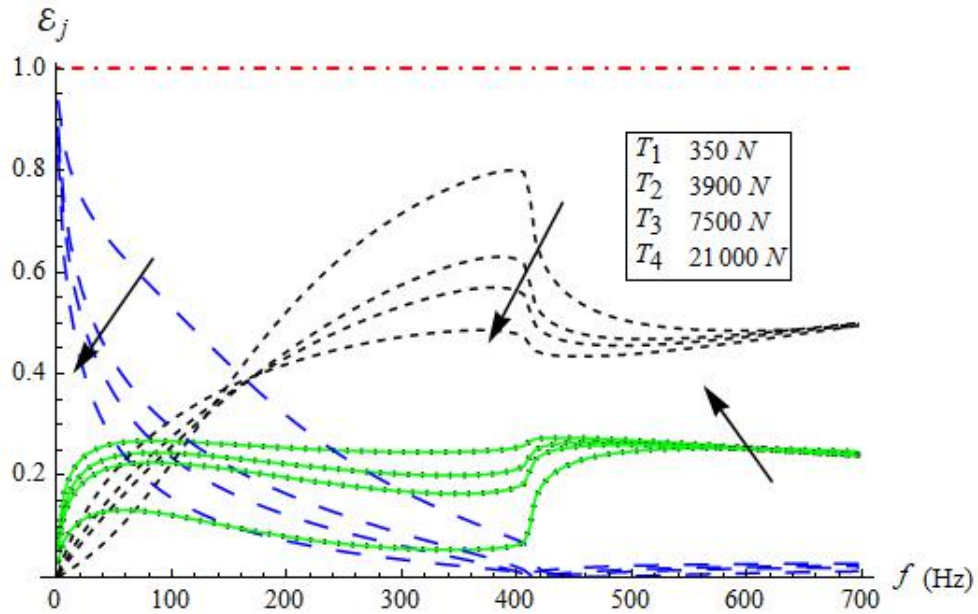


FIGURE 3.7: The scattering energies versus frequency for different values of Tension for discontinuous structure where $\bar{h} = 0.15\text{m}$ and $N = 30$ terms.

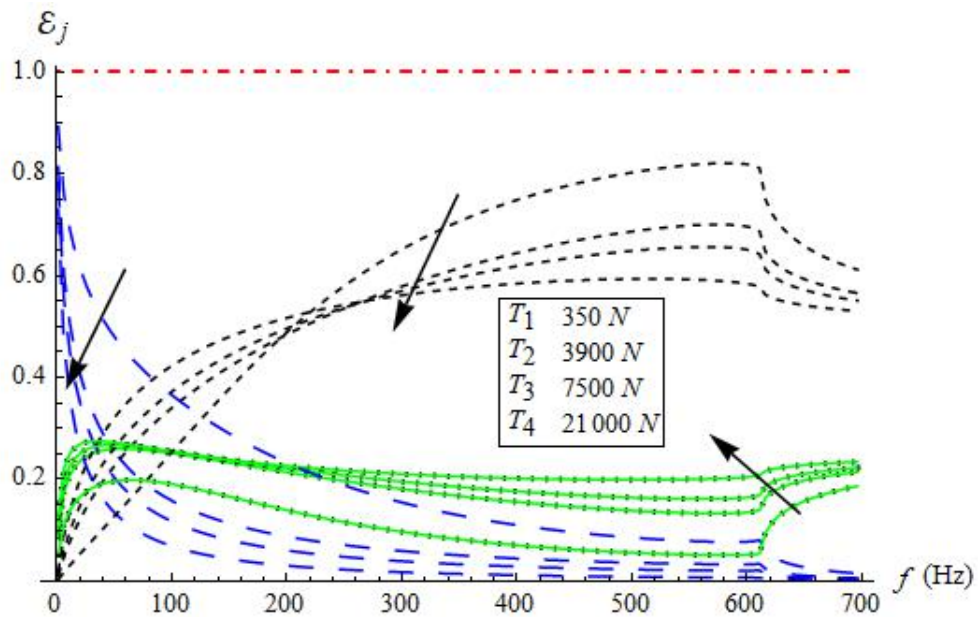


FIGURE 3.8: The scattering energies versus frequency for different values of Tension for continuous structure where $\bar{h} = 0.1\text{m}$ and $N = 30$ terms.

It can be seen that by varying frequency from 1Hz to 700Hz the reflection in inlet region \mathcal{R}_1 is decreased while the transmission through central region is increased. It is noted that by increasing the membrane tension the reflection in inlet region

\mathcal{R}_1 (see long dashed curves in Figure 3.7) and the transmission in central region \mathcal{R}_3 (see small dashed curves in Figure 3.7) are decreased while the transmission in lower region \mathcal{R}_2 and upper region \mathcal{R}_4 (see dotted and solid curves in Figure 3.7) is increased. The dissimilarity of scattering components against membrane tension is more prominent in low frequency range and before the occurrence of new cut-on duct modes. These cut-on modes exist at $f = 401\text{Hz}$ for geometrically discontinuous setting (see Figure 3.7) and occur at $f = 601\text{Hz}$ for planar setting (see Figure 3.8). To look at the accuracy of MM solution computationally against truncation parameter N , Table 3.1, and Figures 3.9 and 3.10 are shown with $\bar{a} = 0.05\text{m}$, $f = 250\text{Hz}$ and $T = 350\text{N}$. Whereas, $\bar{b} = 0.1\text{m}$ and $\bar{h} = 0.15\text{m}$ for discontinuous waveguide and for planar waveguide $\bar{b} = \bar{h} = 0.1\text{m}$.

TABLE 3.1: The scattering energies against truncation parameter N , where $\bar{a} = 0.05\text{m}$, $T=350\text{N}$, $f = 250\text{Hz}$.

Cases	N	\mathcal{E}_1	\mathcal{E}_2	\mathcal{E}_3	\mathcal{E}_4	\mathcal{E}_T
Discontinuous configuration $\bar{b} = 0.1\text{m}$, $\bar{h} = 0.15\text{m}$	7	0.227083	0.0632231	0.646471	0.0632231	1
	16	0.23691	0.0661085	0.630873	0.0661085	1
	25	0.240025	0.0669775	0.62602	0.0669775	1
	40	0.24244	0.0676464	0.622267	0.0676464	1
	49	0.243032	0.0678094	0.621349	0.0678094	1
Planar configuration $\bar{b} = \bar{h} = 0.1\text{m}$	7	0.183255	0.113169	0.590407	0.113169	1
	16	0.190581	0.117277	0.574866	0.117277	1
	25	0.193002	0.118606	0.569787	0.118606	1
	40	0.194921	0.119655	0.565769	0.119655	1
	49	0.195397	0.119915	0.564772	0.119915	1

From Table 3.1 it can be seen that the scattering energies converge upto two and three decimal places even with truncation number $N = 25$. Moreover, the sum of reflected energy (\mathcal{E}_1) and transmitted energies (\mathcal{E}_2 , \mathcal{E}_3 , and \mathcal{E}_4) remains unity for each value of N . The point-wise variation of energies verses N are shown Figures 3.9 and 3.10, which clearly satisfy the conserve energy identity (3.51).

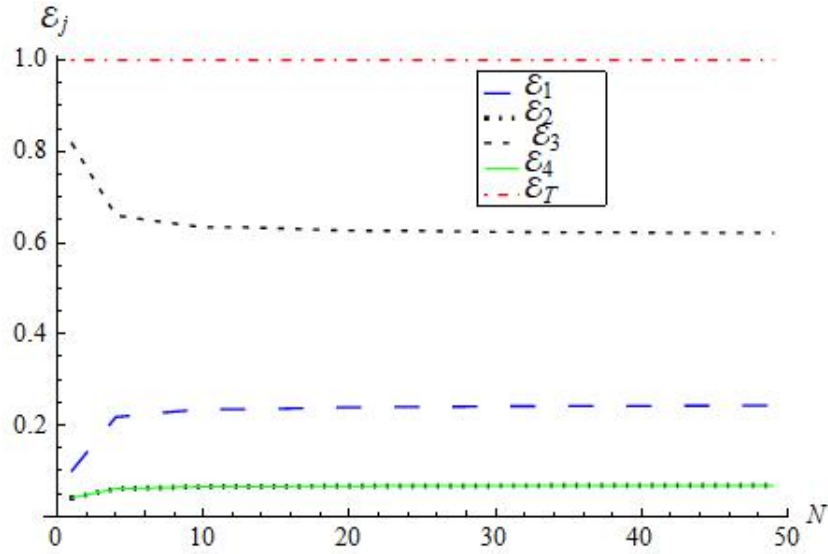


FIGURE 3.9: The scattering energies plotted against number of terms N for discontinuous structure where $\bar{h} = 0.15\text{m}$, $f = 250\text{Hz}$ and $T = 350\text{N}$.

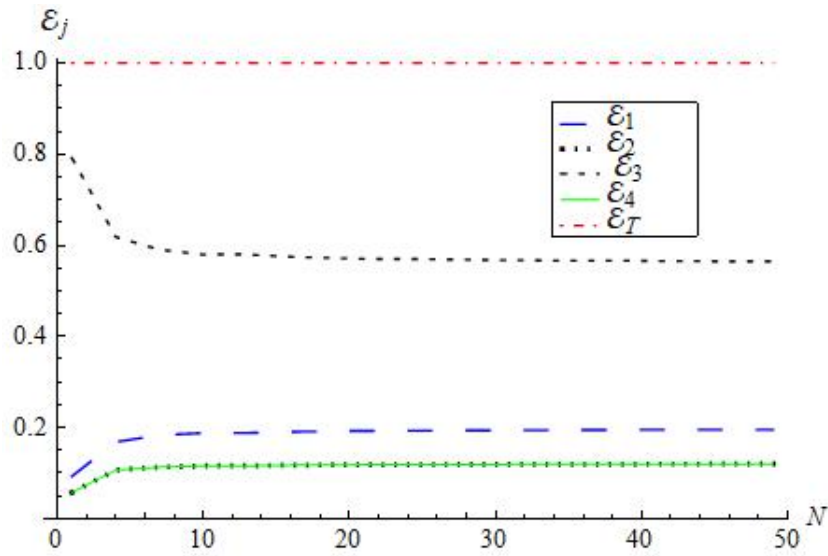


FIGURE 3.10: The scattering energies plotted against number of terms N for planar structure where $\bar{h} = 0.1\text{m}$, $f = 250\text{Hz}$ and $T = 350\text{N}$.

Furthermore, we reconstruct the continuity conditions (3.11)-(3.14) at matching interface to validate the truncated solution. By fixing the waveguide dimensions, at $\bar{a} = 0.05\text{m}$, $\bar{b} = 0.1\text{m}$ and $\bar{h} = 0.15\text{m}$, the real and imaginary parts of dimensionless normal velocities and pressures are plotted in Figures 3.11-3.14. From Figures 3.11 and 3.12, it can be seen that the real and imaginary parts of non-dimensional normal velocity $\psi_{1x}(0, y)$, $-b < y < b$ of inlet region \mathcal{R}_1 match exactly to the

normal velocities $\psi_{jx}(0, y)$, $j = 2, 3, 4$ of regions \mathcal{R}_j , $j = 2, 3, 4$ in their respective regions at aperture. Likewise the real and imaginary parts of non-dimensional pressure $\psi_1(0, y)$, $-b < y < b$ match exactly with the non-dimensional pressures $\psi_j(0, y)$, $j = 2, 3, 4$ in their respective regions at aperture (see Figures 3.4 and 3.14). These are exactly the conditions considered in equations (3.11)-(3.14). However, there appear some oscillations in normal velocities. These oscillations are due to the Gibb's phenomenon that can be removed by increasing the truncation number N or by using the Lanczos filters [31].

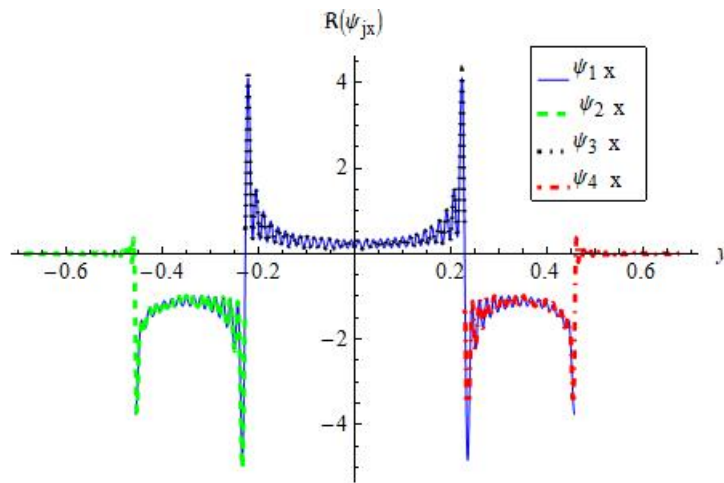


FIGURE 3.11: The real part of normal velocities versus height in non-dimensional form at interface, where, $\bar{h} = 0.15\text{m}$, $f = 250\text{Hz}$ and $N = 120$ terms.

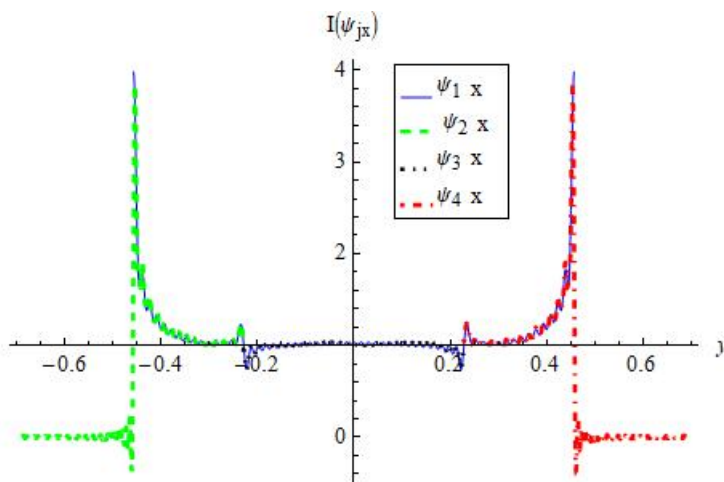


FIGURE 3.12: The imaginary part of normal velocities versus height in non-dimensional form at interface, where $\bar{h} = 0.15\text{m}$, $f = 250\text{Hz}$ and $N = 120$ terms.

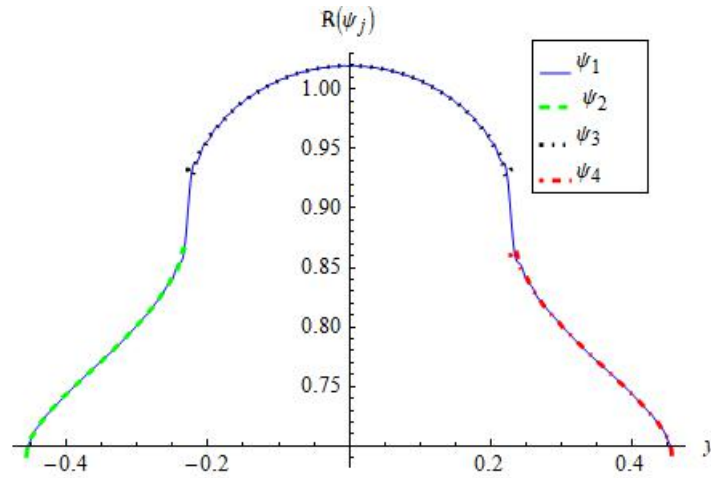


FIGURE 3.13: The real part of pressures versus height in non-dimensional form at interface, where, $\bar{h} = 0.15\text{m}$, $f = 250\text{Hz}$ and $N = 120$ terms.

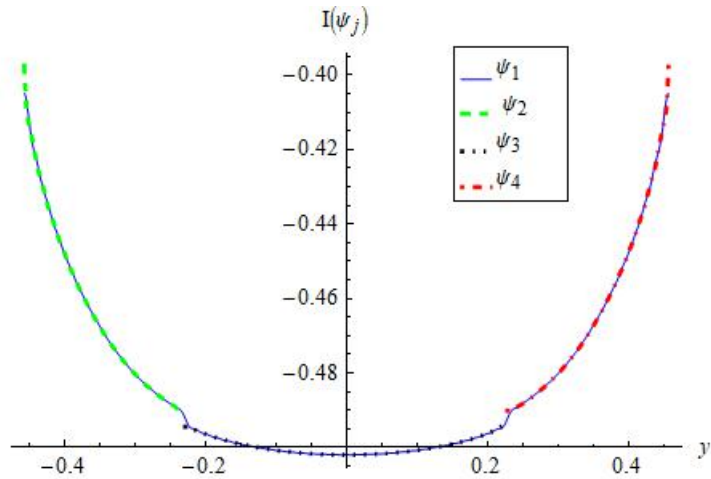


FIGURE 3.14: The imaginary part of pressures versus height in non-dimensional form at interface, where, $\bar{h} = 0.15\text{m}$, $f = 250\text{Hz}$ and $N = 120$ terms.

In this way the truncated form of MM solution not only satisfies the matching conditions of pressures and velocities (3.11)-(3.14) at interface but it also validates the conserved power identity (3.51).

Chapter 4

Scattering Analysis of a Partitioned Wave-Bearing Cavity Containing Different Material Properties

This Chapter, deals with an expansion chamber silencer that contains membrane bounded cavities and horizontal partitioning inside it. The surfaces of partitioning walls are assumed as rigid, soft, impedance or sound absorbing material. The study is general in the sense that it may incorporate the dissipative effects along with the geometric design principles; wherein the sound is attenuated by reflection and/or absorption of acoustic energy within the element. The mode-matching (MM) scheme has been used to obtain the solution of modeled problem. The approach is different from the scheme adopted by Huang [12]. He represented the fields in various duct regions in terms of Fourier integrals and then found the involving coefficients from the membrane conditions. This approach works well if the membranes are in line with the inlet/outlet duct regions. However, has limitation if the membranes are above or below the inlet/outlet sections.

In contrast, the technique employed here contains the discrete wavenumber spectrum of modes in different duct regions of the waveguide. The scattering field

potentials are expressed in the form of eigenfunction expansions which contain the unknown scattering mode amplitudes. Note that in case of rigid or soft type bounding surfaces the duct modes are orthogonal and, thus leads to Sturm-Liouville (SL) systems and thereby the use of usual orthogonal properties yield the accurate solution of the problem. But the cases wherein the boundaries involve higher order derivatives such as membranes boundaries the eigen systems are non-SL. Nevertheless, the systems satisfy the generalized orthogonal properties [24, 28, 47, 54]. The orthogonal and non-orthogonal modes are matched across the interfaces to recast the linear algebraic systems of equations which are then solved numerically. Moreover, the considered physical problem is solved by using the low frequency approximation (LFA) to compare the results in low frequency regime. The LFA used in [30, 31] assumes only the limited number of modes which are subjected to the imposed conditions. Therefore, the solution obtained via this approximation is expected to work in low frequency regime only wherein the planar modes of duct regions take part to propagate energy.

The study is sorted in the following sections. The traveling wave forms of the duct modes and their characteristics are detailed in Section 4.1. The MM solution is found in Section 4.2, whereas, the LFA is used to solve the problem in Section 4.3. The physical importance and the mathematical validation through numerical results are presented in Section 4.4.

4.1 Mathematical Formulation

The traveling wave forms of the duct modes and their characteristics are detailed in this section. The waveguide is stretched infinitely along x -direction and includes a finite trifurcation of the region at $|\bar{x}| \leq \bar{L}$, $-\bar{b} \leq \bar{y} \leq \bar{b}$ with horizontal parallel plates at $\bar{y} = \pm h$. This region can be regarded as an expansion chamber of a physical silencer. The boundary walls of the expansion chamber at $\bar{y} = \pm \bar{b}$ are elastic membranes. The end points of these membranes are attached with the rigid vertical plates which lie along $\bar{x} = \pm \bar{L}$, where, $\bar{a} \leq \bar{y} \leq \bar{b}$ and $-\bar{b} \leq \bar{y} \leq -\bar{a}$. Moreover, the outer surfaces of the parallel plates at $\bar{y} = \pm \bar{h}$ are rigid whilst the

inward surfaces can be rigid, soft or impedance (absorbing linings). Whereas, the regions at $|\bar{x}| \geq \bar{L}$, $-\bar{a} \leq \bar{y} \leq \bar{a}$ serve as inlet and outlet of the chamber. The bounding wall conditions of inlet/outlet duct regions are taken to be acoustically rigid. Note that over-bar here and throughout the article denotes the dimensional setting of co-ordinates. A compressible fluid of density ρ and sound speed c is filled inside the waveguide where the outer region of it is contained in *vacuo*. The geometry of physical problem is as shown in Figure 4.1

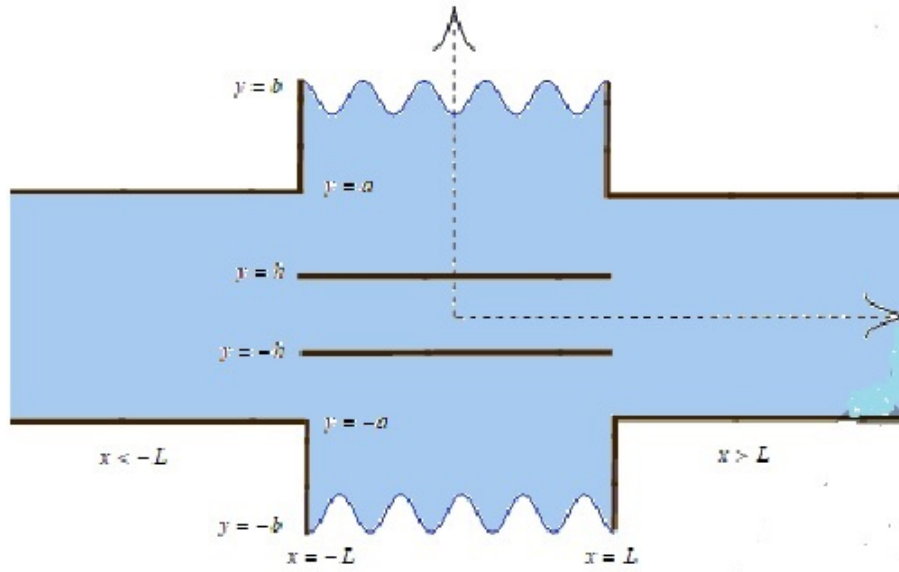


FIGURE 4.1: The geometry of physical problem.

Harmonic time dependence, $\exp(-i\omega\bar{t})$, where ω is the radian frequency, is assumed. Consider an incident wave of harmonic time dependence is propagating from negative x -direction towards the expansion chamber, wherein it is scattered into infinite number of reflected and transmitted modes. The boundary value problem is made dimensionless by taking scales and transformations defined in Chapter 2. Therefore dimensionless form of governing equation is Helmholtz equation [28]

$$(\nabla^2 + 1)\psi(x, y) = 0. \quad (4.1)$$

The propagation of waves and their characteristics subject to the bounding wall properties different duct regions are explained in the subsequent sub-sections 1-3.

4.1.1 Wave Propagation in the Inlet Duct

In the inlet duct, the fluid velocity potential, ψ_I satisfies the Helmholtz's equation (4.1) along with the boundary conditions

$$\frac{\partial \psi_I}{\partial y} = 0, \quad y = \pm a, \quad -\infty < x < -L. \quad (4.2)$$

On using the separation of variable technique, (4.1) and (4.2) yield the eigenfunction expansion form of field potential as

$$\psi_I(x, y) = e^{i(x+L)} + \sum_{n=0}^{\infty} A_n \cos[\beta_n(y+a)] e^{-i\sigma_n(x+L)}, \quad -a \leq y \leq a, \quad (4.3)$$

where, wave numbers $\sigma_n = \sqrt{1 - \beta_n^2}$; $n = 0, 1, 2, \dots$ can be defined in terms of the eigenvalues β_n wherein the eigenvalues satisfy the dispersion relation

$$\sin(2a\beta_n) = 0. \quad (4.4)$$

The admissible eigenfunctions $\cos[\beta_n(y+a)]$, satisfy the usual orthogonality relation (OR), that is

$$\int_{-a}^a \cos[\beta_m(y+a)] \cos[\beta_n(y+a)] dy = a\delta_{mn}\epsilon_m, \quad (4.5)$$

where, δ_{mn} is Kronecker delta and

$$\epsilon_m = \begin{cases} 2 & m = 0, \\ 1 & m \neq 0. \end{cases}$$

Note that in (4.3), the first term represents the incident wave while the second term denotes the reflected field.

4.1.2 Wave Propagation in the Expansion Chamber

The expansion chamber is distributed into three regions: lower region, central region and upper region which comprise respectively the velocity potentials ψ_1 , ψ_2 and ψ_3 . The lower and upper regions are bounded by elastic membranes and rigid walls, that are

$$\left(\frac{\partial^2}{\partial x^2} + \mu^2\right)\psi_{1y} - \alpha\psi_1 = 0, \quad y = -b, \quad |x| < L, \quad (4.6)$$

$$\left(\frac{\partial^2}{\partial x^2} + \mu^2\right)\psi_{3y} + \alpha\psi_3 = 0, \quad y = +b, \quad |x| < L \quad (4.7)$$

and

$$\frac{\partial\psi_1}{\partial y} = 0, \quad y = -h^-, \quad |x| < L, \quad (4.8)$$

$$\frac{\partial\psi_3}{\partial y} = 0, \quad y = h^+, \quad |x| < L, \quad (4.9)$$

respectively. However, the central region contains absorbing lining at $y = h^-$, $-h^+$, that are

$$\Gamma_1\psi_2 + \Gamma_2\frac{\partial\psi_2}{\partial y} = 0, \quad y = h^-, \quad |x| < L \quad (4.10)$$

and

$$\Gamma_1\psi_2 - \Gamma_2\frac{\partial\psi_2}{\partial y} = 0, \quad y = -h^+, \quad |x| < L. \quad (4.11)$$

Note that the parameters Γ_1 and Γ_2 are arbitrary chosen here to consider the boundary walls to be acoustically rigid, soft or absorbing lining. Their values are discussed in later section 5. In order to describe the behavior of membrane at semi-infinite edges two edge conditions are imposed. These conditions also ensure the uniqueness of the solution. At semi-infinite edges the selection of zero displacement conditions yield

$$\frac{\partial\psi_1}{\partial y} = 0, \quad x = \pm L, \quad y = -b, \quad (4.12)$$

$$\frac{\partial\psi_3}{\partial y} = 0, \quad x = \pm L, \quad y = +b. \quad (4.13)$$

Now the eigenfunction expansion forms of fluid potential in expansion chamber take the form

$$\psi_1(x, y) = \sum_{n=0}^{\infty} (B_n e^{-i\nu_n x} + C_n e^{i\nu_n x}) Y_{1n}(y), \quad -b \leq y \leq -h, \quad (4.14)$$

$$\psi_2(x, y) = \sum_{n=0}^{\infty} (D_n e^{-is_n x} + E_n e^{is_n x}) Y_{2n}(y), \quad -h \leq y \leq h, \quad (4.15)$$

$$\psi_3(x, y) = \sum_{n=0}^{\infty} (F_n e^{-i\nu_n x} + G_n e^{i\nu_n x}) Y_{3n}(y), \quad h \leq y \leq b, \quad (4.16)$$

where,

$Y_{1n} = \cosh[\gamma_n(y+h)]$, $Y_{2n}(y) = \Gamma_1 \sin[\tau_n(y+h)] + \tau_n \Gamma_2 \cos[\tau_n(y+h)]$ and $Y_{3n} = \cosh[\gamma_n(y-h)]$ represent the eigenfunctions in their respective regions. Note that wave numbers $\nu_n = \sqrt{1 + \gamma_n^2}$ and $s_n = \sqrt{1 - \tau_n^2}$; $n = 0, 1, 2, \dots$ can be defined in terms of the eigenvalues γ_n and τ_n wherein these eigenvalues respectively satisfy the dispersion relations

$$(\gamma_n^2 + 1 - \mu^2) \gamma_n \sinh[\gamma_n(b-h)] - \alpha \cosh[\gamma_n(b-h)] = 0 \quad (4.17)$$

and

$$2\Gamma_1 \Gamma_2 \tau_n \cos(2h\tau_n) + \Gamma_1^2 \sin(2h\tau_n) - \tau_n^2 \Gamma_2^2 \sin(2h\tau_n) = 0. \quad (4.18)$$

The admissible eigenfunctions Y_{jn} , $j = 1, 2, 3$ for $n = 0, 1, 2, \dots$ satisfy the OR

$$\begin{aligned} \alpha \int_{-b}^{-h} Y_{1n}(y) Y_{1m}(y) dy &= \alpha \int_h^b Y_{3n}(y) Y_{3m}(y) dy \\ &= M_m \delta_{mn} - Y'_{3n}(b) Y'_{3m}(b) \end{aligned} \quad (4.19)$$

and

$$\int_{-h}^h Y_{2n}(y) Y_{2m}(y) dy = J_m \delta_{mn}, \quad (4.20)$$

where,

$$M_m = \frac{(b-h)\alpha}{2} + \left\{ \gamma_m^2 + \frac{1 + \gamma_m^2 - \mu^2}{2} \right\} \sinh^2[\gamma_m(b-h)] \quad (4.21)$$

and

$$J_m = \frac{1}{2} \{ \Gamma_1 \Gamma_2 - \Gamma_1 \Gamma_2 \cos(4h\tau_m) + 2h(\Gamma_1^2 + \Gamma_2^2 \tau_m^2) \} + \frac{1}{\tau_m} \{ -\Gamma_1^2 + \Gamma_2^2 \tau_m^2 \sin(4h\tau_m) \}. \quad (4.22)$$

4.1.3 Wave Propagation in the Outlet Duct

In the outlet duct, the fluid velocity potential, ψ_O satisfies (4.1) along with the boundary conditions

$$\frac{\partial \psi_O}{\partial y} = 0, \quad y = \pm a, \quad L < x < \infty. \quad (4.23)$$

The eigenfunction expansion form of fluid potential in this region is given by

$$\psi_O(x, y) = \sum_{n=0}^{\infty} H_n \cos[\beta_n(y + a)] e^{i\sigma_n(x-L)}. \quad (4.24)$$

Note that (A_n, B_n, D_n, F_n) and (C_n, G_n, E_n, H_n) , are the amplitudes of the n^{th} reflected and transmitted modes in the waveguide regions and are unknowns. These unknowns are found through the matching of pressure and normal velocities modes at interface $x = \pm L$.

4.2 Mode-Matching (MM) Solution

Here we match the pressures and the normal velocities modes of expansion chamber with inlet/outlet duct regions modes at interfaces $x = \pm L$. The normal velocities conditions across lower region of expansion chamber and inlet/outlet duct regions at interfaces are defined by

$$\int_{-b}^{-h} \psi_{1x}(-L, y) dy = \int_{-a}^{-h} \psi_{Ix}(-L, y) dy \quad (4.25)$$

and

$$\int_{-b}^{-h} \psi_{1x}(L, y) dy = \int_{-a}^{-h} \psi_{Ox}(L, y) dy. \quad (4.26)$$

On substituting (4.3), (4.14) and (4.24) into (4.25)-(4.26) and then by using OR (4.19) and after some rearrangement we get:

$$B_m e^{i\nu_m L} - C_m e^{-i\nu_m L} = \frac{Y'_{1m}(-b)}{\nu_m M_m} e_1 - \frac{\alpha}{\nu_m M_m} \left[Q_{m0} - \sum_{n=0}^{\infty} A_n \sigma_n Q_{mn} \right] \quad (4.27)$$

and

$$B_m e^{-i\nu_m L} - C_m e^{i\nu_m L} = \frac{Y'_{1m}(-b)}{\nu_m M_m} e_2 - \frac{\alpha}{\nu_m M_m} \sum_{n=0}^{\infty} H_n \sigma_n Q_{mn}, \quad (4.28)$$

where,

$$Q_{mn} = \int_{-a}^{-h} \cos[\beta_m(y+a)] Y_{1n}(y) dy. \quad (4.29)$$

The quantities $e_1 = -i\psi_{1xy}(-L, -b)$ and $e_2 = -i\psi_{1xy}(L, -b)$ are constants which will be found from the edge condition (4.12).

Now the addition and subtraction of (4.27) and (4.28) yield

$$\zeta_m^+ = \frac{1}{2i \sin(\nu_m L) \nu_m M_m} \left[Y'_{1m}(-b) U^- - \alpha Q_{m0} + \alpha \sum_{n=0}^{\infty} \chi_n^+ \sigma_n Q_{mn} \right] \quad (4.30)$$

and

$$\zeta_m^- = \frac{1}{2 \cos(\nu_m L) \nu_m M_m} \left[Y'_{1m}(-b) U^+ - \alpha Q_{m0} + \alpha \sum_{n=0}^{\infty} \chi_n^- \sigma_n Q_{mn} \right], \quad (4.31)$$

where, $\chi_m^\pm = (A_m \pm H_m)$, $\zeta_m^\pm = (B_m \pm C_m)$, and $U^\pm = (e_1 \pm e_2)$.

By multiplying $2 \sum_{m=0}^{\infty} Y'_{1m}(-b) \cos(\nu_m L)$ with (4.30) and $2i \sum_{m=0}^{\infty} Y'_{1m}(-b) \sin(\nu_m L)$ with (4.31) respectively, we get constants U^\pm and then by using the edge condition (4.12), which result after rearrangements:

$$U^- = \frac{\alpha}{S_1} \sum_{m=0}^{\infty} \frac{Y'_{1m}(-b) \cot(\nu_m L)}{\nu_m M_m} \left[\sum_{m=0}^{\infty} Q_{m0} - \sum_{n=0}^{\infty} \chi_n^+ \sigma_n Q_{mn} \right], \quad (4.32)$$

$$U^+ = \frac{\alpha}{S_2} \sum_{m=0}^{\infty} \frac{Y'_{1m}(-b) \tan(\nu_m L)}{\nu_m M_m} \left[\sum_{m=0}^{\infty} Q_{m0} - \sum_{n=0}^{\infty} \chi_n^- \sigma_n Q_{mn} \right], \quad (4.33)$$

where,

$$S_1 = \sum_{m=0}^{\infty} \frac{[Y'_{1m}(-b)]^2 \cot(\nu_m L)}{\nu_m M_m}, \quad (4.34)$$

$$S_2 = \sum_{m=0}^{\infty} \frac{[Y'_{1m}(-b)]^2 \tan(\nu_m L)}{\nu_m M_m}. \quad (4.35)$$

The normal velocities conditions across central region of expansion chamber and inlet/outlet duct regions at interfaces are defined by:

$$\int_{-h}^h \psi_{2x}(-L, y) dy = \int_{-h}^h \psi_{Ix}(-L, y) dy, \quad (4.36)$$

$$\int_{-h}^h \psi_{2x}(L, y) dy = \int_{-h}^h \psi_{Ox}(L, y) dy. \quad (4.37)$$

On substituting (4.3), (4.15) and (4.24) into (4.36)-(4.37) and then by using the OR (4.20), it is found that

$$D_m e^{is_m L} - E_m e^{-is_m L} = -\frac{1}{s_m J_m} \left[R_{m0} - \sum_{n=0}^{\infty} A_n \sigma_n R_{mn} \right] \quad (4.38)$$

and

$$D_m e^{-is_m L} - E_m e^{is_m L} = -\frac{1}{s_m J_m} \left[\sum_{n=0}^{\infty} H_n \sigma_n R_{mn} \right], \quad (4.39)$$

where,

$$R_{mn} = \int_{-a}^{-h} \cos[\beta_m(y+a)] Y_{2n}(y) dy. \quad (4.40)$$

Now the addition and subtraction of (4.38) and (4.39) yield:

$$\varrho_m^+ = \frac{1}{2i \sin(s_m L) s_m J_m} \left[-R_{m0} + \sum_{n=0}^{\infty} \chi_n^+ \sigma_n R_{mn} \right] \quad (4.41)$$

and

$$\varrho_m^- = \frac{1}{2 \cos(s_m L) s_m J_m} \left[-R_{m0} + \sum_{n=0}^{\infty} \chi_n^- \sigma_n R_{mn} \right], \quad (4.42)$$

where $\varrho_m^{\pm} = (D_m \pm E_m)$.

Now the normal velocities conditions across upper region of expansion chamber and inlet/outlet duct regions at interfaces are defined by:

$$\int_h^b \psi_{3x}(-L, y) dy = \int_h^a \psi_{Ix}(-L, y) dy \quad (4.43)$$

and

$$\int_h^b \psi_{3x}(L, y) dy = \int_h^a \psi_{Ox}(L, y) dy. \quad (4.44)$$

On substituting (4.3), (4.16) and (4.24) into (4.43)-(4.44) and then by using the OR (4.19), it is found that:

$$F_m e^{i\nu_m L} - G_m e^{-i\nu_m L} = \frac{Y'_{3m}(b)}{\nu_m M_m} e_3 - \frac{\alpha}{\nu_m M_m} \left[P_{m0} - \sum_{n=0}^{\infty} A_n \sigma_n P_{mn} \right] \quad (4.45)$$

and

$$F_m e^{-i\nu_m L} - G_m e^{i\nu_m L} = \frac{Y'_{3m}(b)}{\nu_m M_m} e_4 - \frac{\alpha}{\nu_m M_m} \sum_{n=0}^{\infty} H_n \sigma_n P_{mn}, \quad (4.46)$$

where,

$$P_{mn} = \int_h^a \cos[\beta_m(y+a)] Y_{3n}(y) dy. \quad (4.47)$$

The quantities $e_3 = -i\psi_{3xy}(-L, b)$ and $e_4 = -i\psi_{3xy}(L, b)$ are constants which are found by using the edge condition (4.13).

Now the addition and subtraction of (4.46) and (4.47) yield:

$$\Theta_m^+ = \frac{1}{2i \sin(\nu_m L) \nu_m M_m} \left[Y'_{3m}(b) V^- - \alpha P_{m0} + \alpha \sum_{n=0}^{\infty} \chi_n^+ \sigma_n P_{mn} \right] \quad (4.48)$$

and

$$\Theta_m^- = \frac{1}{2 \cos(\nu_m L) \nu_m M_m} \left[Y'_{3m}(b) V^+ - \alpha P_{m0} + \alpha \sum_{n=0}^{\infty} \chi_n^- \sigma_n P_{mn} \right], \quad (4.49)$$

where, $\Theta_m^\pm = (F_m \pm G_m)$ and $V^\pm = (e_3 \pm e_4)$.

The constants V^\pm are determined by multiplying $2 \sum_{m=0}^{\infty} Y'_{3m}(b) \cos(\nu_m L)$ with (4.48) and (4.49) with $2i \sum_{m=0}^{\infty} Y'_{3m}(b) \sin(\nu_m L)$ respectively, and then by using

the edge condition (4.13), which result after rearrangements:

$$V^- = \frac{\alpha}{S_3} \sum_{m=0}^{\infty} \frac{Y'_{3m}(b) \cot(\nu_m L)}{\nu_m M_m} \left[\sum_{m=0}^{\infty} P_{m0} - \sum_{n=0}^{\infty} \chi_n^+ \sigma_n P_{mn} \right], \quad (4.50)$$

$$V^+ = \frac{\alpha}{S_4} \sum_{m=0}^{\infty} \frac{Y'_{3m}(b) \tan(\nu_m L)}{\nu_m M_m} \left[\sum_{m=0}^{\infty} P_{m0} - \sum_{n=0}^{\infty} \chi_n^- \sigma_n P_{mn} \right], \quad (4.51)$$

where,

$$S_3 = \sum_{m=0}^{\infty} \frac{[Y'_{3m}(b)]^2 \cot(\nu_m L)}{\nu_m M_m}, \quad (4.52)$$

$$S_4 = \sum_{m=0}^{\infty} \frac{[Y'_{3m}(b)]^2 \tan(\nu_m L)}{\nu_m M_m}. \quad (4.53)$$

Now finally, the pressures conditions at interfaces are defined by:

$$\int_{-a}^a \psi_I(-L, y) dy = \int_{-a}^{-h} \psi_1(-L, y) dy + \int_{-h}^h \psi_2(-L, y) dy + \int_h^a \psi_3(-L, y) dy \quad (4.54)$$

and

$$\int_{-a}^a \psi_O(L, y) dy = \int_{-a}^{-h} \psi_1(L, y) dy + \int_{-h}^h \psi_2(L, y) dy + \int_h^a \psi_3(L, y) dy. \quad (4.55)$$

On substituting (4.3), (4.14)- (4.16) and (4.24) into (4.54)-(4.55) and using the OR (4.5), it is found that

$$\begin{aligned} A_m = & -\delta_{m0} + \frac{1}{a\epsilon_m} \sum_{n=0}^{\infty} \{ (B_n e^{i\nu_n L} + C_n e^{-i\nu_n L}) Q_{nm} + (D_n e^{is_n L} + E_n e^{-is_n L}) R_{nm} \\ & + (F_n e^{i\nu_n L} + G_n e^{-i\nu_n L}) P_{nm} \} \end{aligned} \quad (4.56)$$

and

$$\begin{aligned} H_m = & \frac{1}{a\epsilon_m} \sum_{n=0}^{\infty} \{ (B_n e^{-i\nu_n L} + C_n e^{i\nu_n L}) Q_{nm} + (D_n e^{-is_n L} + E_n e^{is_n L}) R_{nm} \\ & + (F_n e^{-i\nu_n L} + G_n e^{i\nu_n L}) P_{nm} \}. \end{aligned} \quad (4.57)$$

The addition and subtraction of (4.56) and (4.57) yields:

$$\chi_m^+ = -\delta_{m0} + \frac{2}{a\epsilon_m} \sum_{n=0}^{\infty} \{\zeta_n^+ \cos(\nu_n L) Q_{nm} + \varrho_n^+ \cos(s_n L) R_{nm} + \Theta_n^+ \cos(\nu_n L) P_{nm}\} \quad (4.58)$$

and

$$\chi_m^- = -\delta_{m0} + \frac{2i}{a\epsilon_m} \sum_{n=0}^{\infty} \{\zeta_n^- \sin(\nu_n L) Q_{nm} + \varrho_n^- \sin(s_n L) R_{nm} + \Theta_n^- \sin(\nu_n L) P_{nm}\}. \quad (4.59)$$

In this way the equations (4.58)-(4.59) together with (4.30)-(4.31), (4.41)-(4.42) and (4.48)-(4.49) yield a system of coupled equations in which ζ_n^\pm , ϱ_n^\pm and Θ_n^\pm are unknowns and are truncated upto $n = m = 0, 1, 2, \dots, N$ terms.

4.3 A Low Frequency Approximation (LFA)

A LFA solution is thus developed to compare the results obtained via MM scheme. This approximation relies on the limited number of modes allowed to propagate, in the various duct region, which are subjected to the imposed conditions. Therefore, the velocity potentials in different duct regions are approximated according to the propagating modes as follows:

$$\psi_I(x, y) \approx e^{i(x+L)} + \sum_{n=0}^{\Pi_1} A_n \cos[\beta_n(y+a)] e^{-i\sigma_n(x+L)}, \quad (4.60)$$

$$\psi_1(x, y) \approx \sum_{n=0}^{\Pi_2} (B_n e^{-i\nu_n x} + C_n e^{i\nu_n x}) Y_{1n}(y), \quad (4.61)$$

$$\psi_2(x, y) \approx (D_0 e^{-is_0 x} + E_0 e^{is_0 x}) Y_{20}(y), \quad (4.62)$$

$$\psi_3(x, y) \approx \sum_{n=0}^{\Pi_2} (F_n e^{-i\nu_n x} + G_n e^{i\nu_n x}) Y_{3n}(y), \quad (4.63)$$

$$\psi_O(x, y) \approx \sum_{n=0}^{\Pi_1} H_n \cos[\beta_n(y+a)] e^{i\sigma_n(x-L)}, \quad (4.64)$$

where Π_1 and Π_2 stand for the number of propagating modes in the inlet/outlet duct and the upper/lower region of expansion chamber. Here the modal coefficients (A_n, H_n) , $n = 0, 1, \dots, \Pi_1$, (D_0, E_0) , and (B_n, C_n, F_n, G_n) , $n = 0, 1, \dots, \Pi_2$ are unknowns, and to determine these coefficients, the continuity conditions of velocity flux across the expansion chamber at interfaces can be expressed as:

$$\int_{-a}^{-h} \{\psi_{1x}(-L, y) - \psi_{Ix}(-L, y)\} dy = 0, \quad \int_{-a}^{-h} \{\psi_{1x}(L, y) - \psi_{Ox}(L, y)\} dy = 0, \quad (4.65)$$

$$\int_{-h}^h \{\psi_{2x}(-L, y) - \psi_{Ix}(-L, y)\} dy = 0, \quad \int_{-h}^h \{\psi_{2x}(L, y) - \psi_{Ox}(L, y)\} dy = 0, \quad (4.66)$$

$$\int_h^a \{\psi_{3x}(-L, y) - \psi_{Ix}(-L, y)\} dy = 0, \quad \int_h^a \{\psi_{3x}(L, y) - \psi_{Ox}(L, y)\} dy = 0. \quad (4.67)$$

Likewise, the average pressures across the regions at interfaces, $x \pm L$, can be given by:

$$\int_{-a}^{-h} \{\psi_1(-L, y) - \psi_I(-L, y)\} dy = 0, \quad \int_{-a}^{-h} \{\psi_1(L, y) - \psi_O(L, y)\} dy = 0, \quad (4.68)$$

$$\int_{-h}^h \{\psi_2(-L, y) - \psi_I(-L, y)\} dy = 0, \quad \int_{-h}^h \{\psi_2(L, y) - \psi_O(L, y)\} dy = 0, \quad (4.69)$$

$$\int_h^a \{\psi_3(-L, y) - \psi_I(-L, y)\} dy = 0, \quad \int_h^a \{\psi_3(L, y) - \psi_O(L, y)\} dy = 0. \quad (4.70)$$

On substituting (4.60)-(4.64) into (4.65)-(4.70), then after some rearrangements, we get following two systems of equations:

$$2i \sum_{n=0}^{\Pi_2} \zeta_n^+ \sin(\nu_n l) \nu_n K_n - \sum_{n=0}^{\Pi_1} \sigma_n \chi_n^+ P_n = -P_0, \quad (4.71)$$

$$2i \sum_{n=0}^{\Pi_2} \Theta_n^+ \sin(\nu_n l) \nu_n K_n - \sum_{n=0}^{\Pi_1} (-1)^n \sigma_n \chi_n^+ P_n = -P_0, \quad (4.72)$$

$$2i \varrho_0^+ \sin(s_0 l) s_0 N_0 + \sum_{n=0}^{\Pi_1} \sigma_n \chi_n^+ X_n = X_0, \quad (4.73)$$

$$2 \sum_{n=0}^{\Pi_2} \zeta_n^+ \cos(\nu_n l) K_n - \sum_{n=0}^{\Pi_1} \chi_n^+ P_n = P_0, \quad (4.74)$$

$$2 \sum_{n=0}^{\Pi_2} \Theta_n^+ \cos(\nu_n l) K_n - \sum_{n=0}^{\Pi_1} (-1)^n \chi_n^+ P_n = P_0, \quad (4.75)$$

$$2\varrho_0^+ \cos(s_0 l) N_0 + \sum_{n=0}^{\Pi_1} \chi_n^+ X_n = -X_0 \quad (4.76)$$

and

$$2 \sum_{n=0}^{\Pi_2} \zeta_n^- \cos(\nu_n l) \nu_n K_n - \sum_{n=0}^{\Pi_1} \sigma_n \chi_n^- P_n = -P_0, \quad (4.77)$$

$$2 \sum_{n=0}^{\Pi_2} \Theta_n^- \cos(\nu_n l) \nu_n K_n - \sum_{n=0}^{\Pi_1} (-1)^n \sigma_n \chi_n^- P_n = -P_0, \quad (4.78)$$

$$2\varrho_0^- \cos(s_0 l) s_0 N_0 + \sum_{n=0}^{\Pi_1} \sigma_n \chi_n^- X_n = X_0, \quad (4.79)$$

$$2i \sum_{n=0}^{\Pi_2} \zeta_n^- \sin(\nu_n l) K_n - \sum_{n=0}^{\Pi_1} \chi_n^- P_n = P_0, \quad (4.80)$$

$$2i \sum_{n=0}^{\Pi_2} \Theta_n^- \sin(\nu_n l) K_n - \sum_{n=0}^{\Pi_1} (-1)^n \chi_n^- P_n = P_0, \quad (4.81)$$

$$2i\varrho_0^- \sin(s_0 l) N_0 + \sum_{n=0}^{\Pi_1} \chi_n^- X_n = -X_0, \quad (4.82)$$

where, $K_n = \sinh[\gamma_n(a-h)]/\gamma_n$, $N_0 = 2\Gamma_1 \sin^2(h\tau_0)/\tau_0 + \Gamma_2 \sin(2h\tau_0)$, $P_0 = a-h$, $P_1 = 2a \cos(\frac{h\pi}{2a})/\pi$, $P_2 = a \sin(\frac{h\pi}{a})/\pi$, $X_0 = -2h$, $X_1 = 0$ and $X_2 = 2P_2$. Note that the above found systems do not preserve any information about the edge conditions which have been imposed on membrane edges (4.12)-(4.13). To encounter these, we use (4.60)-(4.64) into (4.12)-(4.13), which after simplification lead to

$$\sum_{n=0}^{\Pi_2} \zeta_n^+ \cos(\nu_n l) Z_n = 0, \quad \sum_{n=0}^{\Pi_2} \Theta_n^+ \cos(\nu_n l) Z_n = 0 \quad (4.83)$$

and

$$\sum_{n=0}^{\Pi_2} \zeta_n^- \sin(\nu_n l) Z_n = 0, \quad \sum_{n=0}^{\Pi_2} \Theta_n^- \sin(\nu_n l) Z_n = 0, \quad (4.84)$$

where, $Z_n = \beta_n \sinh[\beta_n(b-h)]$. Now clearly, the systems of equations defined by (4.71)-(4.82) together with (4.83)-(4.84) are solved simultaneously for the planar geometrical configuration of the expansion chamber. However, for the geometrically discontinuous configuration as shown in Figure 1, the extra modes in discontinuities involving regions are allowed to cater the information along vertical step discontinuities. In rigid vertical step discontinuities, the velocity flux across the interfaces must be zero, that are:

$$\int_{-b}^{-a} \psi_{1x}(\pm L, y) dy = 0, \quad \int_a^b \psi_{3x}(\pm L, y) dy = 0. \quad (4.85)$$

On substituting(4.60)-(4.64) into (4.85) and then rearranging, we found:

$$\sum_{n=0}^{\Pi_2} \zeta_n^+ \sin(\nu_n l) W_n = 0, \quad \sum_{n=0}^{\Pi_2} \Theta_n^+ \sin(\nu_n l) W_n = 0 \quad (4.86)$$

and

$$\sum_{n=0}^{\Pi_2} \zeta_n^- \cos(\nu_n l) W_n = 0, \quad \sum_{n=0}^{\Pi_2} \Theta_n^- \cos(\nu_n l) W_n = 0, \quad (4.87)$$

where, $W_n = i\nu_n \{\sinh[\gamma_n(h-a)] - \sinh[\gamma_n(h-b)]\} / \gamma_n$. Thus, for the geometrical discontinuities involving expansion chamber, the systems of equations (4.71)-(4.84) and (4.86)-(4.87) are solved simultaneously to get the unknown scattering amplitudes. Note that we set $\Pi_1 = \Pi_2 = 2$ in discontinuous case $b > a$, while $\Pi_1 = 2$ and $\Pi_2 = 1$ for the planar case $b = a$.

4.4 Numerical Results and Discussion

In this section, the numerical results obtained via MM scheme and LFA are discussed. Note that in MM case, first we truncate the systems of infinite equations

defined by (4.58)-(4.59) together with (4.30)-(4.31), (4.41)-(4.42) and (4.48)-(4.49) up to N terms and then solve the retained systems through inversion. The truncated solution is used to discuss the scattering of energies and TL verses frequency. The expressions for the reflected and transmitted energy flux in inlet and outlet regions are respectively found to be [28]

$$\mathcal{E}_1 = \frac{1}{2} Re \left\{ \sum_{n=0}^{\infty} |A_n|^2 \eta_n \epsilon_n \right\} \quad (4.88)$$

and

$$\mathcal{E}_2 = \frac{1}{2} Re \left\{ \sum_{n=0}^{\infty} |H_n|^2 \eta_n \epsilon_n \right\}, \quad (4.89)$$

where, the incident power is being scaled at unity. Clearly if unit power is fed into the system it will be equal to the sum of the reflected and transmitted powers, that is:

$$\mathcal{E}_1 + \mathcal{E}_2 = 1, \quad (4.90)$$

which is the conserved power identity. Note that this identity holds if there is no dissipation of energy in the waveguide. But however, if the chamber contains absorbing material such as porous lining, then some power is absorbed i.e., $\mathcal{E}_{abs} = 1 - (\mathcal{E}_1 + \mathcal{E}_2)$. Accordingly, the expansion chamber of the modeled problem comprises partitioning which contains: two side regions that are bounded by isotropic membranes and a central region whose bounding properties can be taken as; absorbent lining, rigid or soft, by fixing the values of parameters Γ_1 and Γ_2 . For instance, to consider the absorbing lining we may set $\Gamma_1 = 1$ and $\Gamma_2 = i\varsigma$; for rigid $\Gamma_1 = 0$ and $\Gamma_2 = 1$ and for soft $\Gamma_1 = 1$ and $\Gamma_2 = 0$ [65]. Note that quantity $\varsigma = \xi + i\eta$ denotes the specific impedance and for the of absorbing lining its following values are representative [49]:

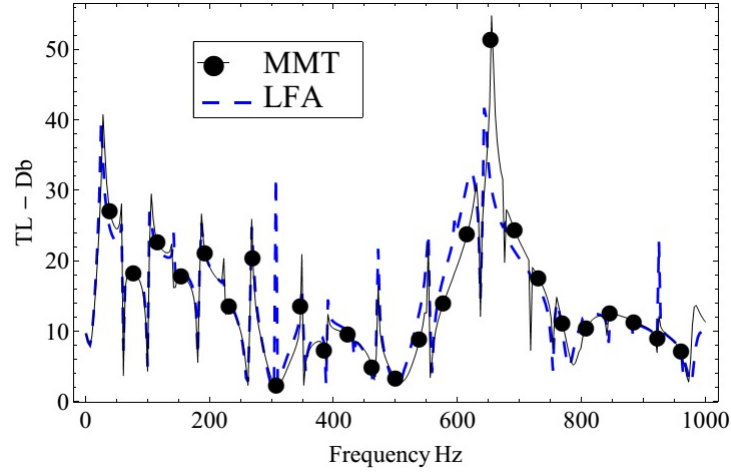
$$\text{fibrous sheet: } \quad \xi = 0.5, \quad -1.0 < \eta < 3.0,$$

$$\text{perforated sheet: } \quad 0 < \xi < 3, \quad -1.0 < \eta < 3.0.$$

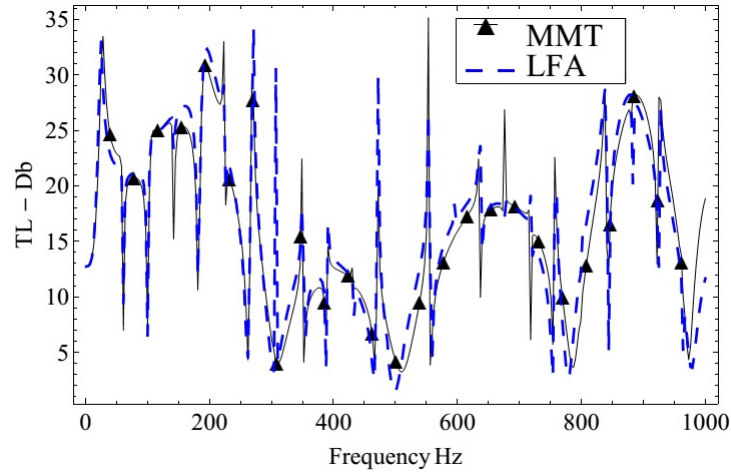
The results with each type of the bounding characteristics of the central region are discussed. The graphical results are shown in term of TL, which is a usual

measure of performance of dissipative silencer, given by [13]:

$$TL = -10 \log_{10} (\mathcal{E}_2 / \mathcal{E}_i). \quad (4.91)$$



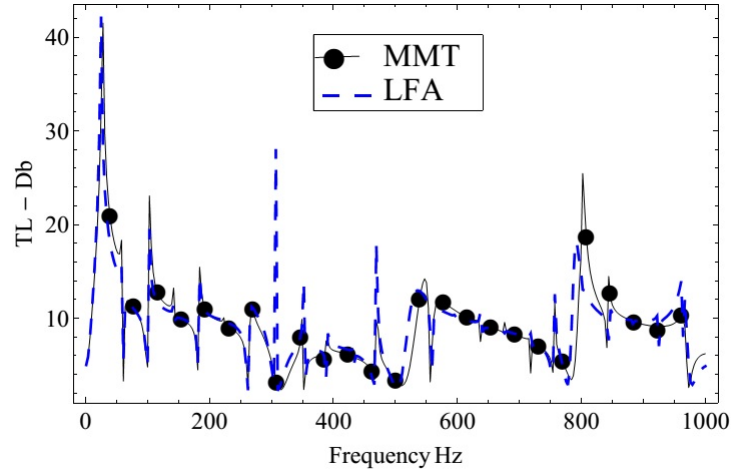
(a)



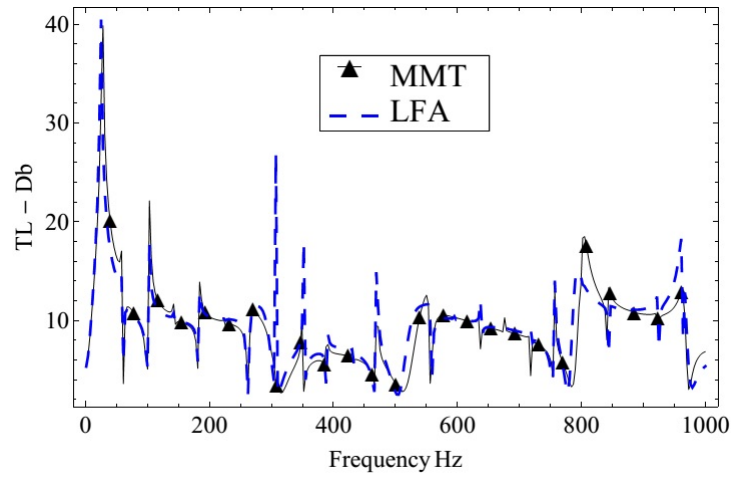
(b)

FIGURE 4.2: Transmission loss against frequency with fibrous sheet along with vertical step-discontinuities for: a) $\eta = -0.5$, b) $\eta = 0$, where, $\bar{a} = 0.15\text{m}$, $\bar{b} = 0.3\text{m}$, $\bar{L} = 0.25\text{m}$ and $N = 20$ terms.

Figures 4.2 and 4.3 show the TL against frequency for the silencer including structural discontinuities. In Figure 4.2 the central region of the expansion chamber contains fibrous sheet, which refers $\xi = 0.5$, and have chosen $\eta = 0.5$ and $\eta = 0$ to get the plots of Figure 4.2(a) and 4.2(b), respectively.



(a)



(b)

FIGURE 4.3: Transmission loss against frequency with perforated sheet along with vertical step-discontinuities for: a) $\eta = -0.5$, b) $\eta = 0$, where, $\bar{a} = 0.15\text{m}$, $\bar{b} = 0.3\text{m}$, $\bar{L} = 0.25\text{m}$ and $N = 20$ terms.

Accordingly, the Figure 4.3 is found by replacing the fibrous sheet of the central region with perforated sheet by setting $\xi = 2$, whereas, the other parameters remain same as used for Figure 4.2. Note that in structural-discontinuities involving expansion chamber ($\bar{b} > \bar{a}$), the TL of 36 dB decreases with fluctuations by increasing frequency in the range of first cut-on mode of each duct region except the central region. This behavior is evident for both fibrous and perforated setting of central region, see Figure 4.2 and 4.3 ($1\text{Hz} < f < 247\text{Hz}$). However, as the

secondary mode of membrane bounded regions (side regions of expansion chamber) becomes cut-on the energy is transmitted via compressional waves and thus a lesser amount of TL in this regime is observed ($247Hz < f < 571Hz$). But at $f = 572Hz$, the next inlet/outlet duct mode start propagating and the TL increases in domain wherein two modes of each element except central region contribute to propagate energy ($572Hz < f < 946Hz$). Even though, at frequency $947Hz$ the third mode of membrane bounded regions start propagating but the central region remained evanescent in the whole given regime due to the presence of porous lining.

TABLE 4.1: Propagating modes in discontinuous waveguide.

Cut-on f (Hz)	Inlet/Outlet	Expansion Chamber		
		Side Regions	Central Region	
			Rigid	Soft
248	1	2	1	1
573	2	2	1	1
859	2	2	2	2
947	2	3	2	2
1146	3	3	2	2
1718	4	3	3	3
1766	4	4	3	3
2290	5	4	3	3
2577	5	4	4	4
2610	5	5	4	4
2863	6	5	4	4
3435	7	5	5	5
3460	7	6	5	5

The list of cut-on modes of each duct region against frequency for discontinuous and planar settings of expansion chamber and by changing the bounding properties of the central region are shown in Tables 4.1 and 4.2. Furthermore, more TL for the

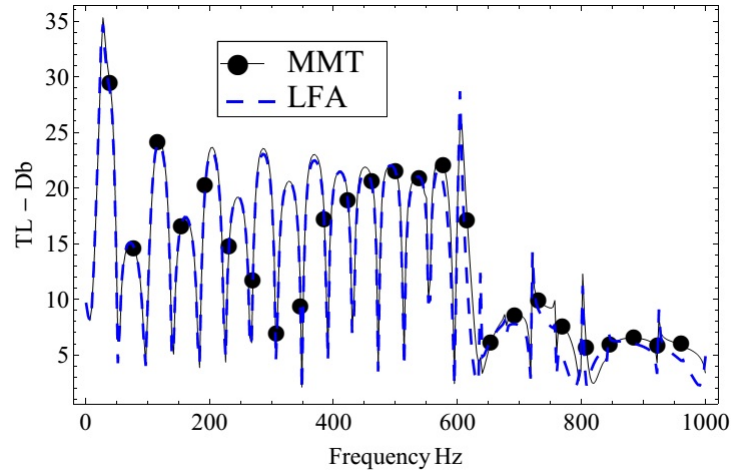
fibrous lining case than perforated sheet is observed. Note that a good agreement between MM scheme and LFA curves is seen, however, there appear some spikes of variation in LFA at some frequencies. These dissimilarities are caused by occurrence of the the interchange of imaginary eigenvalues to real or complex number and vice versa.

TABLE 4.2: Propagating modes in planar waveguide.

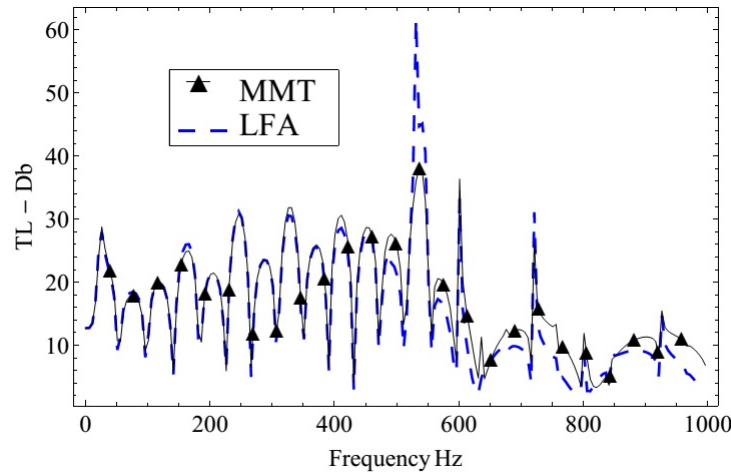
Cut-on f (Hz)	Inlet/Outlet	Expansion Chamber		
		Side Regions	Central Region	
			Rigid	Soft
562	1	2	1	1
573	2	2	1	1
859	2	2	2	2
1146	3	2	2	2
1718	4	2	3	3
2290	5	2	3	3
2577	5	2	4	4
2863	6	2	4	4
3435	7	2	5	5
3533	7	3	5	5

In Figures 4.4 and 4.5 the TL against frequency for planar expansion chamber ($\bar{b} = \bar{a}$) is depicted. Clearly, more fluctuations in TL curves than vertical step-discontinuities involving expansion chamber case are observed. These fluctuations are due to trigonometric terms present in equations (4.58)-(4.59), and whose effect is comparatively greater in planar case than discontinuous case. A good agreement between MM scheme and LFA solutions in low frequency range is seen. Nevertheless, the maximum two modes of each component except central lined component finch energy dissemination in the given regime. Clearly, when $1Hz < f < 561Hz$ there exists one-one cut-on mode of each duct region except the central region, however, in regime $561Hz < f < 571Hz$ two modes of membrane bounded region

and one mode of inlet/outlet region contribute in energy propagation. The list of cut-on modes in planar case given Table 4.2. Also it is important note that by changing the value of porosity parameter η , the TL is altered significantly for planar as well as discontinuity involving expansion chamber.



(a)

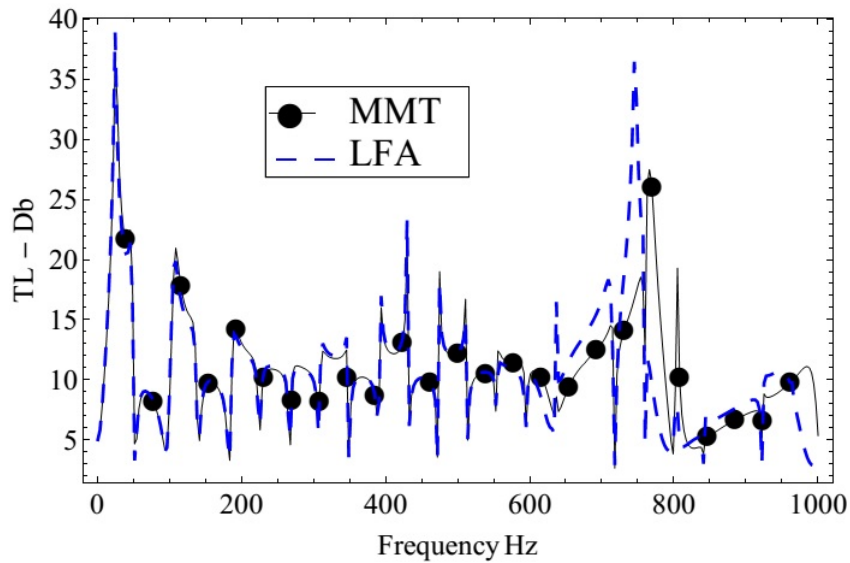


(b)

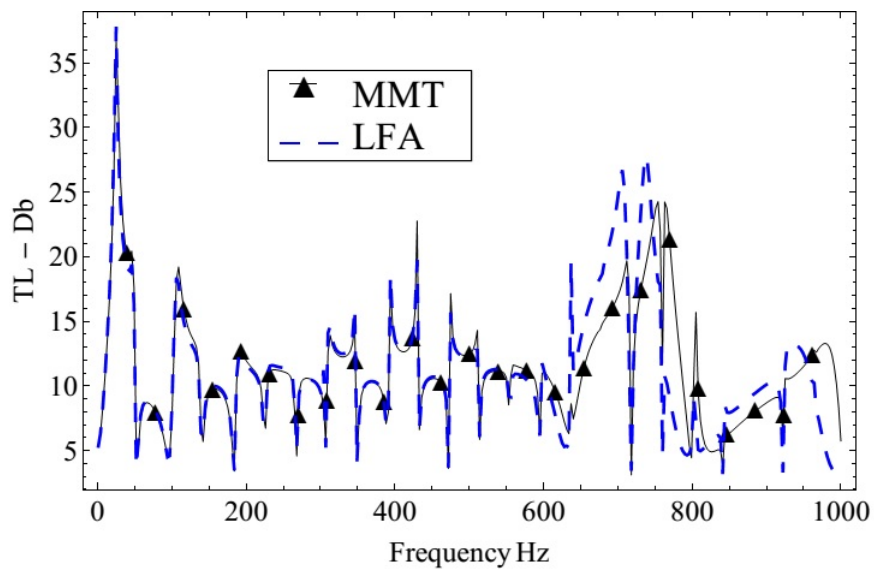
FIGURE 4.4: Transmission loss against frequency with fibrous sheet and planar expansion chamber for: a) $\eta = -0.5$, b) $\eta = 0$, where, $\bar{a} = \bar{b} = 0.15\text{m}$, $\bar{L} = 0.25\text{m}$ and $N = 20$ terms.

The graphs in Figures 4.6 and 4.7 are plotted for vertical step-discontinuities containing expansion chamber ($\bar{b} > \bar{a}$), whereas, the central region of the expansion chamber is assumed to be bounded by rigid or soft type wall conditions. Note that

for the rigid case, the device is tuned only for the low frequency range of noise $< 200Hz$.



(a)

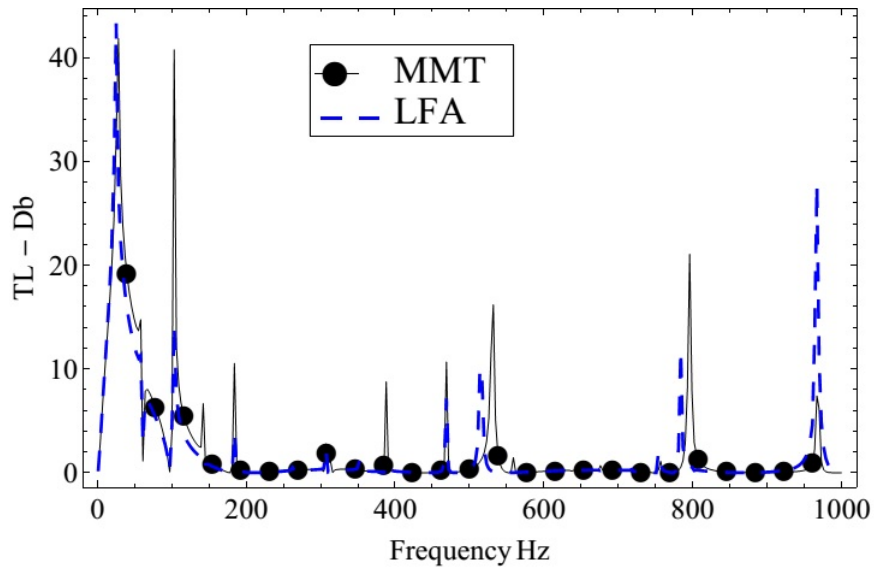


(b)

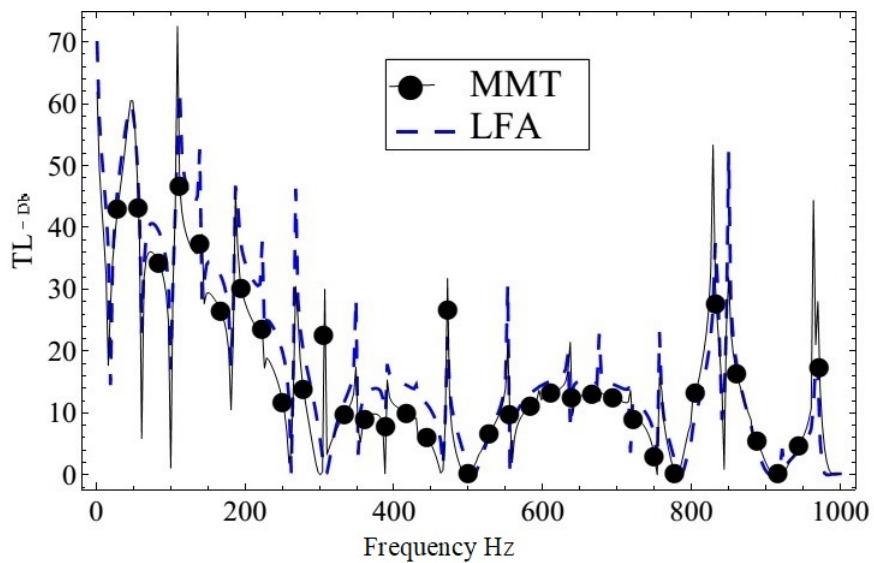
FIGURE 4.5: Transmission loss against frequency with perforated sheet and planar expansion chamber for: a) $\eta = -0.5$, b) $\eta = 0$, where, $\bar{a} = \bar{b} = 0.15m$, $\bar{L} = 0.25m$ and $N = 20$ terms.

On the other hand, the attenuation region is distributed over frequency for the acoustically soft setting of central region (see Figure 4.6). Clearly, the overall TL against frequency in soft case is much higher than rigid case. However, the

variation of tension T significantly affect the TL. It not only varies the TL but also changes the distribution of optimal TL over frequency (see Figure 4.7).



(a)

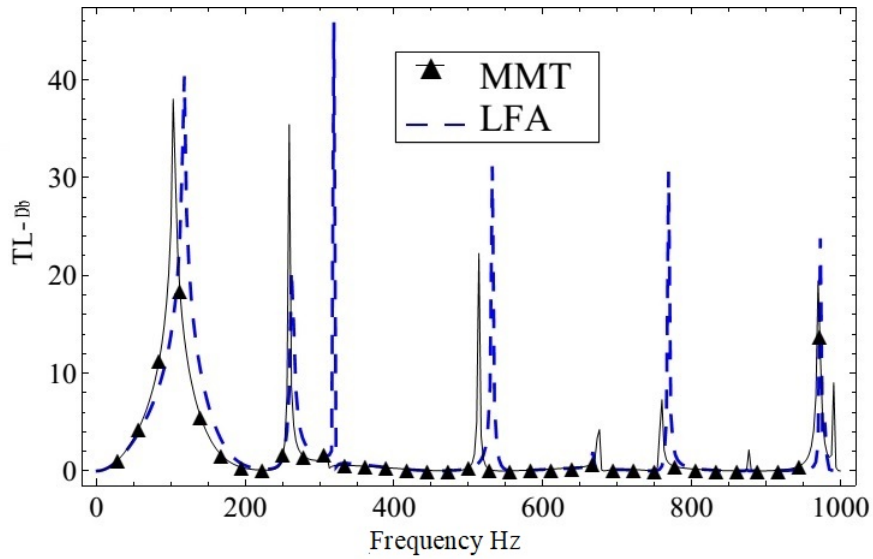


(b)

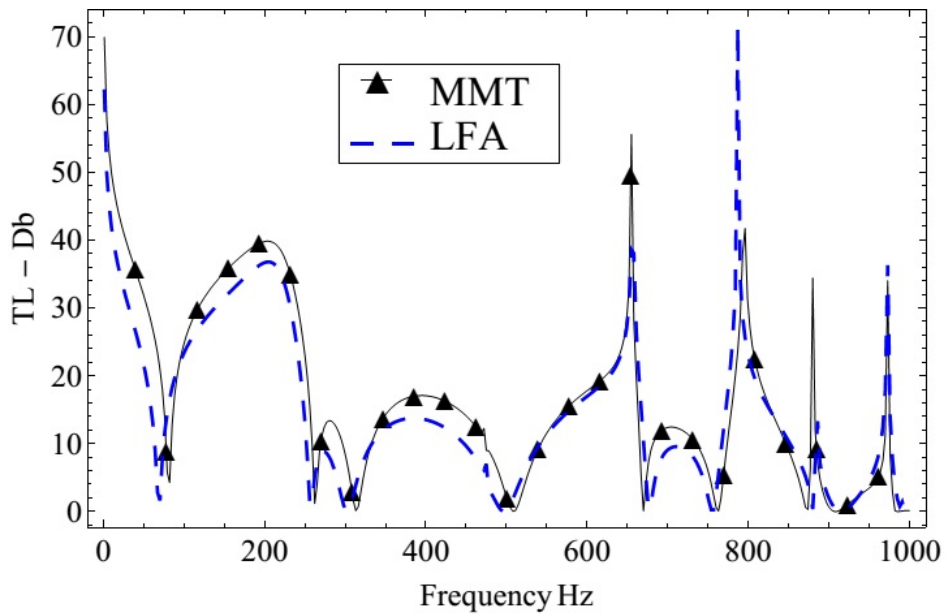
FIGURE 4.6: Transmission loss against frequency with vertical step-discontinuities involving expansion chamber while the central region comprises; a) rigid walls, b) soft walls, where, $\bar{a} = 0.15\text{m}$, $\bar{b} = 0.3\text{m}$, $\bar{L} = 0.25\text{m}$, $T=350\text{N}$ and $N = 20$ terms.

The TL against frequency for planar expansion chamber case including the rigid or soft type bounding characteristics of central region is shown in Figures 4.8 and 4.9.

Note that the pattern of TL curves for this case are similar to the discontinuous case but the magnitude of TL is less than that of the previous case.



(a)

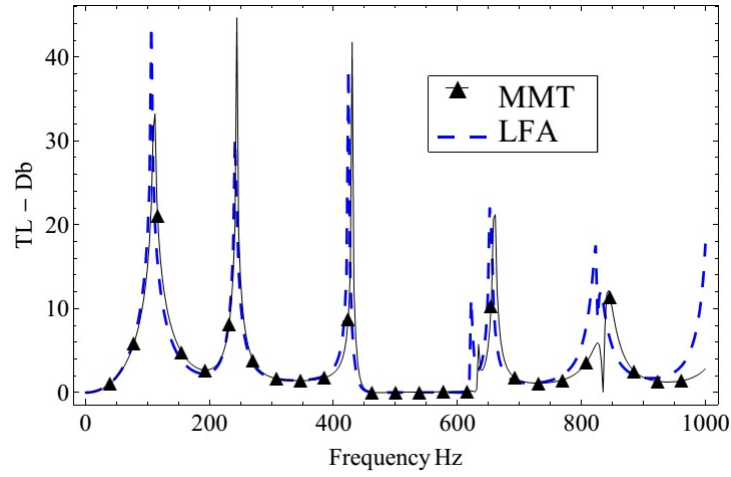


(b)

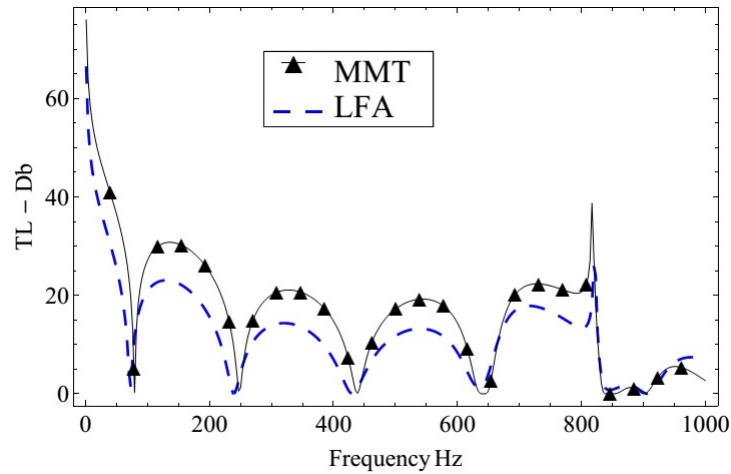
FIGURE 4.7: Transmission loss against frequency with vertical step-discontinuities involving expansion chamber while the central region comprises: a) rigid walls, b) soft walls, where, $\bar{a} = 0.15\text{m}$, $\bar{b} = 0.3\text{m}$, $\bar{L} = 0.25\text{m}$, $T=7500\text{N}$ and $N = 20$ terms.

As in planar case the compressional waves along the boundaries take part to

encompass both orthogonal and non-orthogonal modes, thus, the use of orthogonal characteristics defined in [48, 64], is indispensable.



(a)



(b)

FIGURE 4.9: Transmission loss against frequency with planar expansion chamber while the central region comprises: a) rigid b) soft, where, $\bar{a} = \bar{b} = 0.15\text{m}$, $\bar{L} = 0.25\text{m}$, $T=7500\text{N}$ and $N = 20$ terms.

The results for the reflected power in inlet (ε_1) and the transmitted power in outlet (ε_2) by for different values of truncation parameter N are shown in Table 4.3 and Table 4.4. Note that the sum of scattering energies for different value of N remains unity as given in (4.90). It clearly, authenticate the accuracy of algebra for both planar (Table 4.3) and discontinuous (Table 4.4) configurations of expansion chamber.

TABLE 4.3: Discontinuous expansion chamber, where,
 $\bar{a} = 0.15\text{m}$, $\bar{b} = 0.3\text{m}$, $\bar{h} = 0.1\text{m}$, $\bar{L} = 0.25\text{m}$, $T = 350\text{N}$, $f = 581\text{Hz}$.

Cases	N	\mathcal{E}_1	\mathcal{E}_2	$\mathcal{E}_1 + \mathcal{E}_2$	\mathcal{E}_{abs}
Rigid	15	0.0143675	0.985633	1	-
	20	0.0107053	0.989295	1	-
	25	0.00949543	0.990505	1	-
Soft	15	0.94091	0.0590905	1	-
	20	0.948663	0.0513374	1	-
	25	0.951804	0.0481963	1	-
Perforated ($\xi = 2, \eta = -0.5$)	15	0.145304	0.0723007	0.217604	0.782396
	20	0.150846	0.0701236	0.22097	0.77903
	25	0.154398	0.0677306	0.222128	0.777872
Fibrous ($\xi = 0.5, \eta = -0.5$)	15	0.311264	0.03	0.341264	0.658736
	20	0.315129	0.0324887	0.347618	0.652382
	25	0.316804	0.0339668	0.35077	0.64923

TABLE 4.4: Planar expansion chamber, where,
 $\bar{a} = 0.15\text{m}$, $\bar{b} = 0.15\text{m}$, $\bar{h} = 0.1\text{m}$, $\bar{L} = 0.25\text{m}$, $T = 350\text{N}$, $f = 581\text{Hz}$.

Cases	N	\mathcal{E}_1	\mathcal{E}_2	$\mathcal{E}_1 + \mathcal{E}_2$	\mathcal{E}_{abs}
Rigid	15	0.132295	0.867705	1	-
	20	0.136184	0.863816	1	-
	25	0.137554	0.862446	1	-
Soft	15	0.957819	0.0421806	1	-
	20	0.970748	0.0292522	1	-
	25	0.974552	0.0254479	1	-
Perforated ($\xi = 2, \eta = -0.5$)	15	0.0973971	0.0730003	0.170397	0.829603
	20	0.0957027	0.0716832	0.167386	0.832614
	25	0.0937829	0.0702737	0.164057	0.835943
Fibrous ($\xi = 0.5, \eta = -0.5$)	15	0.231671	0.00770542	0.239376	0.760624
	20	0.225837	0.00745078	0.233288	0.766712
	25	0.219545	0.00726535	0.226811	0.773189

It is evident for the rigid or soft type wall conditions of the central region. It essentially referred to the conservation of energies when no dissipation is involved. But, however, when porous lining (absorbent material) is considered along the boundaries of the central region instead of being rigid, soft or impedance, the maximum of incident energy goes on absorption. It is depicted for both planar (Table 4.3) and discontinuous (Table 4.4) expansion chamber. Note that comparatively more energy is absorbed in perforated case instead of fibrous case, see Tables 4.3 and 4.4. Also more energy is absorbed in planar case instead of discontinuous setting. This fact is because of the presence of extra propagating mode in discontinuity involving regions at given fixed frequency. Additional power pass into that regions and thus reflection is increased. This setting of devise works well when interested in getting more internal reflection. In contrast, for the planar case the internal reflection is less than that of discontinuous expansion chamber and thus absorption is increased.

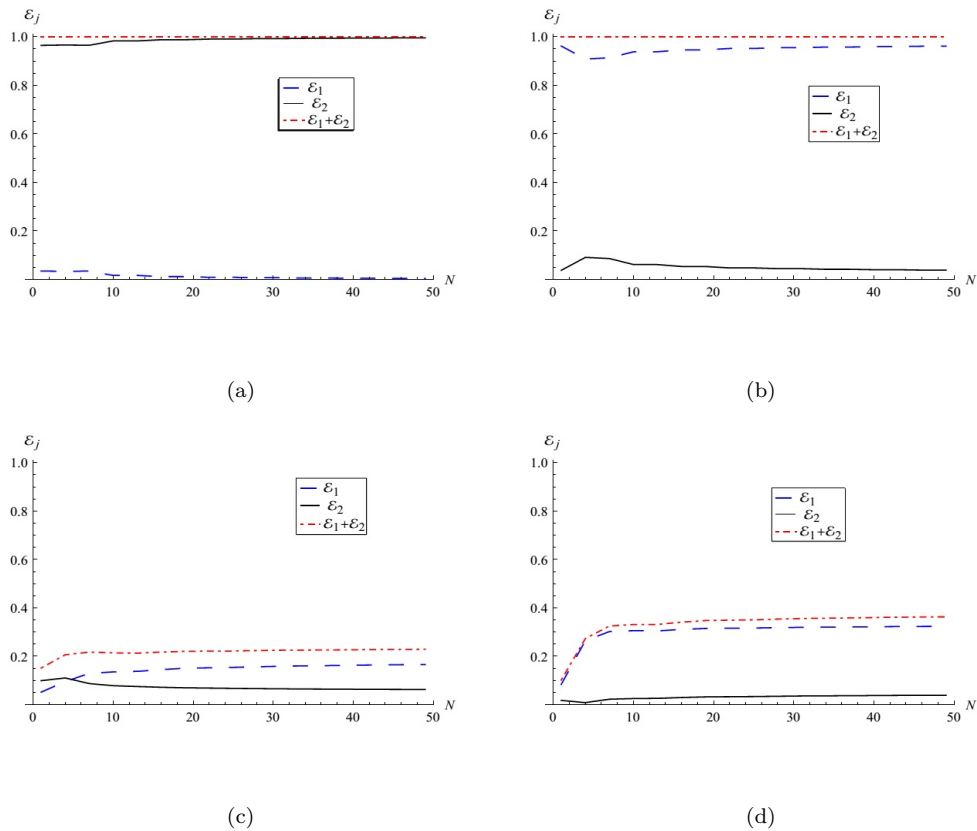


FIGURE 4.10: Discontinuous expansion chamber comprises: a) rigid b) soft c) perforated d) fibrous, where, $\bar{a} = 0.15\text{m}$, $\bar{b} = 0.3\text{m}$, $\bar{h} = 0.1\text{m}$, $\bar{L} = 0.25\text{m}$, $T=350\text{N}$ and $f = 581\text{Hz}$

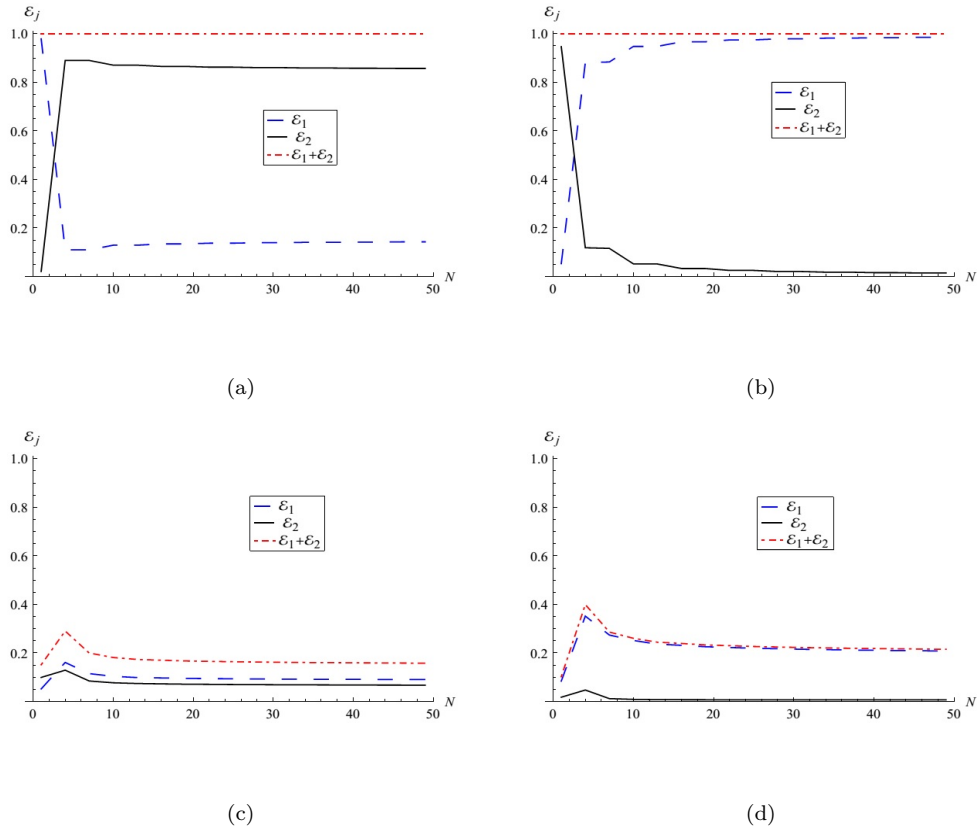


FIGURE 4.11: Planar expansion chamber comprises: a) rigid b) soft c) perforated d) fibrous, where, $\bar{a} = \bar{b} = 0.15\text{m}$, $\bar{h} = 0.1\text{m}$, $\bar{L} = 0.25\text{m}$, $T=350\text{N}$ and $f = 581\text{Hz}$.

Furthermore, the accuracy of truncated solution is confirmed through the reconstruction of matching conditions for truncation $N = 20$ terms. It leads to $8N \times 8N$ system of equations that are solved numerically for unknown scattering amplitudes. As two silencers configurations together with various bounding characteristics have been considered for analysis, and in each case their matching conditions have also been confirmed. But here we show limited graphs only. Thus, the graphs of matching conditions for geometrically discontinuous expansion chamber are shown. In Figures 4.12 and 4.13, the real and imaginary parts of dimensionless pressures and normal velocities are plotted at interfaces $x = \pm L$.

It can be seen that real and imaginary components of pressures and normal velocities curves match exactly. In this way the truncated solution successfully reconstructs the matching conditions.

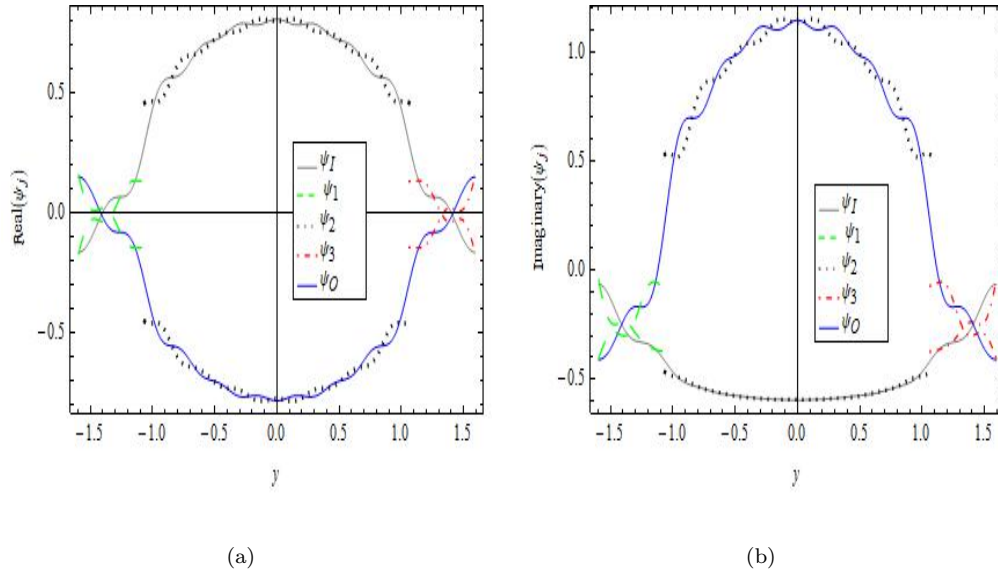


FIGURE 4.12: The real and imaginary parts of pressures against duct height at $x = \pm L$ and $N = 20$ terms.

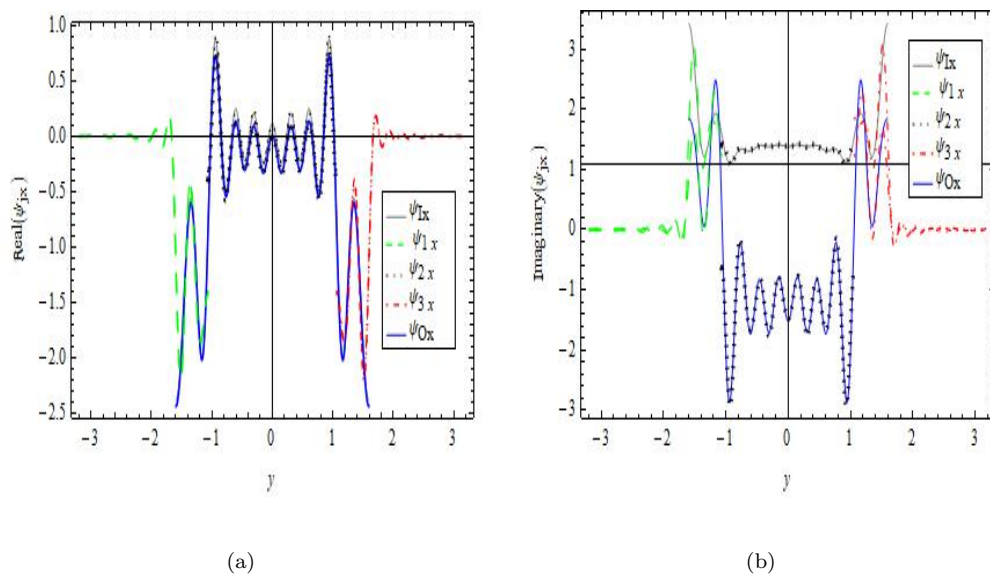


FIGURE 4.13: The real and imaginary parts of velocities against duct height at $x = \pm L$ and $N = 20$ terms.

Chapter 5

The Traveling Wave Formulation of a Splitting Chamber Containing Reactive Components

In this Chapter, scattering of through a splitting expansion chamber radiated by the incident duct mode is discussed. The segments of the expansion chamber contain absorbent linings and sandwiched elastic membranes backed by rigid cavities. Lee and Kim [10] showed that the internal partitioning of the muffler expansion chamber significantly effects the transmission characteristics of devise at some specific values of frequency. The current work anticipates a mathematical frame work of the physical model that incorporates the silencing objects capable of noise attenuation at low, mid and high range of frequencies. The mode-matching (MM) solution is developed to analyze the physical problem. The adopted scheme is different from the approach discussed by Huang [12], wherein the elastic membranes are present in line with the inlet and outlet duct walls, and the sound field is specified by means of Fourier integrals. Whereas, the coefficients of Fourier integrals are determined through the substitution of sound field into the membrane conditions. But the case considered here is somehow general with reference to the position of elastic components, and contain elastic components that may or may not be in line with the inlet and outlet duct walls, which undoubtedly leads to

discontinuity in geometry. Moreover, the considered physical problem is solved by using the low frequency approximation (LFA) to compare the results in low frequency regime.

The study is sorted in the following sections. The formulation of boundary value problem and the traveling wave formulation together with characteristics of eigenfunctions are discussed in Section 5.1. The MM solution is presented in Section 5.2, whilst, LFA solution is constructed in the Section 5.3. The numerical results and discussion results are displayed in Section 5.4.

5.1 Mathematical Formulation

In this section, the eigenforms of propagating duct modes in various regions of waveguides and their properties are discussed. The waveguide is rectangular, infinite and comprises finite expansion chamber including horizontal partitionings. The interior of the waveguide is filled with compressible fluid having density ρ and sound speed c , whilst its is in *vacuo*. In dimensional coordinates setting $(\bar{x}, \bar{y}, \bar{t})$, the sections at $|\bar{x}| \geq \bar{L}$, $-\bar{a} \leq \bar{y} \leq \bar{a}$ assist as inlet and outlet, whereas, the section at $|\bar{x}| \leq \bar{L}$, $-\bar{b} \leq \bar{y} \leq \bar{b}$ are taken for the expansion chamber. Note that the over bar here and henceforth represents a dimensional quantity. The surfaces at $\bar{y} = \pm \bar{d}^{\mp}$ include lining of absorbing material and there lie sandwiched membranes at $\bar{y} = \pm \bar{h}$. All the other boundaries are assumed acoustically rigid. The acoustic impedance of the absorbent lining is the ratio of acoustic pressure to normal velocity defined by [65].

$$\bar{Z} = \bar{P}/(\bar{\mathbf{u}} \cdot \bar{\mathbf{n}}),$$

where $\bar{P} = -\rho \partial \bar{\Phi} / \partial \bar{t}$ and $\bar{\mathbf{u}} = \text{grad} \bar{\Phi}$ are pressure and normal velocity vector, respectively, and $\bar{\mathbf{n}}$ is the normal vector directed into the lining. It yields the boundary condition for absorbent linings (impedance's type) as:

$$\left\{ \bar{\mathbf{n}} \cdot \text{grad} + \bar{\beta} c^{-1} \frac{\partial}{\partial \bar{t}} \right\} \bar{\Phi} = 0, \quad (5.1)$$

where $\bar{\beta}$ is specific impedance and its value is $\rho c \bar{Z}^{-1}$.

Let us assume the isotropic membrane lying at $\bar{y} = \pm \bar{h}$. The dimensional membrane displacement $\bar{w}(\bar{x}, \bar{y}, \bar{t})$ satisfies dimensional equation of motion:

$$\left\{ \frac{\partial^2}{\partial \bar{x}^2} - \frac{1}{c_m^2} \frac{\partial^2}{\partial \bar{t}^2} \right\} \bar{w} = \frac{1}{T} [\bar{P}]_{-}^{+}. \quad (5.2)$$

The geometry of physical problem is as shown in Figure 5.1.

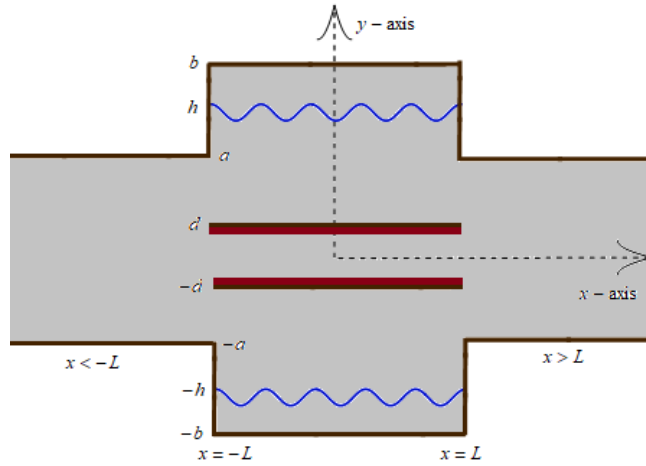


FIGURE 5.1: The geometry of physical problem.

The boundary value problem is made dimensionless by taking scales and transformations defined in Chapter 2. Moreover, the harmonic time dependence $\exp(-i\omega\bar{t})$ is suppressed throughout the governing equations. Thus, the time independent, non-dimensional velocity potential $\phi(x, y)$ satisfies the boundary value problem:

$$(\nabla^2 + 1)\phi(x, y) = 0, \quad (5.3)$$

$$\frac{\partial \phi}{\partial y} = 0, \quad y = \pm a, \quad \pm b, \quad \pm d^{\pm}, \quad (5.4)$$

$$\phi \pm i\zeta \frac{\partial \phi}{\partial y} = 0, \quad y = \pm d^{\mp}, \quad |x| < L, \quad (5.5)$$

$$\left(\frac{\partial^2}{\partial x^2} + \mu^2 \right) \frac{\partial \phi}{\partial y} \pm \alpha [\phi]_{h^{\pm}}^{\mp} = 0, \quad y = \pm h, \quad |x| < L \quad (5.6)$$

and

$$\frac{\partial \phi}{\partial y}(x, \pm h^+) = \frac{\partial \phi}{\partial y}(x, \pm h^-), \quad |x| < L, \quad (5.7)$$

where $\varsigma = \beta^{-1}$, $\beta = k\bar{\beta}$, the non-dimensional specific impedance. In addition, edge conditions are imposed on the edges of membranes. These conditions not only ensure the uniqueness of solution but also define the physical behavior of membrane at the edges or joints. At semi-infinite edges the selection of zero displacement conditions yield:

$$\frac{\partial \phi}{\partial y} = 0, \quad x = \pm L, \quad y = \pm h. \quad (5.8)$$

We assume an incident wave of fundamental inlet duct mode from negative x -direction towards the expansion chamber, where it will scatter into infinite number of scattering modes. The propagation of the reflecting and transmitting modes can be discussed through determining the eigenfunctions of guiding regions and their orthogonal properties. First we discuss, the region at $|x| < L$ (expansion chamber). It contains further partitioning with respect to height y as: lower region $-b \leq y \leq -d$, central region $|y| \leq d$ and upper region $d \leq y \leq b$. On applying the separation of variable method in (5.3)-(5.5), the eigenmodes for the central region are found as

$$\phi_1(\tau_n, x, y) = Y_1(\tau_n, y)e^{\pm i s_n x}, \quad -d \leq y \leq d, \quad (5.9)$$

where, $Y_1(\tau_n, y) = \sin[\tau_n(y+d)] + i\tau_n\varsigma \cos[\tau_n(y+d)]$, $n = 0, 1, 2, \dots$ are eigenfunctions. Note that $s_n = \sqrt{1 - \tau_n^2}$ be the n^{th} mode wave numbers containing eigenvalues τ_n . These eigenvalues satisfy the dispersion relation:

$$2i\varsigma\tau_n \cos[2d\tau_n] + \sin[2d\tau_n] + \tau_n^2\varsigma^2 \sin[2d\tau_n] = 0. \quad (5.10)$$

These roots can be found numerically and satisfy the condition $0 < \text{Im } s_0 < \text{Im } s_1 < \text{Im } s_2 < \dots$, and $\text{Re } s_n > 0$ for all $n = 0, 1, 2, \dots$. Furthermore, the eigenfunctions $Y_1(\tau_n, y)$ for $n = 0, 1, 2, \dots$ are orthogonal and satisfy the orthogonality relation (OR)

$$\int_{-d}^d Y_1(\tau_n, y)Y_1(\tau_m, y)dy = J_m\delta_{mn}, \quad (5.11)$$

where,

$$J_m = \frac{1}{2} \left\{ i\zeta - i\zeta \cos(4d\tau_m) + 2d(1 - \zeta^2\tau_m^2) \right\} + \frac{1}{\tau_m} \left\{ -1 - \zeta^2\tau_m^2 \sin(4d\tau_m) \right\}. \quad (5.12)$$

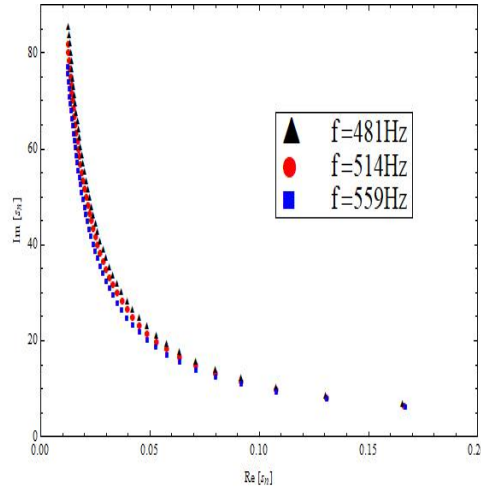


FIGURE 5.2: The plot of first few wave numbers in s -plane, where $\eta = 0.5$, $\bar{a} = 0.15m$, $\bar{d} = 0.1m$, $\bar{h} = 0.2m$, $\bar{b} = 0.3m$, $\bar{L} = 0.25m$ and $T = 3250N$.

Now for lower and upper regions, (5.3)-(5.4) and (5.6)-(5.7) yield the traveling eigenmodes formulation as

$$\begin{aligned} \phi_2(\gamma_n, x, y) &= Y_2(\gamma_n, y)e^{\pm i\nu_n x}, & -b \leq y \leq -d, \\ \phi_3(\gamma_n, x, y) &= Y_3(\gamma_n, y)e^{\pm i\nu_n x}, & d \leq y \leq b, \end{aligned} \quad (5.13)$$

where, $\nu_n = \sqrt{1 + \gamma_n^2}$ be the n^{th} mode wave number containing eigenvalues γ_n , respectively. Note that due to sandwiched membranes in upper and lower regions, the eigenmodes are of two forms; coupled modes and uncoupled modes. We discuss these modes one by one. The eigenfunctions for coupled eigenmodes can be expressed as

$$Y_2(\gamma, y) = \begin{cases} \Upsilon(\gamma) \cosh[\gamma(b+y)] & -b \leq y < -h, \\ \cosh[\gamma(y+d)] & -h \leq y \leq -d, \end{cases} \quad (5.14)$$

$$Y_3(\gamma, y) = \begin{cases} \cosh[\gamma(y-d)] & d \leq y \leq h, \\ \Upsilon(\gamma) \cosh[\gamma(b-y)] & h < y \leq b, \end{cases} \quad (5.15)$$

where, $\Upsilon(\gamma) = -\sinh[\gamma(h-d)] / \sinh[\gamma(b-h)]$ and the eigenvalue γ , satisfies dispersion relation:

$$(\gamma^2 + 1 - \mu^2)\gamma \sinh[\gamma(h-d)] + \alpha\Upsilon(\gamma) = 0. \quad (5.16)$$

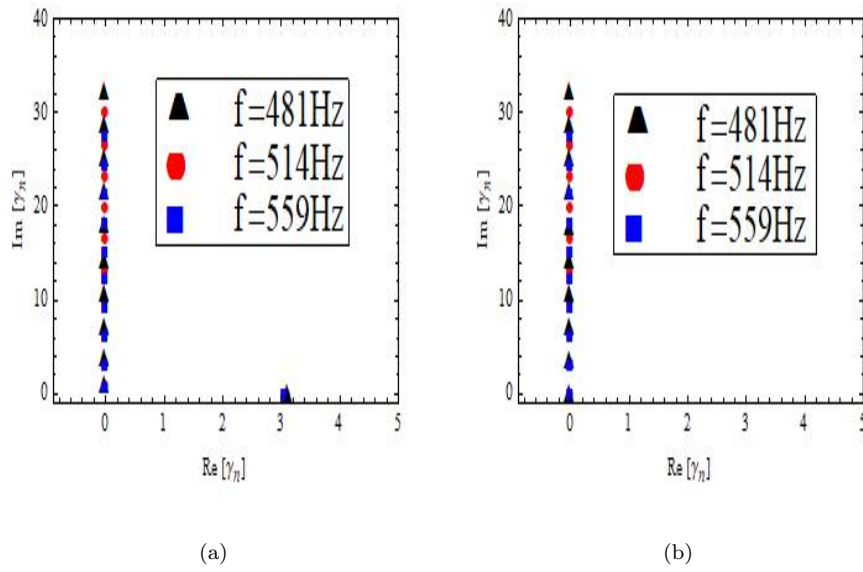


FIGURE 5.3: The plot of first few roots in γ -plane, where $\eta = 0.5$, $\bar{a} = 0.15m$, $\bar{d} = 0.1m$, $\bar{h} = 0.2m$, $\bar{b} = 0.3m$, $\bar{L} = 0.25m$ and $T = 3250N$: (a) Coupled modes and (b) Uncoupled modes.

There are infinite many values of γ which satisfy (5.16). These values can be found numerically and contain one real root $\gamma_0 > 0$, and infinite number of imaginary roots such that for each root γ_n , there is another root $-\gamma_n$ for $n = 1, 2, \dots$. These roots are arranged by employing a convention that the real root appears first and then the positive imaginary roots which are sorted sequentially in an ascending order. However, the negative imaginary roots are omitted.

In addition to the fluid-structure coupled modes as discussed above there are other waveforms in membrane containing regions, the plane acoustic waves of the form $\exp(ix)$. These waveforms always exist in membrane bounded regions without

interaction with membranes and are the trivial solution of equations (5.3), (5.6) and (5.7). Other waveforms of interest are the subset of usual rigid duct modes: those that have zero velocity normal to the membrane at $y = \pm h$. These are known as the uncoupled modes and exist only if the duct height $b - d$ can be expressed in the form $b - d = \frac{p(h - d)}{q}$, for integer values of p and q . It is convenient to express the eigenfunctions corresponding to uncoupled modes can be written as

$$Y_2(\gamma_j, y) = \begin{cases} (-1)^j \cosh [\gamma_j (b + y)] & -b \leq y < -h, \\ \cosh [\gamma_j (y + d)] & -h \leq y \leq -d, \end{cases} \quad (5.17)$$

$$Y_3(\gamma_j, y) = \begin{cases} \cosh [\gamma_j (y - d)] & d \leq y \leq h, \\ (-1)^j \cosh [\gamma_j (b - y)] & h < y \leq b, \end{cases} \quad (5.18)$$

where the eigenvalues for uncoupled modes are $\gamma_1 = 0$ (always present) and $\gamma_j = \frac{ij\pi q}{p(h - d)}$, $j = p, 2p, 3p, \dots$ (present only for $b - d = \frac{p(h - d)}{q}$). Note that these wave numbers are not roots of the given dispersion relation.

Now the eigenfunctions corresponding to coupled and uncoupled duct modes take the form

$$Y_2(\gamma_n, y) = \begin{cases} \Gamma_n \cosh [\gamma_n (b + y)] & -b \leq y < -h, \\ \cosh [\gamma_n (y + d)] & -h \leq y \leq -d, \end{cases} \quad (5.19)$$

$$Y_3(\gamma_n, y) = \begin{cases} \cosh [\gamma_n (y - d)] & d \leq y \leq h, \\ \Gamma_n \cosh [\gamma_n (b - y)] & h < y \leq b, \end{cases} \quad (5.20)$$

where

$$\Gamma_n = \begin{cases} \Upsilon(\gamma_n), & n \neq 1 \quad \text{and} \quad \gamma_n \neq \frac{ij\pi q}{p(h - d)}, \\ 1, & n = 1, \\ (-1)^j, & n \neq 1 \quad \text{and} \quad \gamma_n = \frac{ij\pi q}{p(h - d)}. \end{cases} \quad (5.21)$$

It is important to note that the set of all values, $\gamma_n, n = 0, 1, 2, \dots$ now includes

all admissible eigenvalues for both fluid-membrane coupled and uncoupled modes, ordered γ_0, γ_1 and then by increasing imaginary part. The eigenfunctions $Y_j(\gamma_n, y)$ for $j = 1, 3$ satisfy the generalized OR

$$\begin{aligned} \alpha \int_{-b}^{-d} Y_2(\gamma_n, y) Y_2(\gamma_m, y) dy &= \alpha \int_d^b Y_3(\gamma_n, y) Y_3(\gamma_m, y) dy \\ &= M_m \delta_{mn} - Y_3'(\gamma_n, h) Y_3'(\gamma_m, h), \end{aligned} \quad (5.22)$$

where

$$M_m = \begin{cases} \frac{\alpha}{2} \{e_m(h-d) + \Gamma_m^2 e_m(b-h)\}, & m \neq 1 \text{ and } \gamma_m \neq \frac{ij\pi q}{p(h-d)}, \\ \alpha(b-d), & m = 1, \\ \frac{\alpha(b-d)}{2}, & m \neq 1 \text{ and } \gamma_m = \frac{ij\pi q}{p(h-d)} \end{cases} \quad (5.23)$$

in which

$$e_m(x) = x + \frac{2\gamma_m^2 + \nu_m^2 - \mu^2}{2\gamma_m(\nu_m^2 - \mu^2)} \sinh(2\gamma_m x). \quad (5.24)$$

Likewise the inlet/outlet which contains both rigid type boundaries and thus yield eigenfunctions $\cos\left\{\frac{n\pi}{2a}(y+a)\right\}$, $n = 0, 1, 2, \dots$ which satisfy the usual form OR given by

$$\int_{-a}^a \cos\left(\frac{n\pi}{2a}(y+a)\right) \cos\left(\frac{m\pi}{2a}(y+a)\right) dy = a\delta_{mn}\epsilon_m. \quad (5.25)$$

In the next section MM solution is developed for the boundary value problem of the present section.

5.2 Mode-Matching (MM) Solution

To formulate the MM solution, we first find the eigenfunction expansion forms of propagating and scattering modes in the various duct regions. For inlet/outlet and expansion chamber, these expansions of velocity potentials are

$$\phi^-(x, y) = e^{i(x+L)} + \sum_{n=0}^{\infty} A_n \cos\left(\frac{n\pi}{2a}(y+a)\right) e^{-i\sigma_n(x+L)}, \quad x < L, \quad |y| \leq a, \quad (5.26)$$

$$\phi_2(x, y) = \sum_{n=0}^{\infty} (B_n e^{-i\nu_n x} + C_n e^{i\nu_n x}) Y_2(\gamma_n, y), \quad |x| < L, \quad -b \leq y \leq -d, \quad (5.27)$$

$$\phi_1(x, y) = \sum_{n=0}^{\infty} (D_n e^{-is_n x} + E_n e^{is_n x}) Y_1(\tau_n, y), \quad |x| < L, \quad |y| \leq d, \quad (5.28)$$

$$\phi_3(x, y) = \sum_{n=0}^{\infty} (F_n e^{-i\nu_n x} + G_n e^{i\nu_n x}) Y_3(\gamma_n, y), \quad |x| < L, \quad d \leq y \leq b, \quad (5.29)$$

$$\phi^+(x, y) = \sum_{n=0}^{\infty} H_n \cos\left(\frac{n\pi}{2a}(y+a)\right) e^{i\sigma_n(x-L)} \quad x > L, \quad |y| \leq a. \quad (5.30)$$

Here $\sigma_n = \sqrt{1 - n^2\pi^2/(4a^2)}$, $n = 0, 1, 2, \dots$ be the n^{th} mode wave numbers. Note that $\{A_n, B_n, \dots, H_n\}$, $n = 0, 1, 2, \dots$, are the amplitudes of the n^{th} scattering modes in the waveguide regions. These amplitudes are found by matching the fluid pressure and normal velocity at the interfaces $x = \pm L$. The continuity conditions of normal velocities at matching interfaces are

$$\int_{-b}^{-d} \alpha Y_2(\gamma_n, y) \frac{\partial \phi_1}{\partial x}(\pm L, y) dy = \alpha \int_{-a}^{-d} Y_2(\gamma_n, y) \frac{\partial \phi^{\pm}}{\partial x}(\pm L, y) dy. \quad (5.31)$$

On invoking (5.26), (5.27) and (5.30) into (5.31) and then by making use of the orthogonality relation (5.22), after some rearrangements it is found that:

$$\Xi_m^{\pm} = \frac{1}{2\Lambda^{\pm}(\nu_m L)\nu_m M_m} \left[Y_2'(\gamma_m, -h)\Theta^{\mp} - \alpha Q_{m0} + \alpha \sum_{n=0}^{\infty} \psi_n^{\pm} \sigma_n Q_{mn} \right], \quad (5.32)$$

where, $\psi_m^{\pm} = (A_m \pm H_m)$, $\Xi_m^{\pm} = (B_m \pm C_m)$, $\Theta^{\pm} = (e_1 \pm e_2)$, $\Lambda^+(x) = i \sin x$, $\Lambda^-(x) = \cos x$ and

$$Q_{mn} = \int_{-a}^{-d} Y_2(\gamma_m, y) \cos\left[\frac{n\pi}{2a}(y+a)\right] dy. \quad (5.33)$$

Here $e_1 = -i\phi_{1xy}(-L, -h)$ and $e_2 = -i\phi_{1xy}(L, -h)$ are constants. To determine these constants we use the edge conditions (5.8). For this, we multiply the equation (5.32) with $2 \sum_{m=0}^{\infty} Y_2'(\gamma_m, -h)\Lambda^{\mp}(\nu_m L)$, and then simplify the resulting equations

with the help of edge conditions (5.8), to get:

$$\Theta^\mp = \frac{\alpha}{S_1^\mp} \sum_{m=0}^{\infty} \frac{Y_2'(\gamma_m, -h) \kappa^\mp(\nu_m L)}{\nu_m M_m} \left[\sum_{m=0}^{\infty} Q_{m0} - \sum_{n=0}^{\infty} \psi_n^\pm \sigma_n Q_{mn} \right], \quad (5.34)$$

where, $\kappa^+(x) = \tan(x)$, $\kappa^-(x) = 1/\kappa^+(x)$ and

$$S_1^\mp = \sum_{m=0}^{\infty} \frac{[Y_2'(\gamma_m, -h)]^2 \kappa^\mp(\nu_m L)}{\nu_m M_m}. \quad (5.35)$$

The continuity conditions of normal velocities at matching interfaces are

$$\int_{-d}^d Y_1(\tau_n, y) \frac{\partial \phi_2}{\partial x}(\pm L, y) dy = \int_{-d}^d Y_1(\tau_n, y) \frac{\partial \phi^\pm}{\partial x}(\pm L, y) dy. \quad (5.36)$$

On invoking (5.26), (5.28) and (5.30) into (5.36) and then making use of the OR (5.11), after some rearrangement it is found that

$$\chi_m^\pm = \frac{1}{2\Lambda^\pm(s_m L) s_m J_m} \left[-R_{m0} + \sum_{n=0}^{\infty} \psi_n^\pm \sigma_n R_{mn} \right], \quad (5.37)$$

where $\chi_m^\pm = (D_m \pm E_m)$ and

$$R_{mn} = \int_{-d}^d Y_1(\tau_m, y) \cos\left[\frac{n\pi}{2a}(y+a)\right] dy. \quad (5.38)$$

The continuity conditions of normal velocities at matching interfaces are

$$\int_d^b \alpha Y_3(\gamma_n, y) \frac{\partial \phi_3}{\partial x}(\pm L, y) dy = \alpha \int_d^a Y_3(\gamma_n, y) \frac{\partial \phi^\pm}{\partial x}(\pm L, y) dy. \quad (5.39)$$

On invoking (5.26), (5.29) and (5.30) into (5.39) and then by using orthogonality (5.22), after simplification we get:

$$\varpi_m^\pm = \frac{1}{2\Lambda^\pm(\nu_m L) \nu_m M_m} \left[Y_3'(\gamma_m, h) \varphi^\mp - \alpha P_{m0} + \alpha \sum_{n=0}^{\infty} \psi_n^\pm \sigma_n P_{mn} \right], \quad (5.40)$$

where, $\varpi_m^\pm = (F_m \pm G_m)$, $\varphi^\pm = (e_3 \pm e_4)$ and

$$P_{mn} = \int_d^a Y_3(\gamma_m, y) \cos\left[\frac{n\pi}{2a}(y+a)\right] dy. \quad (5.41)$$

Again the quantities $e_3 = -i\phi_{3xy}(-L, h)$ and $e_4 = -i\phi_{3xy}(L, h)$ are constants. To find these constants we use edge conditions (5.8). For this we multiply (5.40) with $2\sum_{m=0}^{\infty} Y_3'(\gamma_m, h)\Lambda^{\mp}(\nu_m L)$ and, then simplify the resulting equation with the aid of edge conditions (5.8), to get

$$\varphi^{\mp} = \frac{\alpha}{S_2^{\mp}} \sum_{m=0}^{\infty} \frac{Y_3'(\gamma_m, h)\kappa^{\mp}(\nu_m L)}{\nu_m M_m} \left[\sum_{m=0}^{\infty} P_{m0} - \sum_{n=0}^{\infty} \psi_n^{\pm} \sigma_n P_{mn} \right], \quad (5.42)$$

where,

$$S_2^{\mp} = \sum_{m=0}^{\infty} \frac{[Y_3'(\gamma_m, h)]^2 \kappa^{\mp}(\nu_m L)}{\nu_m M_m}. \quad (5.43)$$

Now finally, we match the pressure modes across the duct regions at interfaces. The matching conditions for these modes reveal the forms as

$$\begin{aligned} \int_{-a}^a \cos\left(\frac{n\pi}{2a}(y+a)\right) \phi^{\pm}(\pm L, y) dy &= \int_{-a}^{-d} \phi_1(\pm L, y) \cos\left(\frac{n\pi}{2a}(y+a)\right) dy \\ + \int_{-d}^d \phi_2(\pm L, y) \cos\left(\frac{n\pi}{2a}(y+a)\right) dy &+ \int_d^a \phi_3(\pm L, y) \cos\left(\frac{n\pi}{2a}(y+a)\right) dy. \end{aligned} \quad (5.44)$$

On invoking (5.26)-(5.30) into (5.44) and then by making use of the OR (5.25), it is found that

$$\psi_m^{\pm} = -\delta_{m0} + \frac{2}{a\epsilon_m} \sum_{n=0}^{\infty} \{\Xi_n^{\pm} Q_{nm} \Lambda^{\mp}(\nu_n L) + \chi_n^{\pm} R_{nm} \Lambda^{\mp}(s_n L) + \varpi_n^{\pm} P_{nm} \Lambda^{\mp}(\nu_n L)\}. \quad (5.45)$$

In this way, we found two systems of linear algebraic equations having infinite number of unknowns. These systems are defined by the equations (5.45), (5.32), (5.37) and (5.40) in which Ξ_n^{\pm} , χ_n^{\pm} and ϖ_n^{\pm} are unknowns. To solve these systems we truncate with $n = m = 0, 1, 2, \dots, N$ terms and then solve the retained systems simultaneously.

5.3 A Low Frequency Approximation (LFA)

In this section LFA solution is provided. The aim of this solution is to analyze its validation with MM solution. The LFA based on matching integral quantities such

as mean pressure and mean velocity instead of using OR. So only the fundamental forcing incident is considered herein and LFA is not expected to valid for higher mode incident. The expressions for velocity potentials remain valid in this case with truncation of $n = \Pi_2 = 2$. That are as follows:

$$\phi^-(x, y) \approx e^{i(x+L)} + \sum_{n=0}^{\Pi_2} A_n \cos\left(\frac{n\pi}{2a}(y+a)\right) e^{-i\sigma_n(x+L)}, \quad x < L, \quad |y| \leq a, \quad (5.46)$$

$$\phi_1(x, y) \approx \sum_{n=0}^{\Pi_2} (B_n e^{-i\nu_n x} + C_n e^{i\nu_n x}) Y_2(\gamma_n, y), \quad |x| < L, \quad -b \leq y \leq -d, \quad (5.47)$$

$$\phi_2(x, y) \approx (D_0 e^{-is_0 x} + E_0 e^{is_0 x}) Y_1(\tau_0, y), \quad |x| < L, \quad |y| \leq d, \quad (5.48)$$

$$\phi_3(x, y) \approx \sum_{n=0}^{\Pi_2} (F_n e^{-i\nu_n x} + G_n e^{i\nu_n x}) Y_3(\gamma_n, y), \quad |x| < L, \quad d \leq y \leq -b, \quad (5.49)$$

$$\phi^+(x, y) \approx \sum_{n=0}^{\Pi_2} H_n \cos\left(\frac{n\pi}{2a}(y+a)\right) e^{i\sigma_n(x-L)}, \quad x > L, \quad |y| \leq a. \quad (5.50)$$

The continuity conditions of normal velocities and mean pressures are expressed as:

$$\int_{-h}^{-d} \frac{\partial \phi_1}{\partial x}(\pm L, y) dy = \int_{-a}^{-d} \frac{\partial \phi^\pm}{\partial x}(\pm L, y) dy, \quad (5.51)$$

$$\int_{-d}^d \frac{\partial \phi_2}{\partial x}(\pm L, y) dy = \int_{-d}^d \frac{\partial \phi^\pm}{\partial x}(\pm L, y) dy, \quad (5.52)$$

$$\int_d^h \frac{\partial \phi_3}{\partial x}(\pm L, y) dy = \int_d^a \frac{\partial \phi^\pm}{\partial x}(\pm L, y) dy \quad (5.53)$$

and

$$\int_{-a}^{-d} \phi_1(\pm L, y) dy = \int_{-a}^{-d} \phi^\pm(\pm L, y) dy, \quad (5.54)$$

$$\int_{-d}^d \phi_2(\pm L, y) dy = \int_{-d}^d \phi^\pm(\pm L, y) dy, \quad (5.55)$$

$$\int_d^a \phi_3(\pm L, y) dy = \int_d^a \phi^\pm(\pm L, y) dy \quad (5.56)$$

respectively. On invoking (5.46)-(5.50) into (5.51)-(5.56), then after simplification, we get following systems of equations:

$$2 \sum_{n=0}^{\Pi 2} \Xi_n^{\pm} \nu_n K_n \Lambda^{\pm} (\nu_n L) - \sum_{n=0}^{\Pi 2} \sigma_n \psi_n^{\pm} P_n = -P_0, \quad (5.57)$$

$$2 \sum_{n=0}^{\Pi 2} \varpi_n^{\pm} \nu_n K_n \Lambda^{\pm} (\nu_n L) - \sum_{n=0}^{\Pi 2} (-1)^n \sigma_n \psi_n^{\pm} P_n = -P_0, \quad (5.58)$$

$$2\chi_0^{\pm} s_0 N_0 \Lambda^{\pm} (s_0 L) + \sum_{n=0}^{\Pi 2} \sigma_n \psi_n^{\pm} X_n = X_0, \quad (5.59)$$

$$2 \sum_{n=0}^{\Pi 2} \Xi_n^{\pm} T_n \Lambda^{\mp} (\nu_n L) - \sum_{n=0}^{\Pi 2} \psi_n^{\pm} P_n = P_0, \quad (5.60)$$

$$2 \sum_{n=0}^{\Pi 2} \varpi_n^{\pm} T_n \Lambda^{\mp} (\nu_n L) - \sum_{n=0}^{\Pi 2} (-1)^n \psi_n^{\pm} P_n = P_0 \quad (5.61)$$

and

$$2\chi_0^{\pm} N_0 \Lambda^{\mp} (s_0 L) + \sum_{n=0}^{\Pi 2} \psi_n^{\pm} X_n = -X_0, \quad (5.62)$$

where, $K_0 = \sinh[\gamma_0(h-d)]/\gamma_0$, $K_1 = h-d$, $K_2 = \sinh[\gamma_2(h-d)]/\gamma_2$, $T_0 = \sinh[\gamma_0(a-d)]/\gamma_0$, $T_2 = \sinh[\gamma_2(a-d)]/\gamma_2$, $N_0 = \frac{2}{\tau_0} \sin^2(d\tau_0) + i\zeta \sin(2d\tau_0)$, $T_1 = P_0 = a-d$, $P_1 = \frac{2a}{\pi} \cos\left(\frac{d\pi}{2a}\right)$, $P_2 = \frac{a}{\pi} \sin\left(\frac{d\pi}{a}\right)$, $X_0 = -2d$, $X_1 = 0$ and $X_2 = 2P_2$.

To determine the edge conditions, we use (5.47) and (5.49) into (5.8), which after simplification lead to:

$$\sum_{n=0}^{\Pi 2} \Xi_n^{\pm} Z_n \Lambda^{\mp} (\nu_n L) = 0, \quad \sum_{n=0}^{\Pi 2} \varpi_n^{\pm} Z_n \Lambda^{\mp} (\nu_n L) = 0, \quad (5.63)$$

where, $Z_0 = \gamma_0 \sinh[\gamma_0(d-h)]$, $Z_1 = 0$, $Z_2 = \gamma_2 \sinh[\gamma_2(d-h)]$. Now as the vertical surfaces inside of the cavities are acoustically rigid, therefore the velocity flux along these surfaces must satisfy the conditions:

$$\int_{-b}^{-h} \frac{\partial \phi_1}{\partial x} (\pm L, y) dy = 0, \quad \int_h^b \frac{\partial \phi_3}{\partial x} (\pm L, y) dy = 0. \quad (5.64)$$

By invoking (5.47) and (5.49) into (5.64), after some rearrangements, we found:

$$\sum_{n=0}^{\Pi 2} \Xi_n^{\pm} W_n \Lambda^{\pm} (\nu_n L) = 0, \quad \sum_{n=0}^{\Pi 2} \varpi_n^{\pm} W_n \Lambda^{\pm} (\nu_n L) = 0, \quad (5.65)$$

where, $W_0 = i\nu_0 \{\Gamma_0 \sinh[\gamma_0(b-h)]\} / \gamma_0$, $W_1 = i\nu_1 \{\Gamma_1(b-h)\}$, $W_2 = i\nu_2 \{\Gamma_2 \sinh[\gamma_2(b-h)]\} / \gamma_2$. Thus, to determine the unknowns, the systems of equations (5.57)-(5.63) and (5.65) are solved simultaneously.

5.4 Numerical Results and Discussion

The performance of HVAC component is usually measured in terms of power transmission loss (TL), that is $TL = -10 \log_{10} (\mathcal{E}_2 / \mathcal{E}_i)$, where \mathcal{E}_2 denotes the transmitted energy flux in outlet region and \mathcal{E}_i is the incident energy taken as unity.

$$\mathcal{E}_2 = \frac{1}{2} \text{Re} \left[\sum_{n=0}^{\infty} |H_n|^2 \sigma_n \epsilon_n \right]. \quad (5.66)$$

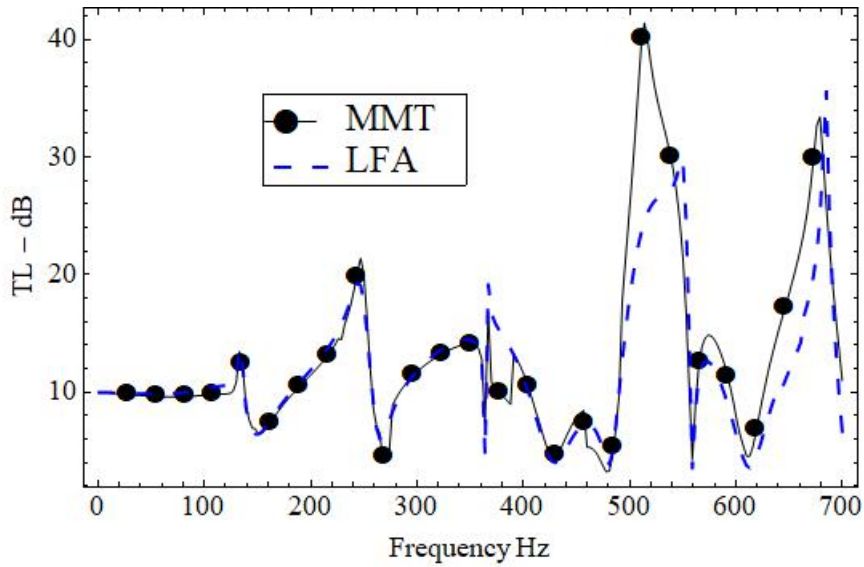
Likewise the reflected energy flux \mathcal{E}_r denotes the reflected energy in inlet region

$$\mathcal{E}_1 = \frac{1}{2} \text{Re} \left[\sum_{n=0}^{\infty} |A_n|^2 \sigma_n \epsilon_n \right]. \quad (5.67)$$

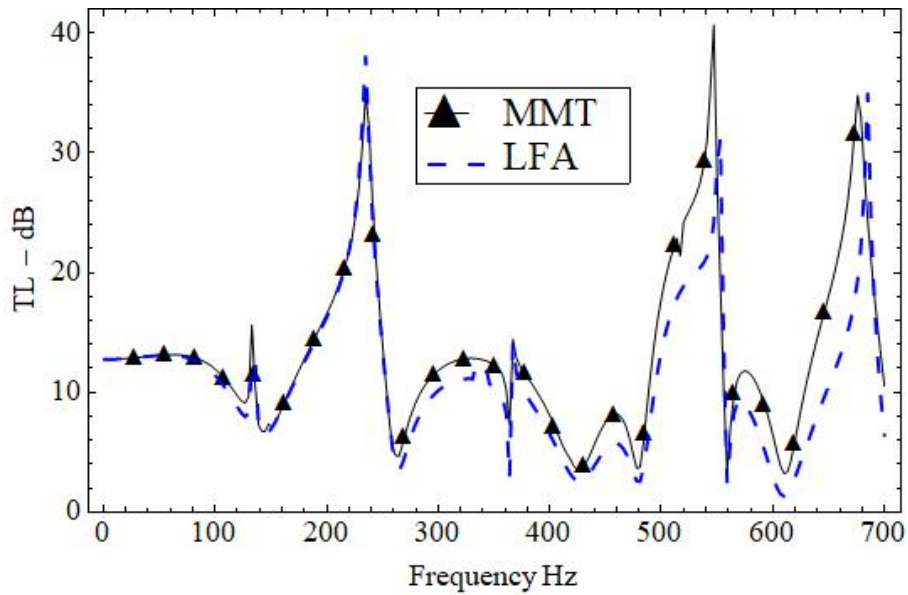
Note we fed unit energy into the system which will be equal to the sum of reflected energy in inlet \mathcal{E}_1 , transmitted energy in outlet \mathcal{E}_2 and absorbed energy \mathcal{E}_{abs} due to the lining of central region. This is conserved power identity and thus we may write $\mathcal{E}_{abs} = 1 - (\mathcal{E}_1 + \mathcal{E}_2)$. The specific impedance $\varsigma = \xi + i\eta$ of the absorbent lining follows the values [49]. For fibrous sheet: $\xi = 0.5$ and $-1.0 < \eta < 3.0$, whereas, for perforated sheet: $0 < \xi < 3$ and $-1.0 < \eta < 3.0$.

The TL associated with the properties of dissipative material used in the central region of the expansion chamber, material properties of sandwiched elastic components and/or the configurations of the chamber is analyzed in Figures. 5.4-5.10.

Figures 5.4-5.5 depict respectively the TL versus frequency with fibrous and perforated types of absorbing lining while the elastic components are pinned inside of the cavities ($\bar{h} > \bar{a}$). To perform numerical computations, $\rho = 1.2043kgm^{-3}$, $c = 343ms^{-1}$, $\rho_m = 0.2kgm^{-3}$, $T = 3250Nm^{-2}$ and the duct dimensions $\bar{d} = 0.1m$, $\bar{a} = 0.15m$, $\bar{h} = 0.2m$, $\bar{b} = 0.25m$, $\bar{L} = 0.25m$ remain fixed.

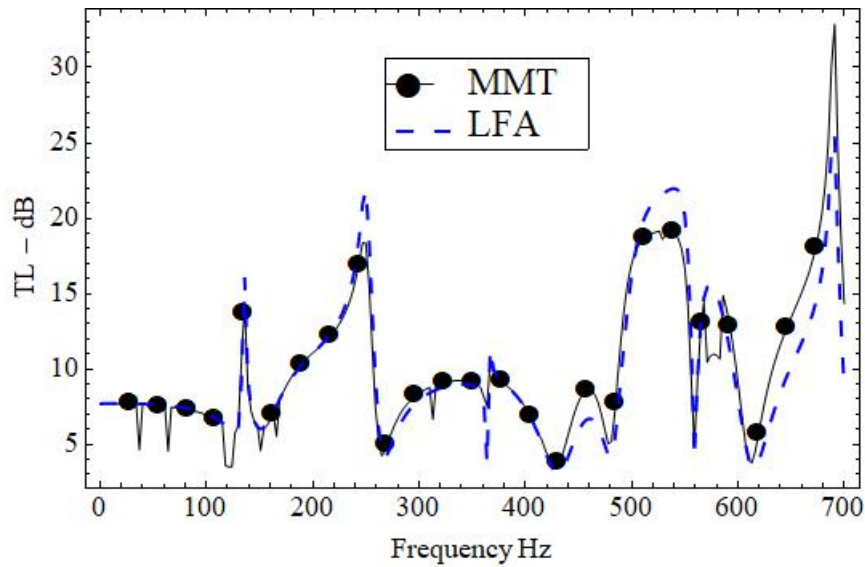


(a)

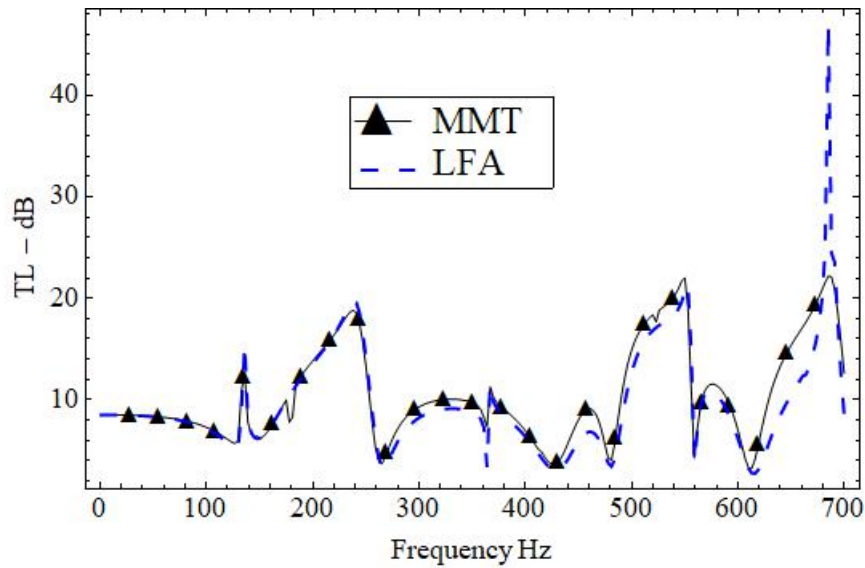


(b)

FIGURE 5.4: For fibrous coating and the elastic components pinned inside the cavities ($\bar{h} > \bar{a}$), the Transmission loss against frequency, where, (a) $\eta = 0.5$ and (b) $\eta = 0$, for $N = 25$ terms.



(a)



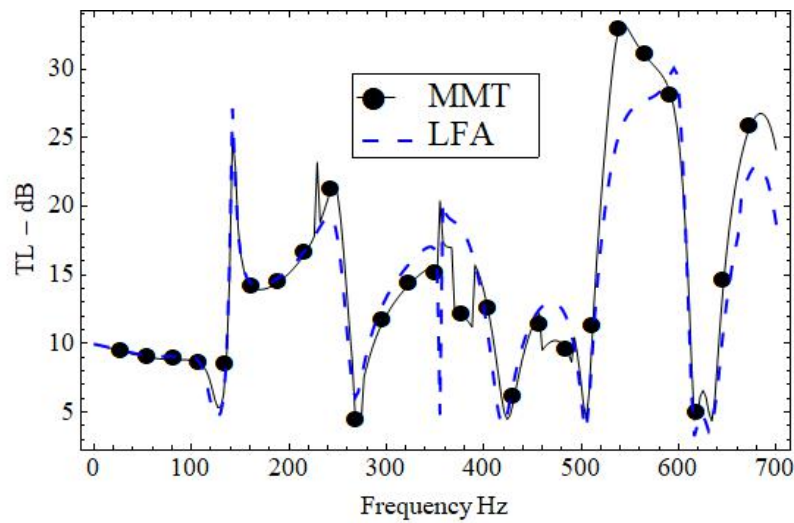
(b)

FIGURE 5.5: For perforated coating and the elastic components pinned inside the cavities ($\bar{h} > \bar{a}$), the Transmission loss against frequency, where, (a) $\eta = 0.5$ and (b) $\eta = 0$, for $N = 25$ terms.

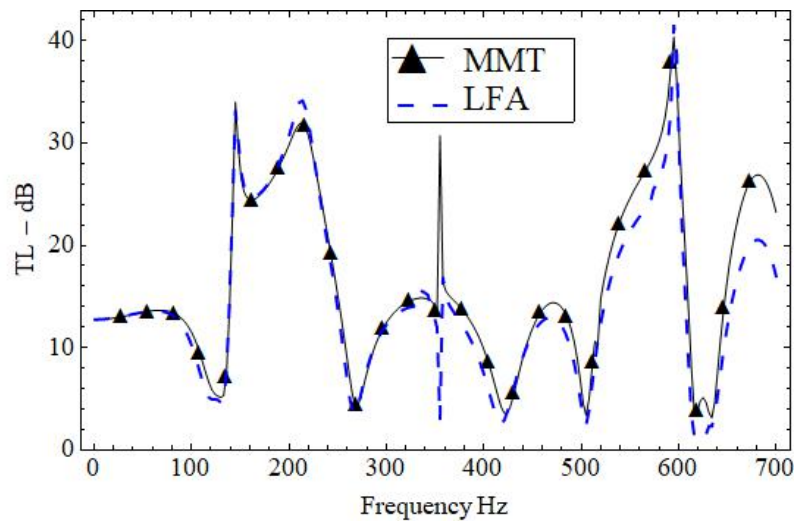
For graphs in Figure 5.4, the surfaces of the central region assume the fibrous material that refers $\xi = 0.5$, and have taken $\eta = 0.5$ and $\eta = 0$ respectively to obtain the curves of Figure 5.4(a) and 5.4(b). Accordingly, in Figure 5.5 the perforated type of coating is taken along the surfaces of the central region of expansion chamber which refers $\xi = 1$, while rest of parameters are same as

assumed to plot Figure 5.4. Note that the TL curves of Figures 5.4 and 5.5 depict almost similar behavior. Nevertheless, fibrous coating yields greater TL as compared with the perforated linings. Also the stopbands with larger bandwidths for fibrous case relatively to perforated case, according to the criterion as given in [49], at different frequency ranges are revealed.

Now by altering the position of membranes of the cavity regions, the TL results against frequency are shown in Figures 5.6 and 5.7.

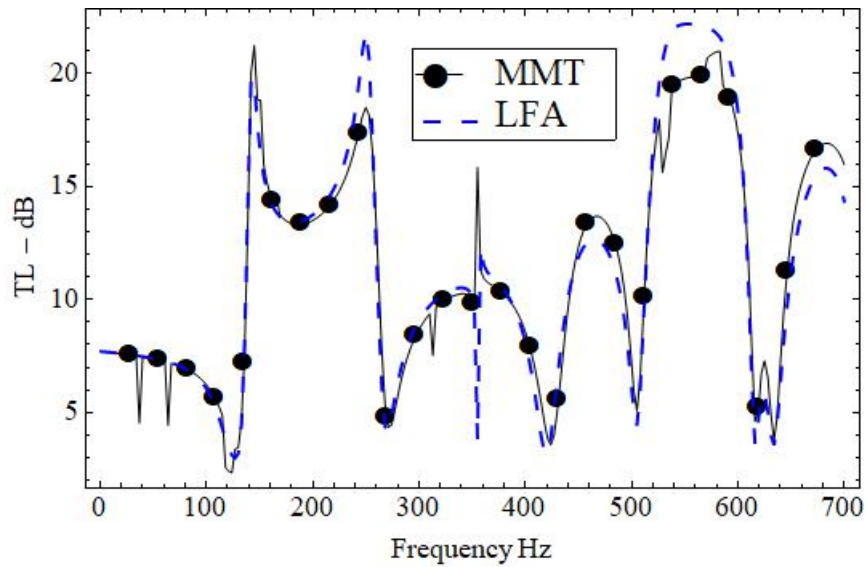


(a)

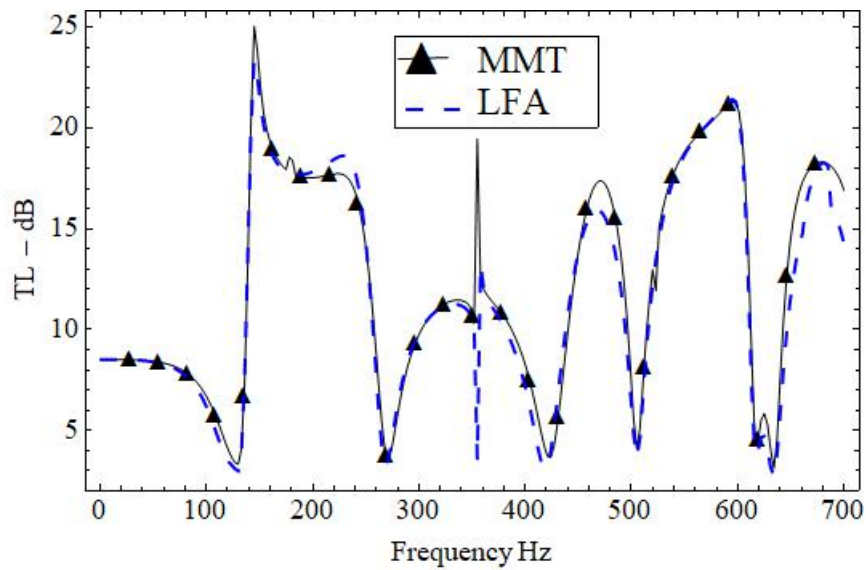


(b)

FIGURE 5.6: For fibrous coating and elastic components attached at apertures of cavities ($\bar{h} = \bar{a}$), the Transmission loss against frequency, where, (a) $\eta = 0.5$ and (b) $\eta = 0$, for $N = 25$ terms.



(a)



(b)

FIGURE 5.7: For perforated coating and elastic components attached at apertures of cavities ($\bar{h} = \bar{a}$), the Transmission loss against frequency, where, (a) $\eta = 0.5$ and (b) $\eta = 0$, for $N = 25$ terms.

In this case the elastic membranes are attached at the apertures of the cavities ($\bar{h} = \bar{a} = 0.2m$), whereas, rest of the dimensional variables and involving physical parameters remain invariant. Form the graphs in Figures 5.6 and 5.7, comparatively wide stopbands at different ranges of frequencies are revealed. The reason

behind is the variation of cut-on modes of the cavities. The cut-on mode frequencies for the elastic membranes pinned inside the cavities and attached at the aperture positions are presented in Table 5.1 and Table 5.2, respectively.

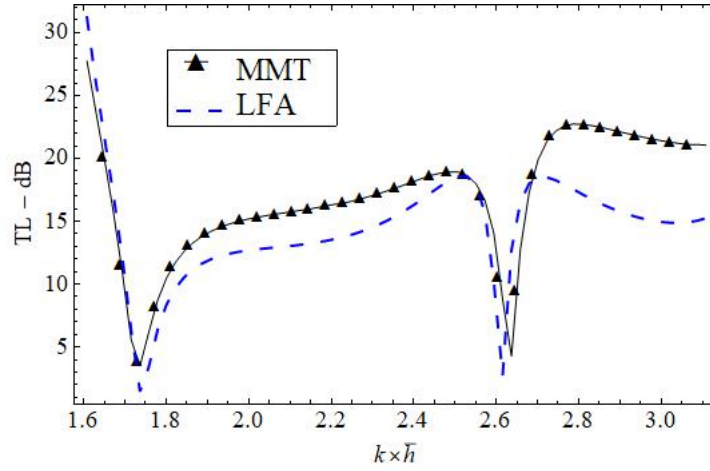
TABLE 5.1: Cut-on mode frequencies when the elastic components are pinned inside of the cavities ($\bar{a} < \bar{h}$).

Cut-on f (Hz)	Inlet/Outlet	Expansion Chamber
		Side Regions
1	1	2
496	1	3
573	2	3
1145	3	3
1718	4	4
1894	4	5
2290	5	5
2863	6	5

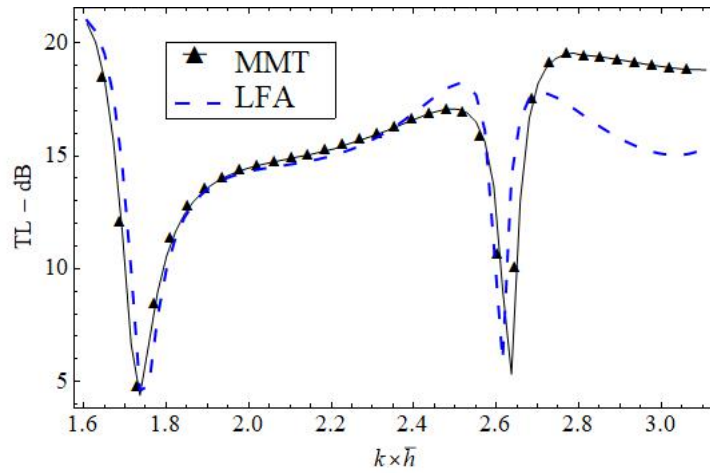
TABLE 5.2: Cut-on mode frequencies when the elastic components attached at apertures of cavities ($\bar{h} = \bar{a}$).

Cut-on f (Hz)	Inlet/Outlet	Expansion Chamber
		Side Regions
1	1	2
565	1	3
573	2	3
1145	3	3
1247	3	4
1718	4	4
2290	5	4
2336	5	5
2863	6	5

Furthermore, fibrous coating of the central region leads to more TL than the perforated coating. Also it is worth noting that the variation of porosity parameter η , significantly alter the TL. Moreover, it can be seen that both MM and LFA curves have a good agreement, however, in LFA at some frequency ranges there appear some dissimilarities. These variations are due to the exchange imaginary eigenvalues to real or complex number and vice versa.



(a)



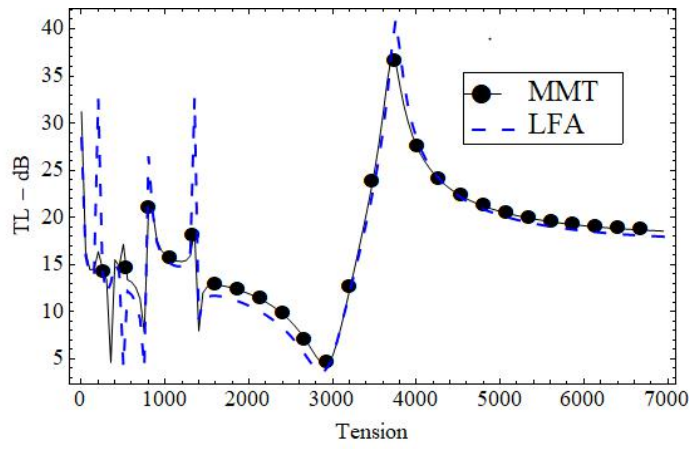
(b)

FIGURE 5.8: TL against the position of membrane h in cavities for; a) fibrous coating and b) perforated coating, where, $\bar{a} = 0.15m$, $\bar{d} = 0.1m$, $\bar{b} = 0.3m$, $\bar{L} = 0.25m$, $T=350N$, $f = 586Hz$ and $N = 20$ terms.

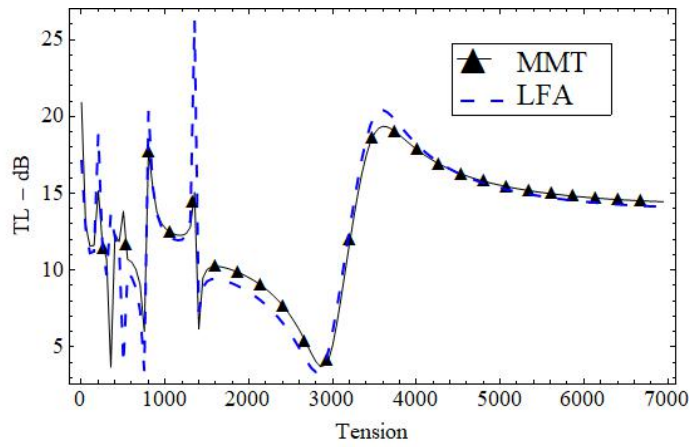
Figure 5.8 is found to analyze TL verses the position of sandwiched membranes by varying \bar{h} from 1.5m to 3m, whereas, frequency $f = 586Hz$ and dimensional

lengths $\bar{a} = 0.15m$, $\bar{d} = 0.1m$, $\bar{b} = 0.3m$, $\bar{L} = 0.25m$ remain fixed. Note that there appear downward spikes in TL curves at $k \times \bar{h} \approx 1.74$ and 2.64 . These occur due to the appearance of new cut-on duct modes. Nevertheless, the advent of additional modes reveal dissimilarities in LFA and MM curves due inability of LFA with higher order modes propagation. Furthermore, comparatively more TL in fibrous case than perforated lining is found.

In Figures 5.9 and 5.10 TL are shown against membrane tension T. Again the fibrous and perforated materials are chosen by fixing the parameters $\xi = 0.5$ and $\xi = 1$, respectively and have taken respectively $\eta = 0.5$ and $\eta = 0$ to obtain the (a) and (b) parts of Figures 5.9 and 5.10.

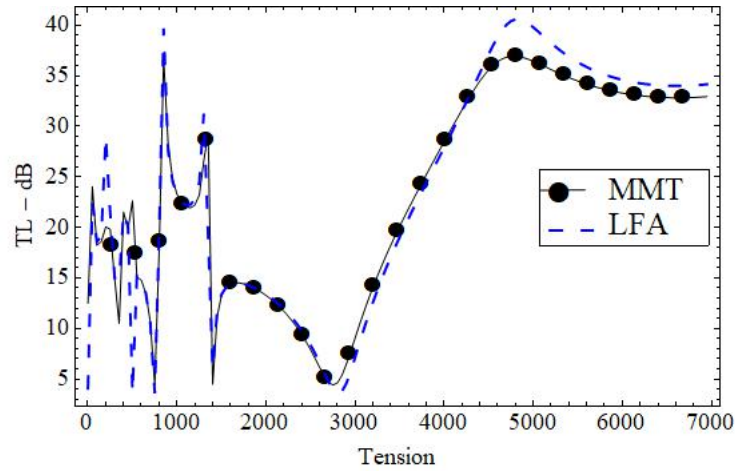


(a)

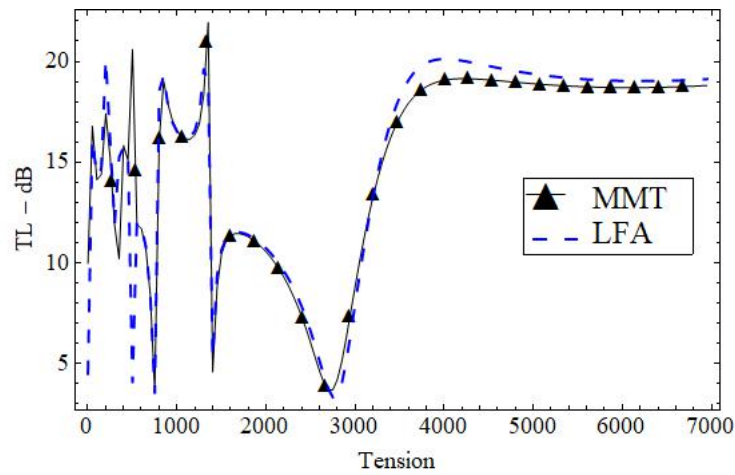


(b)

FIGURE 5.9: TL against tension when elastic components are pinned inside the cavities ($\bar{h} > \bar{a}$) for; a) fibrous case, and b) perforated case, where, $\bar{a} = 0.15m$, $\bar{h} = 0.2m$, $\bar{d} = 0.1m$, $\bar{b} = 0.3m$, $\bar{L} = 0.25m$, $f = 250Hz$ and $N = 20$ terms.



(a)



(b)

FIGURE 5.10: TL against tension when elastic components are attached at the aperture of the the cavities for; a) fibrous case and b) perforated case, where, $\bar{a} = \bar{h} = 0.15m$, $\bar{d} = 0.1m$, $\bar{b} = 0.3m$, $\bar{L} = 0.25m$, $f = 250Hz$ and $N = 20$ terms.

From Figure 5.9(b), it can be seen that the TL for the perforated case is within 25dB in whole tension regime, whereas, for fibrous case TL is within 32dB upto tension 3000N, after that TL increases to 40dB while $3000N < T < 4000N$ and then decreases by increasing the value of tension. In Figures. 5.10(a) and 5.10(b), we alter the position of membranes by taking $\bar{a} = \bar{h}$. Note that for the fibrous type of linings of the central region, there achieved TL of 22dB in whole tension regime, whilst, the value of TL in porous lining case reaches to 40dB. It clearly reveals that the variation of tension of elastic membranes of the cavities significantly alter

the TL results. Furthermore, a good comparison in LFA and MM curves for the case wherein the elastic membranes are pinned inside of the cavities is found (see FIGURE 5.9). However, there appear some dissimilarities in LFA and MM curves for case when the elastic membranes are attached along the apertures (see Figure 5.10). These variation are due to conversion of real eigenvalues to imaginary or complex eigenvalues and vice versa.

Now to analyze the energy propagation and absorption in conjunction with the truncation parameter N, Table 5.3 and Table 5.4 are shown. For different values of N the reflected power (\mathcal{E}_1), the transmitted power(\mathcal{E}_2) and absorbed power \mathcal{E}_{abs} are portrayed in these Tables. Note that at N=20, the reflected, transmitted and absorbed energies converge upto 3 decimal places. Moreover, the it can be seen that by changing the material properties of the absorbent material the absorbed power is changed; i.e., more energy is absorbed in perforated case as compared with fibrous case (see Tables 5.3 and 5.4). Also more energy is absorbed in the case when elastic membranes are pinned inside of the cavities than the elastic membranes attached at the mouths of cavities.

TABLE 5.3: The case when elastic membranes pinned inside of the cavities, where, $\bar{a} = 0.15\text{m}$, $\bar{b} = 0.3\text{m}$, $\bar{d} = 0.1\text{m}$, $\bar{h} = 0.2\text{m}$, $\bar{L} = 0.25\text{m}$, $T=350\text{N}$, $f = 500\text{Hz}$.

Cases	N	\mathcal{E}_1	\mathcal{E}_2	$\mathcal{E}_1 + \mathcal{E}_2$	\mathcal{E}_{abs}
Perforated ($\xi = 1, \eta = 0.5$)	10	0.13431	0.019996	0.154306	0.845694
	15	0.13416	0.0198787	0.154038	0.845962
	20	0.133337	0.0195743	0.152911	0.847089
	25	0.133337	0.0195743	0.152911	0.847089
	30	0.133337	0.0195743	0.152911	0.847089
Fibrous ($\xi = 0.5, \eta = 0.5$)	10	0.161157	0.00997624	0.171133	0.828867
	15	0.159394	0.0102694	0.169663	0.830337
	20	0.156658	0.0105658	0.167223	0.832777
	25	0.156658	0.0105658	0.167223	0.832777
	30	0.156658	0.0105658	0.167223	0.832777

TABLE 5.4: The case when elastic membranes are attached at aperture of cavities, where, $\bar{a} = \bar{h} = 0.2\text{m}$, $\bar{b} = 0.3\text{m}$, $\bar{d} = 0.1\text{m}$, $\bar{L} = 0.25\text{m}$, $T=350\text{N}$, $f = 500\text{Hz}$.

Cases	N	\mathcal{E}_1	\mathcal{E}_2	$\mathcal{E}_1 + \mathcal{E}_2$	\mathcal{E}_{abs}
Perforated ($\xi = 1, \eta = 0.5$)	10	0.217865	0.0218471	0.239712	0.760288
	15	0.212584	0.0213132	0.233898	0.766102
	20	0.210714	0.021119	0.231833	0.768167
	25	0.210714	0.021119	0.231833	0.768167
	30	0.210714	0.021119	0.231833	0.768167
Fibrous ($\xi = 0.5, \eta = 0.5$)	10	0.249567	0.0110724	0.260639	0.739361
	15	0.241169	0.0113076	0.252477	0.747523
	20	0.237378	0.0115346	0.248913	0.751087
	25	0.237378	0.0115346	0.248913	0.751087
	30	0.237378	0.0115346	0.248913	0.751087

On the other hand, comparatively less reflection with membranes pinned inside of the cavities than at the apertures of the cavities. The fact is because of the presence of extra propagating modes in pinned inside case, that help some additional power pass to pass through the cavities. It clearly reveals that the tuning of device is subject to setting of elastic components as well as the material properties of components and the dissipative materials used in the central region of the chamber.

In Figures 5.11 and 5.12 reflected, transmitted and their sum are plotted against the truncation number N. The graphs in Figure 5.11 are achieved by keeping the elastic components inside the cavities whilst for Figure 5.12 these the elastic components are attached at the apertures of cavities. In Figures 5.11 and 5.12 reflected, transmitted and their sum are plotted against the truncation number N. The graphs in Figure 5.11 are achieved by keeping the elastic components inside the cavities whilst for Figure 5.12 these the elastic components are attached at the apertures of cavities. The bounding wall surfaces of the central region are taken as the fibrous and the perforated types to get respectively (a) and (b) parts of these Figures. It can be seen that by increasing the truncation number N the scattering

components converge adequately to three decimal places even with smaller value of $N = 20$ terms.

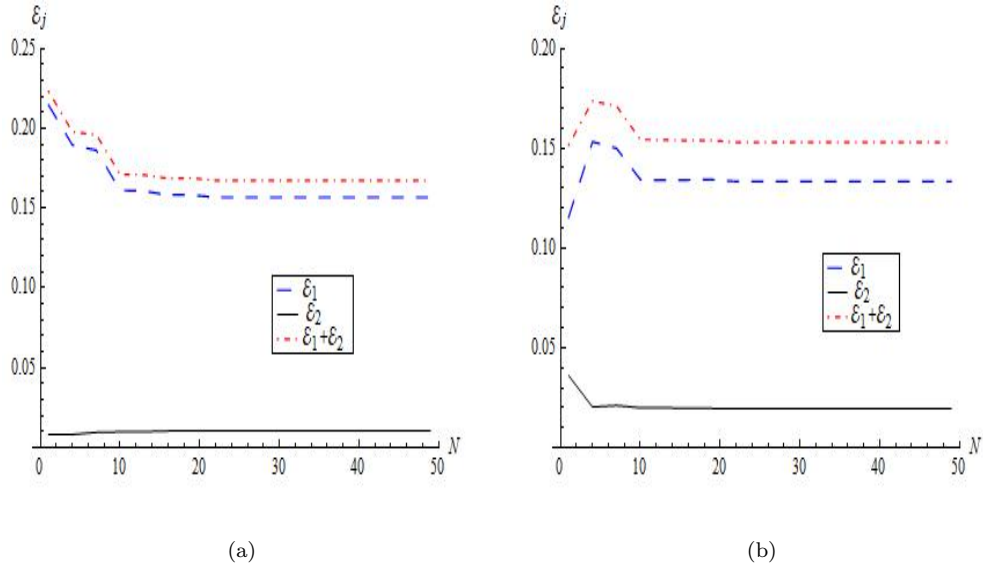


FIGURE 5.11: Energy flux against truncation number N when the elastic components are pinned inside the cavities for; ($\bar{h} > \bar{a}$) a) fibrous case and b) perforated case, where, $\bar{a} = 0.15\text{m}$, $\bar{b} = 0.3\text{m}$, $\bar{h} = 0.2\text{m}$, $\bar{d} = 0.1\text{m}$ $\bar{L} = 0.25\text{m}$, $T=350\text{N}$ and $f = 500\text{Hz}$.

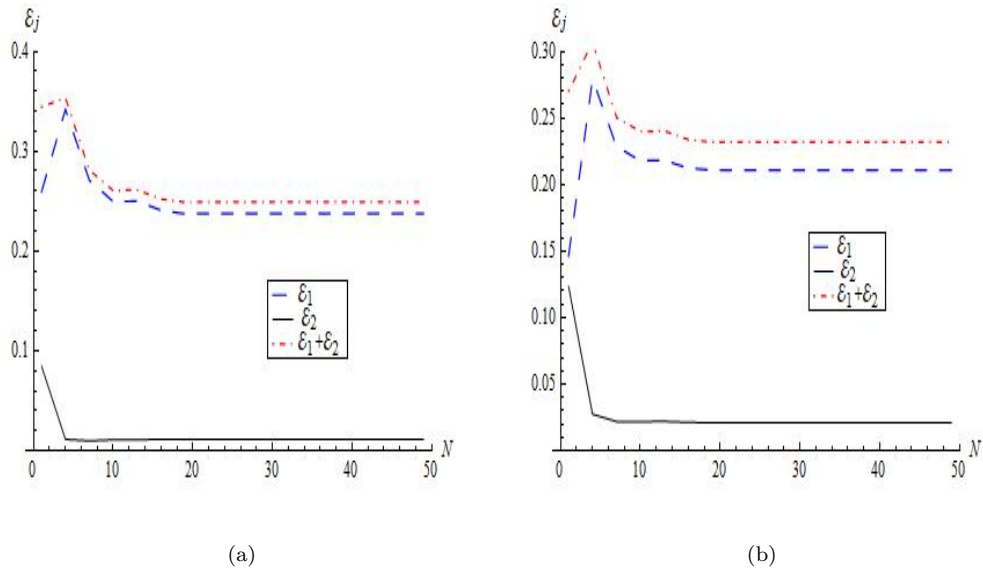
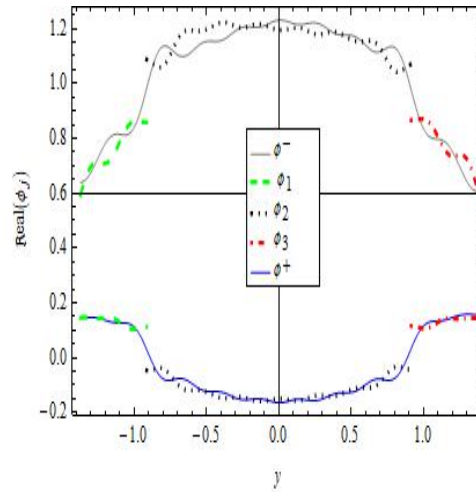
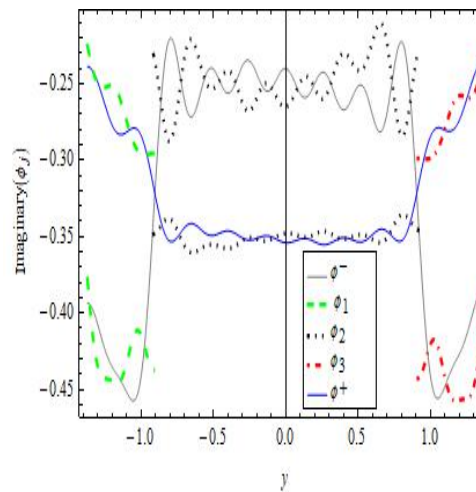


FIGURE 5.12: Energy flux against truncation number N when the elastic components are attached at the apertures of cavities ($\bar{h} = \bar{a}$) for; a) fibrous case b) perforated case, where, $\bar{a} = \bar{h} = 0.2\text{m}$, $\bar{b} = 0.3\text{m}$, $\bar{d} = 0.1\text{m}$ $\bar{L} = 0.25\text{m}$, $T=350\text{N}$ and $f = 500\text{ Hz}$.

Furthermore, the truncated form of solution is used to reconstruct the matching conditions of pressures and normal velocities at interfaces with truncation $N=20$ terms. It clearly reveals two $8(N + 1) \times 8(N + 1)$ systems of linear algebraic equations. These systems are solved numerically to determine unknown scattering amplitudes. In Figures 5.13 and 5.14, the non-dimensional form of pressures and normal velocities are shown at interfaces $x = \pm L$.



(a)

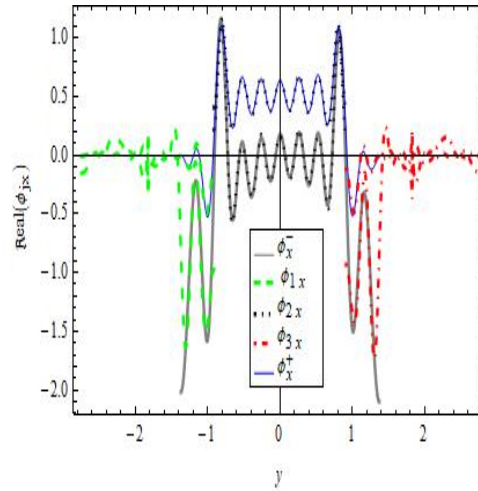


(b)

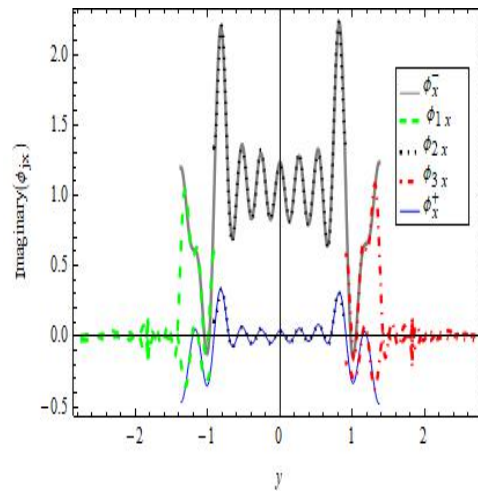
FIGURE 5.13: The real and imaginary parts of pressures against duct height at $x = \pm L$ and $N = 20$ terms.

Both the real and imaginary parts are portrayed. From these Figures it can be seen that the both real and imaginary parts of pressures and normal velocities across

the regions match exactly at interfaces as considered in matching conditions. It not only confirm the accuracy of truncated solution but also justifies the correctness of performed algebra.



(a)



(b)

FIGURE 5.14: The real and imaginary parts of velocities against duct height at $x = \pm L$ and $N = 20$ terms.

Chapter 6

Scattering Characteristics of Splitting Chamber Loaded by Elastic Components with Material Contrast

In this Chapter a generalization of the silencer investigated by Lawrie and Guled is considered. The device comprises a two-dimensional silencer in which the expansion chamber is split. The segments of the expansion chamber contain a sandwich elastic membrane and two splitters in its central region. These splitters contain bulk reacting porous materials separated from the airway by a thin perforated sheet. These perforated sheets are joined to metallic fairing and porous wall at either end of the splitter thereby lowering the static air pressure loss across the silencer. This article aims to investigate the effect of splitter fairing and the porous wall on the performance of the silencer.

The MM approach is utilized for the resolution and analysis of the physical problem. The separation of variable technique is used to determine an eigenfunction expansion of the scattering field potentials in different regions of the waveguide

that contain unknown modal coefficients. Later on, these unknowns are determined from the matching conditions on the pressure and normal velocities at the interface. In the case where the duct has flexible bounding properties (such as the membranes or elastic plates), the pressure or normal velocity modes prove to be non-orthogonal and thus yield a non-Sturm-Liouville (non-SL) system. Consequently, the use of generalized orthogonal characteristics becomes indispensable in elastic membrane-containing regions.

The study is sorted in the following sections. The formulation of the relevant boundary value problem is discussed in Section 6.1. A MM approach-based solution is presented in Section 6.2. The numerical simulations and the discussion on the results are provided in Section 6.3

6.1 Problem Formulation

The primary goal of the current study is to analyze the acoustic attenuation performance of a physical silencer whose expansion chamber is loaded with thin elastic components backed by slender cavities and a dissipative material. The silencer is excited with fundamental or incident modes and the performance of the splitter silencer is analyzed. A two-dimensional prototype geometry is displayed in Figure 6.1.

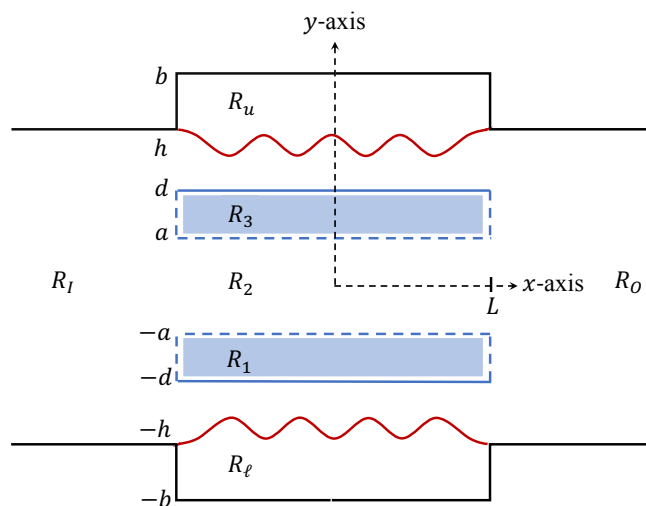


FIGURE 6.1: The geometry of physical problem.

For convenience, the problem is dealt with in a non-dimensional setting using the scales and transmissions defined in Chapter 2.

The acoustic velocity potential, denoted by $\Phi(x, y; t)$, is assumed to be time-harmonic, i.e., $\Phi(x, y; t) = \phi(x, y)e^{-i\omega t}$, where $i = \sqrt{-1}$ throughout this article. The non-dimensional time-independent velocity potential $\phi(x, y)$ in the duct satisfies Helmholtz equation

$$(\nabla^2 + \tilde{\Gamma})\phi(x, y) = 0, \tag{6.1}$$

where

$$\tilde{\Gamma} := \begin{cases} 1, & \text{if the inside region contains a compressible fluid,} \\ \Gamma, & \text{if the inside region contains a porous material.} \end{cases}$$

The guiding structure consists of three sub-domains: the inlet, the outlet, and the expansion chamber. The expansion chamber is further divided into upper, lower, and central regions (see Figure 6.1). The bounding characteristics and traveling-wave formulations in different regions of the structure are discussed in the subsequent subsections.

6.1.1 Inlet and Outlet

The silencer consist of inlet region $R_I := \{(\bar{x}, \bar{y}) \in \mathbb{R}^2 \mid \bar{x} < -\bar{L}, |\bar{y}| \leq \bar{h}\}$ and the outlet region $R_O := \{(\bar{x}, \bar{y}) \in \mathbb{R}^2 \mid \bar{x} > \bar{L}, |\bar{y}| \leq \bar{h}\}$, respectively. A multi-mode sound source propagating in the positive x direction in region R_I excites the silencer. The duct is terminated anechoically in region R_O . The duct walls in these regions are assumed to be rigid. The traveling wave formulation in R_I and R_O can be expressed as

$$\phi_n^\pm(x, y) = Y_n(y)e^{\pm i\sigma_n x}, \quad -h \leq y \leq h,$$

where $\sigma_n = \sqrt{1 - n^2\pi^2/4h^2}$ for $n = 0, 1, 2, \dots$, and $Y_n(y)$ are eigenfunctions which satisfy

$$\frac{dY_n}{dy} = 0, \quad y = \pm h. \quad (6.2)$$

Equation (6.1), together with (6.2), yields $Y_n(y) = \cos(n\pi(y + h)/2h)$. These eigenfunctions satisfy usual OR, i.e.,

$$\int_{-h}^h Y_n(y)Y_m(y)dy = h\delta_{mn}\epsilon_m, \quad (6.3)$$

where δ_{mn} is the Kronecker's delta function and $\epsilon_m = 1$ if $m \neq 0$, otherwise $\epsilon_0 = 2$.

6.1.2 Expansion Chamber

The finite expansion chamber of the silencer is partitioned into the upper, lower, and central regions. The characteristics and traveling-wave formulations in these regions are discussed separately.

6.1.2.1 Upper and Lower Regions

The expansion chamber consist of $R_u := \{(\bar{x}, \bar{y}) \in \mathbb{R}^2 \mid |\bar{x}| \leq \bar{L}, \bar{d} \leq \bar{y} \leq \bar{b}\}$ upper region and $R_\ell := \{(\bar{x}, \bar{y}) \in \mathbb{R}^2 \mid |\bar{x}| \leq \bar{L}, -\bar{b} \leq \bar{y} \leq -\bar{d}\}$ lower region, respectively. The segments $\bar{y} = \bar{h}$ and $\bar{y} = -\bar{h}$ embedded, respectively, in the upper and lower sections are elastic membranes having edges connected to the inlet and outlet regions. The membrane boundaries are characterized by the transmission conditions

$$\left(\frac{\partial^2}{\partial x^2} + \mu^2\right) \frac{\partial \phi}{\partial y} = \mp \alpha \left[\phi\right]_{y=\mp h^\pm}^{y=\mp h^\mp}, \quad |x| < L, \quad y = \pm h, \quad (6.4)$$

$$\frac{\partial \phi}{\partial y}(x, \pm h^\mp) = \frac{\partial \phi}{\partial y}(x, \pm h^\pm). \quad (6.5)$$

We specify that the quantities $\mu = c/c_m$ and $\alpha = \omega^2\rho/(Tk^3)$ in (6.4)-(6.5) are, respectively, the non-dimensional *in vacuo* membrane wave-number and the fluid loading parameter where ρ is the density and c is sound speed of the compressible

fluid loaded inside the waveguide. Here, $c_m = T/\rho_m$ is the *in vacuo* wave speed which is defined in terms of the membrane density ρ_m and tension T .

Let $\phi_n^\ell(x, y)$ and $\phi_n^u(x, y)$ represent the traveling wave forms of n^{th} eigenmode, where superscripts ℓ and u specify that the scattered fields correspond to the lower and upper regions, respectively. Then,

$$\phi_n^\ell(x, y) = U_n(y)e^{\pm i\nu_n x}, \quad -b \leq y \leq -d,$$

$$\phi_n^u(x, y) = V_n(y)e^{\pm i\nu_n x}, \quad d \leq y \leq b,$$

where $\nu_n = \sqrt{1 + \gamma_n^2}$ is defined in terms of the eigenvalues γ_n , and $U_n(y)$ and $V_n(y)$ are the eigenfunctions in the lower and upper regions, respectively. If we set

$$U_n(y) := \begin{cases} U_{1n}(y), & -h \leq y \leq -d, \\ U_{2n}(y), & -b \leq y < -h, \end{cases}$$

$$V_n(y) := \begin{cases} V_{1n}(y), & d \leq y \leq h, \\ V_{2n}(y), & h < y \leq b, \end{cases}$$

then these eigenfunctions satisfy the transverse boundary conditions

$$\begin{cases} \frac{dU_{1n}}{dy} = 0, & y = -d, \\ \frac{dU_{2n}}{dy} = 0, & y = -b, \\ \frac{dV_{1n}}{dy} = 0, & y = d, \\ \frac{dV_{2n}}{dy} = 0, & y = b, \end{cases}$$

along with the embedded membrane conditions

$$\begin{cases} (-\nu_n^2 + \mu^2) \frac{dU_{1n}}{dy} = -\alpha U_n \Big|_{y=-h^+}^{y=-h^-}, & y = -h, \\ (-\nu_n^2 + \mu^2) \frac{dV_{1n}}{dy} = \alpha V_n \Big|_{y=h^-}^{y=h^+}, & y = h, \\ \frac{dU_{1n}}{dy} \Big|_{y=-h^+} = \frac{dU_{2n}}{dy} \Big|_{y=-h^-}, \\ \frac{dV_{1n}}{dy} \Big|_{y=h^-} = \frac{dV_{2n}}{dy} \Big|_{y=h^+}. \end{cases} \quad (6.6)$$

Besides, conditions are imposed at the edges of the membranes. These edge conditions not only ensure the uniqueness of the solution but also characterize the physical behavior of the membranes at the joints. The zero-displacement conditions at semi-infinite edges are given by

$$\frac{\partial}{\partial y} \phi_n^\ell(x, y) = 0, \quad x = \pm L, \quad y = -h, \quad (6.7)$$

$$\frac{\partial}{\partial y} \phi_n^u(x, y) = 0, \quad x = \pm L, \quad y = h. \quad (6.8)$$

Notice that the eigenmodes due to the sandwiched membranes in the upper and lower regions are of two forms; coupled modes and uncoupled modes. The eigenfunctions corresponding to the coupled and uncoupled duct modes take the form

$$\begin{cases} U_{1n}(y) = \cosh(\gamma_n (y + d)), \\ U_{2n}(y) = \Upsilon_n \cosh(\gamma_n (b + y)), \\ V_{1n}(y) = \cosh(\gamma_n (y - d)), \\ V_{2n}(y) = \Upsilon_n \cosh(\gamma_n (b - y)), \end{cases}$$

where

$$\Upsilon_n = \begin{cases} \frac{-\sinh(\gamma_n (h - d))}{\sinh(\gamma_n (b - h))}, & n \neq 1, & \gamma_n \neq \frac{in\pi q}{p(h - d)}, \\ (-1)^n, & n \neq 1, & \gamma_n = \frac{in\pi q}{p(h - d)}, \\ 1, & n = 1. \end{cases}$$

Here p and q are integers, and the eigenvalue γ_n satisfies the dispersion relation

$$(\gamma_n^2 + 1 - \mu^2)\gamma_n \sinh(\gamma_n(h - d)) - \alpha \frac{\sinh(\gamma_n(b - d))}{\sinh(\gamma_n(b - h))} = 0. \tag{6.9}$$

There are infinitely many values of γ_n that satisfy (6.9). These values can be found numerically. The solution set contains one real root $\gamma_0 > 0$ and an infinite number of imaginary roots such that for each root γ_n , for $n = 1, 2, \dots$, there is another root $-\gamma_n$. These roots are arranged by employing the convention that the real root appears first and then the positive imaginary roots are sorted in ascending order of their magnitude. However, the negative imaginary roots are omitted.

In addition to the fluid-structure coupled modes, there are other wave-forms in membrane containing-regions such as the plane acoustic waves of the form e^{ix} . These wave-forms always exist in membrane bounded-regions without interaction with the membranes. They are the trivial solutions of the system of equations (6.1) and (6.6). Other wave-forms of interest are the subset of usual rigid duct modes; those that have zero velocity normal to the membrane at $y = \pm h$. These are known as the uncoupled modes and they exist only if the duct height $(b - d)$ can be expressed in the form $(b - d) = p(h - d)/q$ for some integers p and q . The eigenvalues for uncoupled modes are $\gamma_1 = 0$ (which is always present) and $\gamma_n = in\pi q/p(h - d)$, for $n = p, 2p, 3p, \dots$, (which is present only when $(b - d)$ is of the form $p(h - d)/q$). Notice that these wave-numbers are not roots of the given dispersion relation.

It is important to note that the set of all values γ_n , for $n = 0, 1, 2, \dots$, includes all admissible eigenvalues for both fluid-membrane coupled and uncoupled modes, ordered as γ_0, γ_1 , and then by increasing the imaginary parts in the magnitude. The functions U_n and V_n , for $n = 0, 1, 2, \dots$, satisfy generalized OR

$$\begin{cases} \alpha \int_{-b}^{-d} U_n(y)U_m(y)dy = M_m\delta_{mn} - U'_n(-h)U'_m(-h), \\ \alpha \int_d^b V_n(y)V_m(y)dy = M_m\delta_{mn} - V'_n(h)V'_m(h), \end{cases} \tag{6.10}$$

where

$$M_m = \begin{cases} \frac{\alpha}{2} \{ \tilde{\varepsilon}_m (h - d) + \Upsilon_m^2 \tilde{\varepsilon}_m (b - h) \}, & m \neq 1, \quad \gamma_m \neq \frac{im\pi q}{p(h-d)}, \\ \frac{\alpha (b - d)}{2}, & m \neq 1, \quad \gamma_m = \frac{im\pi q}{p(h-d)}, \\ \alpha (b - d), & m = 1, \end{cases}$$

with

$$\tilde{\varepsilon}_m(x) := x + \frac{2\gamma_m^2 + \nu_m^2 - \mu^2}{2\gamma_m(\nu_m^2 - \mu^2)} \sinh(2\gamma_m x).$$

6.1.2.2 Central Region

The central region consists of three sub-domains,

$$R_1 := \{ (\bar{x}, \bar{y}) \in \mathbb{R}^2 \mid |\bar{x}| \leq \bar{L}, -\bar{d} \leq \bar{y} \leq -\bar{a} \},$$

$$R_2 := \{ (\bar{x}, \bar{y}) \in \mathbb{R}^2 \mid |\bar{x}| \leq \bar{L}, -\bar{a} \leq \bar{y} \leq \bar{a} \},$$

$$R_3 := \{ (\bar{x}, \bar{y}) \in \mathbb{R}^2 \mid |\bar{x}| \leq \bar{L}, \bar{a} \leq \bar{y} \leq \bar{d} \}.$$

Regions R_1 and R_3 are loaded with a porous material and are separated from the air containing region R_2 by means of porous linings at $\bar{y} = \pm\bar{a}$. Regions R_1 and R_3 are terminated by the line segments

$$\ell_1^\pm : \{ (\bar{x}, \bar{y}) \in \mathbb{R}^2 \mid \bar{x} = \pm\bar{L}, -\bar{d} \leq \bar{y} \leq -\bar{a} \}, \tag{6.11}$$

$$\ell_3^\pm : \{ (\bar{x}, \bar{y}) \in \mathbb{R}^2 \mid \bar{x} = \pm\bar{L}, \bar{a} \leq \bar{y} \leq \bar{d} \}, \tag{6.12}$$

which are considered to be either porous walls (see Figure 6.2(a)) or rigid metallic fairings (see Figure 6.2(b)). The compressible fluid is loaded inside the waveguide except in R_2 whose outer region is contained in *vacuo*. The physical configuration

of the central region of the expansion chamber is shown in Figure 6.2. Let $\phi_n^c(x, y)$

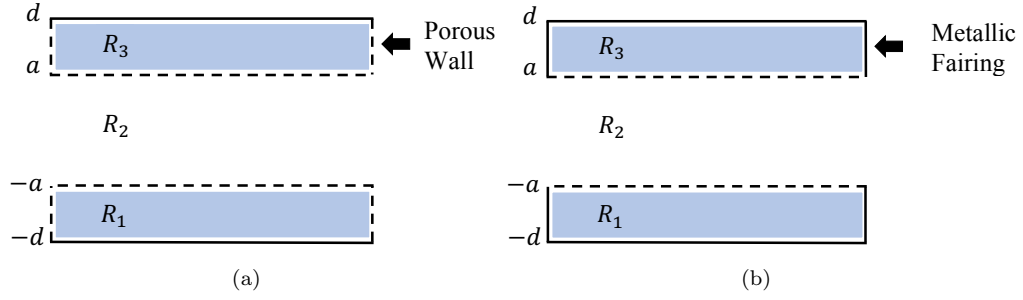


FIGURE 6.2: Configuration of the central region of the expansion chamber.

represent the traveling wave form of the n^{th} eigenmode corresponding to the central region. Then, ϕ_n^c is of the form

$$\phi_n^c(x, y) = Z_n(y)e^{\pm is_n x}, \quad -d < y < d,$$

with

$$Z_n(y) := \begin{cases} Z_{1n}, & -d < y < -a, \\ Z_{2n}, & -a < y < a, \\ Z_{3n}, & a < y < d, \end{cases}$$

where the wave-numbers s_n are the roots of a dispersion relation (see Eq. (6.16) below) and Z_{jn} are the eigenfunctions of the central regions R_j , for $j = 1, 2, 3$, as depicted in Figure 6.2. These functions satisfy the transverse boundary and continuity conditions

$$\left\{ \begin{array}{ll} \frac{dZ_{1n}}{dy} = 0, & y = -d^+, \\ \frac{dZ_{3n}}{dy} = 0, & y = d^-, \\ \frac{dZ_{2n}}{dy} = \frac{dZ_{1n}}{dy}, & y = -a, \\ Z_{2n}(y) = \beta Z_{1n}(y), & y = -a, \\ \frac{dZ_{2n}}{dy} = \frac{dZ_{3n}}{dy}, & y = a, \\ Z_{2n}(y) = \beta Z_{3n}(y), & y = a. \end{array} \right.$$

It is specified that $\beta = \rho(\omega)/\rho_0$ is normalised complex density of the porous material and is defined in terms of the equivalent complex density of the porous material $\rho(\omega)$ and the density of the air ρ_0 (refer, for instance, to [77]).

The functions Z_{jn} are given by

$$\begin{cases} Z_{1n}(y)\eta_n \cosh(\lambda_n(y+d)), \\ Z_{2n}(y) = \lambda_n \sinh(\lambda_n(d-a)) \sinh(\eta_n(y+a)) + \eta_n\beta \cosh(\lambda_n(d-a)) \cosh(\eta_n(y+a)), \\ Z_{3n}(y) = \left(-\eta_n \cosh(2\eta_na) - \frac{\eta_n^2}{\lambda_n}\beta \coth(\lambda_n(d-a)) \sinh(2\eta_na)\right) \cosh(\lambda_n(y-d)), \end{cases} \quad (6.13)$$

where $\lambda_n = \sqrt{s_n^2 - \Gamma_n^2}$ and $\eta_n = \sqrt{s_n^2 - 1}$. Moreover, Z_{jn} satisfy OR

$$\beta \int_{-d}^{-a} Z_{1n}(y)Z_{1m}(y)dy + \int_{-a}^a Z_{2n}(y)Z_{2m}(y)dy + \beta \int_a^d Z_{3n}(y)Z_{3m}(y)dy = J_m\delta_{mn}, \quad (6.14)$$

where

$$J_m = \beta \int_{-d}^{-a} Z_{1m}^2(y)dy + \int_{-a}^a Z_{2m}^2(y)dy + \beta \int_a^d Z_{3m}^2(y)dy. \quad (6.15)$$

The quantities s_n , for $n = 0, 1, 2, \dots$, can be determined from the dispersion relation

$$\begin{aligned} I(s) := & 2\lambda_n\eta_n\beta \sinh(\lambda_n(d-a)) \cosh(\eta_n(2a)) \cosh(\lambda_n(d-a)) \\ & + \sinh(\eta_n(2a)) (\lambda_n^2 \sinh^2(\lambda_n(d-a)) + \eta_n^2\beta^2 \cosh^2(\lambda_n(d-a))) = 0. \end{aligned} \quad (6.16)$$

The dispersion relation (6.16) may be solved for the wave-number s_n using any root-finding technique such as Newton-Raphson or secant method. The success of the analytic MM scheme depends on the accurate computation of all the required roots. It is a challenging task for complex roots and is sensitive to the choice of the initial guess supplied to the root-finding algorithm. At low Helmholtz numbers, the low-frequency approximations of the dispersion relation may be adopted for selecting appropriate initial guesses. One may also employ the *argument principle* to ascertain that all the roots in a specified region of the complex plane have been

found. However, searching for the roots in the complex plane is a laborious and cumbersome process, especially, at high Helmholtz numbers where a large number of roots must be found. Towards this end, it is common to use a successfully located root to provide the initial guess at the next, say, frequency interval, and to track a root through the complex plane as the frequency is altered.

6.2 Mode-Matching (MM) Solution

We first find the eigenfunction expansion forms of the propagating and scattering modes in different duct regions to formulate the MM solution. For expansion chamber and inlet/outlet regions, these expansions of the velocity potentials are defined as

$$\phi^-(x, y) = e^{i(x+L)} + \sum_{n=0}^{\infty} A_n Y_n(y) e^{-i\sigma_n(x+L)}, \quad (6.17)$$

$$\phi^\ell(x, y) = \sum_{n=0}^{\infty} (B_n e^{-i\nu_n x} + C_n e^{i\nu_n x}) U_n(y), \quad (6.18)$$

$$\phi^c(x, y) = \sum_{n=0}^{\infty} (D_n e^{-is_n x} + E_n e^{is_n x}) Z_n(y), \quad (6.19)$$

$$\phi^u(x, y) = \sum_{n=0}^{\infty} (F_n e^{-i\nu_n x} + G_n e^{i\nu_n x}) V_n(y), \quad (6.20)$$

$$\phi^+(x, y) = \sum_{n=0}^{\infty} H_n Y_n(y) e^{i\sigma_n(x-L)}, \quad (6.21)$$

where A_n, B_n, \dots, H_n are the amplitudes of n^{th} scattering modes in the waveguide regions. The amplitudes are found by matching the fluid pressure and normal velocity at the interfaces $x = \pm L$.

6.2.1 Porous Wall

When the terminal line segments ℓ_1^\pm and ℓ_3^\pm , defined in (6.11)-(6.12), are considered to be porous walls, the coefficients of expansion chamber regions are determined by

the normal velocity conditions while inlet/outlet duct coefficients are determined by the normal pressure conditions. Here,

$$\phi^c(\pm L, y) = \begin{cases} \beta Z_{1n}(y), & -d \leq y \leq -a, \\ Z_{2n}(y), & -a \leq y \leq a, \\ \beta Z_{3n}(y), & a \leq y \leq d, \end{cases}$$

and normal velocities conditions at matching interfaces are defined as

$$\frac{\partial \phi^\ell}{\partial x}(\pm L, y) = \begin{cases} 0, & -b \leq y \leq -h, \\ \frac{\partial \phi^\pm}{\partial x}(\pm L, y), & -h \leq y \leq -d. \end{cases} \quad (6.22)$$

Multiplying (6.22) by $\alpha U_n(y)$ and integrating over $(-b, -d)$ furnishes

$$\int_{-b}^{-d} \alpha U_n(y) \frac{\partial \phi^\ell}{\partial x}(\pm L, y) dy = \alpha \int_{-h}^{-d} U_n(y) \frac{\partial \phi^\pm}{\partial x}(\pm L, y) dy. \quad (6.23)$$

Using (6.17), (6.18), and (6.21) in (6.23) and then invoking OR (6.10), we arrive at the relationships

$$B_m e^{i\nu_m L} - C_m e^{-i\nu_m L} = \frac{U'_m(-h)}{\nu_m M_m} e_1 - \frac{\alpha}{\nu_m M_m} \left[Q_{m0} - \sum_{n=0}^{\infty} A_n \sigma_n Q_{mn} \right], \quad (6.24)$$

$$B_m e^{-i\nu_m L} - C_m e^{i\nu_m L} = \frac{U'_m(-h)}{\nu_m M_m} e_2 - \frac{\alpha}{\nu_m M_m} \sum_{n=0}^{\infty} H_n \sigma_n Q_{mn}, \quad (6.25)$$

with

$$Q_{mn} := \int_{-h}^{-d} U_m(y) \cos\left(\frac{n\pi}{2h}(y+h)\right) dy. \quad (6.26)$$

Addition and subtraction of (6.24) and (6.25) yield

$$\Xi_m^\pm = \frac{1}{2\zeta^\pm(\nu_m L)\nu_m M_m} \left[U'_m(-h)\Theta^\mp - \alpha Q_{m0} + \alpha \sum_{n=0}^{\infty} \psi_n^\pm \sigma_n Q_{mn} \right], \quad (6.27)$$

where

$$\begin{aligned} \psi_m^\pm &:= (A_m \pm H_m), & \Xi_m^\pm &:= (B_m \pm C_m), & \Theta^\pm &:= (e_1 \pm e_2), \\ \zeta^+(x) &:= i \sin x, & \zeta^-(x) &:= \cos x, \\ e_1 &:= -i\phi_{xy}^\ell(-L, -h), & e_2 &:= -i\phi_{xy}^\ell(L, -h). \end{aligned}$$

To determine constants e_1 and e_2 , we use the edge conditions in (6.7). Towards this end, we multiply (6.27) on both sides with $2U'_m(-h)\zeta^\mp(\nu_m L)$, take sum over m , and simplify the resulting equation with the help of edge condition (6.7). This renders

$$\Theta^\mp = \frac{\alpha}{S_1^\mp} \sum_{m=0}^{\infty} \frac{U'_m(-h)\kappa^\mp(\nu_m L)}{\nu_m M_m} \left[Q_{m0} - \sum_{n=0}^{\infty} \psi_n^\pm \sigma_n Q_{mn} \right], \quad (6.28)$$

where $\kappa^+(x) := i \tan(x)$, $\kappa^-(x)\kappa^+(x) := 1$ and

$$S_1^\mp := \sum_{m=0}^{\infty} \frac{[U'_m(-h)]^2 \kappa^\mp(\nu_m L)}{\nu_m M_m}.$$

Recall that normal velocities conditions at matching interfaces are

$$\frac{\partial \phi^c}{\partial x}(\pm L, y) = \frac{\partial \phi^\pm}{\partial x}(\pm L, y), \quad -d \leq y \leq d. \quad (6.29)$$

On multiplying (6.29) by $Z_n(y)$ and integrating over $(-d, d)$, we get

$$\int_{-d}^d Z_n(y) \frac{\partial \phi^c}{\partial x}(\pm L, y) dy = \int_{-d}^d Z_n(y) \frac{\partial \phi^\pm}{\partial x}(\pm L, y) dy. \quad (6.30)$$

Substituting (6.17), (6.19), and (6.21) in (6.30) and then making use of OR (6.14), it is found that

$$D_m e^{is_m L} - E_m e^{-is_m L} = -\frac{1}{s_m J_m} \left[R_{m0} - \sum_{n=0}^{\infty} A_n \sigma_n R_{mn} \right], \quad (6.31)$$

$$D_m e^{-is_m L} - E_m e^{is_m L} = -\frac{1}{s_m J_m} \left[\sum_{n=0}^{\infty} H_n \sigma_n R_{mn} \right]. \quad (6.32)$$

Consequently, the addition and subtraction of (6.31) and (6.32) yield

$$\chi_m^\pm = \frac{1}{2\zeta^\pm(s_m L)s_m J_m} \left[-R_{m0} + \sum_{n=0}^{\infty} \psi_n^\pm \sigma_n R_{mn} \right], \quad (6.33)$$

where

$$\chi_m^\pm := (D_m \pm E_m) \quad \text{and} \quad R_{mn} := \int_{-d}^d Z_m(y) \cos\left(\frac{n\pi}{2h}(y+h)\right) dy. \quad (6.34)$$

Now, multiplying normal velocities conditions at matching interfaces,

$$\frac{\partial \phi^u}{\partial x}(\pm L, y) = \begin{cases} \frac{\partial \phi^\pm}{\partial x}(\pm L, y), & d \leq y \leq h, \\ 0, & h \leq y \leq b, \end{cases} \quad (6.35)$$

by $\alpha V_n(y)$ and integrating over (d, b) , we arrive at

$$\int_d^b \alpha V_n(y) \frac{\partial \phi^u}{\partial x}(\pm L, y) dy = \alpha \int_d^h V_n(y) \frac{\partial \phi^\pm}{\partial x}(\pm L, y) dy. \quad (6.36)$$

As before, substituting (6.17), (6.20), and (6.21) in (6.36) and then making use of OR (6.10), we get

$$F_m e^{i\nu_m L} - G_m e^{-i\nu_m L} = \frac{V'_m(h)}{\nu_m M_m} e_3 - \frac{\alpha}{\nu_m M_m} \left[P_{m0} - \sum_{n=0}^{\infty} A_n \sigma_n P_{mn} \right], \quad (6.37)$$

$$F_m e^{-i\nu_m L} - G_m e^{i\nu_m L} = \frac{V'_m(h)}{\nu_m M_m} e_4 - \frac{\alpha}{\nu_m M_m} \sum_{n=0}^{\infty} H_n \sigma_n P_{mn}, \quad (6.38)$$

where

$$P_{mn} := \tilde{\varepsilon}_m \int_d^h V_m(y) \cos\left(\frac{n\pi}{2h}(y+h)\right) dy. \quad (6.39)$$

This time the addition and subtraction of (6.37) and (6.38) yield

$$\varpi_m^\pm = \frac{1}{2\zeta^\pm(\nu_m L)\nu_m M_m} \left[V'_m(h)\varphi^\mp - \alpha P_{m0} + \alpha \sum_{n=0}^{\infty} \psi_n^\pm \sigma_n P_{mn} \right], \quad (6.40)$$

with $\varpi_m^\pm := (F_m \pm G_m)$ and $\varphi^\pm := (e_3 \pm e_4)$. Here, $e_3 := -i\phi_{xy}^u(-L, h)$ and $e_4 := -i\phi_{xy}^u(L, h)$ are constants to be determined. Towards this end, we make use

of edge conditions (6.8). Accordingly, we multiply (6.40) by $2V'_m(h)\zeta^\mp(\nu_m L)$, take sum over m , and simplify the resulting equation with the help of edge conditions (6.8). This yields

$$\varphi^\mp = \frac{\alpha}{S_2^\mp} \sum_{m=0}^{\infty} \frac{V'_m(h)\kappa^\mp(\nu_m L)}{\nu_m M_m} \left[P_{m0} - \sum_{n=0}^{\infty} \psi_n^\pm \sigma_n P_{mn} \right], \quad (6.41)$$

where

$$S_2^\mp := \sum_{m=0}^{\infty} \frac{[V'_m(h)]^2 \kappa^\mp(\nu_m L)}{\nu_m M_m}.$$

Finally, we match the pressure modes across the duct regions at interfaces. The matching conditions for these modes suggest that

$$\phi^\pm(\pm L, y) = \begin{cases} \phi^\ell(\pm L, y), & -h \leq y \leq -d, \\ \phi^c(\pm L, y), & -d \leq y \leq d, \\ \phi^u(\pm L, y), & d \leq y \leq h. \end{cases} \quad (6.42)$$

Multiplying (6.42) by $Y_n(y)$ and integrating over $(-h, h)$ yield

$$\begin{aligned} \int_{-h}^h Y_n(y) \phi^\pm(\pm L, y) dy &= \int_{-h}^{-d} \phi^\ell(\pm L, y) Y_n(y) dy + \int_{-d}^d \phi^c(\pm L, y) Y_n(y) dy \\ &+ \int_d^h \phi^u(\pm L, y) Y_n(y) dy. \end{aligned} \quad (6.43)$$

Substituting (6.17)-(6.21) in (6.43) and making use of orthogonality relation (6.3),

it is found that

$$\begin{aligned} A_m &= -\delta_{m0} + \frac{1}{h\epsilon_m} \sum_{n=0}^{\infty} \left\{ (B_n e^{i\nu_n L} + C_n e^{-i\nu_n L}) Q_{nm} + (D_n e^{is_n L} + E_n e^{-is_n L}) R_{nm} \right. \\ &\quad \left. + (F_n e^{i\nu_n L} + G_n e^{-i\nu_n L}) P_{nm} \right\}, \end{aligned} \quad (6.44)$$

$$\begin{aligned} H_m &= \frac{1}{h\epsilon_m} \sum_{n=0}^{\infty} \left\{ (B_n e^{-i\nu_n L} + C_n e^{i\nu_n L}) Q_{nm} + (D_n e^{-is_n L} + E_n e^{is_n L}) R_{nm} \right. \\ &\quad \left. + (F_n e^{-i\nu_n L} + G_n e^{i\nu_n L}) P_{nm} \right\}. \end{aligned} \quad (6.45)$$

The addition and subtraction of (6.44) and (6.45) yield

$$\psi_m^\pm = -\delta_{m0} + \frac{2}{h\epsilon_m} \sum_{n=0}^{\infty} \left\{ \Xi_n^\pm Q_{nm} \zeta^\mp(\nu_n L) + \chi_n^\pm R_{nm} \zeta^\mp(s_n L) + \varpi_n^\pm P_{nm} \zeta^\mp(\nu_n L) \right\}. \tag{6.46}$$

This entire procedure furnishes an infinite system of linear algebraic equations formed by the (6.27), (6.33), (6.40), and (6.46) in the unknown quantities Ξ_n^\pm , χ_n^\pm , ϖ_n^\pm , and ψ_m^\pm . To solve the problem numerically, we only consider a finite number of equations in finite number of unknowns and neglect the rest. Specifically, we retain the terms with $n = m = 0, 1, 2, \dots, N$ where $N \in \mathbb{N}$ is a sufficiently large truncation parameter. Subsequently, we solve the truncated finite system, simultaneously.

6.2.2 Metallic Fairing

In metallic fairing case, the coefficients of expansion chamber regions are found by using the normal pressure conditions while the inlet and outlet duct coefficients are found by using the normal velocity conditions. With metallic faring, $Z_{1n}(y) = 0 = Z_{3n}(y)$ and

$$\phi^c(\pm L, y) = \begin{cases} 0, & -d \leq y \leq -a, \\ Z_{2n}(y), & -a \leq y \leq a, \\ 0, & a \leq y \leq d. \end{cases}$$

We multiply the continuity conditions of pressures at matching interfaces,

$$\phi^\ell(\pm L, y) = \begin{cases} 0, & -b \leq y \leq -h, \\ \phi^\pm(\pm L, y), & -h \leq y \leq -d, \end{cases} \tag{6.47}$$

by $\alpha U_n(y)$ and integrate over $(-b, -d)$ to get

$$\int_{-b}^{-d} \alpha U_n(y) \phi^\ell(\pm L, y) dy = \alpha \int_{-h}^{-d} U_n(y) \phi^\pm(\pm L, y) dy. \tag{6.48}$$

Substituting (6.17), (6.18), and (6.21) into (6.48) and making use of relation (6.10), we get

$$B_m e^{i\nu_m L} + C_m e^{-i\nu_m L} = \frac{U'_m(-h)}{M_m} e_1 + \frac{\alpha}{M_m} \left[Q_{m0} + \sum_{n=0}^{\infty} A_n Q_{mn} \right], \quad (6.49)$$

$$B_m e^{-i\nu_m L} + C_m e^{i\nu_m L} = \frac{U'_m(-h)}{M_m} e_2 + \frac{\alpha}{M_m} \sum_{n=0}^{\infty} H_n Q_{mn}. \quad (6.50)$$

Then, the addition and subtraction of (6.49) and (6.50) yield

$$\Xi_m^{\pm} = \frac{1}{2\zeta^{\pm}(\nu_m L)M_m} \left[U'_m(-h)\Theta^{\mp} + \alpha Q_{m0} + \alpha \sum_{n=0}^{\infty} \psi_n^{\pm} Q_{mn} \right]. \quad (6.51)$$

Thanks to the edge condition (6.7), it is found that $e_1 = 0 = e_2$ and consequently, $\Theta^{\pm} = 0$.

Now, multiplying the continuity conditions of pressure modes at matching interfaces,

$$\phi^c(\pm L, y) = \begin{cases} 0, & d \leq y \leq -a, \\ \phi^{\pm}(\pm L, y), & -a \leq y \leq a, \\ 0, & a \leq y \leq d, \end{cases} \quad (6.52)$$

by $Z_n(y)$ and integrating over $(-d, d)$, we get

$$\int_{-d}^d Z_n(y) \phi^c(\pm L, y) dy = \int_{-a}^a Z_n(y) \phi^{\pm}(\pm L, y) dy. \quad (6.53)$$

Substituting(6.17), (6.19), and (6.21) into (6.53) and invoking relation (6.14), we obtain

$$D_m e^{is_m L} + E_m e^{-is_m L} = \frac{1}{J_m} \left[R_{m0} + \sum_{n=0}^{\infty} A_n R_{mn} \right], \quad (6.54)$$

$$D_m e^{-is_m L} + E_m e^{is_m L} = \frac{1}{J_m} \left[\sum_{n=0}^{\infty} H_n R_{mn} \right]. \quad (6.55)$$

Therefore, the addition and subtraction of (6.54) and (6.55) yield

$$\chi_m^\pm = \frac{1}{2\zeta^\pm(s_m L)J_m} \left[R_{m0} + \sum_{n=0}^{\infty} \psi_n^\pm R_{mn} \right]. \quad (6.56)$$

Further, by multiplying the continuity conditions of pressure modes at matching interfaces,

$$\phi^u(\pm L, y) = \begin{cases} \phi^\pm(\pm L, y), & d \leq y \leq h, \\ 0, & h \leq y \leq b, \end{cases} \quad (6.57)$$

by $\alpha V_n(y)$ and integrating over (d, b) , we get

$$\int_d^b \alpha V_n(y) \phi^u(\pm L, y) dy = \alpha \int_d^h V_n(y) \phi^\pm(\pm L, y) dy. \quad (6.58)$$

Substitution of (6.17), (6.20), and (6.21) into (6.58) together with relation (6.10) leads to

$$F_m e^{i\nu_m L} + G_m e^{-i\nu_m L} = \frac{V'_m(h)}{M_m} e_3 + \frac{\alpha}{M_m} \left[P_{m0} + \sum_{n=0}^{\infty} A_n P_{mn} \right], \quad (6.59)$$

$$F_m e^{-i\nu_m L} + G_m e^{i\nu_m L} = \frac{V'_m(h)}{M_m} e_4 - \frac{\alpha}{M_m} \sum_{n=0}^{\infty} H_n P_{mn}. \quad (6.60)$$

Then, the addition and subtraction of (6.59) and (6.60) provide

$$\varpi_m^\pm = \frac{1}{2\zeta^\pm(\nu_m L)M_m} \left[V'_m(h) \varphi^\mp + \alpha P_{m0} + \alpha \sum_{n=0}^{\infty} \psi_n^\pm P_{mn} \right]. \quad (6.61)$$

Once again, since $e_3 = 0 = e_4$ thanks to the edge condition (6.8), $\phi^\mp = 0$ for metallic fairing. Finally, since normal velocities conditions at matching interfaces

are

$$\frac{\partial \phi^\pm}{\partial x}(\pm L, y) = \begin{cases} \frac{\partial \phi^\ell}{\partial x}(\pm L, y), & -h \leq y \leq -d, \\ 0, & -d \leq y \leq -a, \\ \frac{\partial \phi^c}{\partial x}(\pm L, y), & -a \leq y \leq a, \\ 0, & a \leq y \leq d, \\ \frac{\partial \phi^u}{\partial x}(\pm L, y), & d \leq y \leq h, \end{cases} \quad (6.62)$$

on multiplying (6.62) by $Y_n(y)$, we get

$$\begin{aligned} \int_{-h}^h Y_n(y) \frac{\partial \phi^\pm}{\partial x}(\pm L, y) dy &= \int_{-h}^{-d} Y_n(y) \frac{\partial \phi^\ell}{\partial x}(\pm L, y) dy + \int_{-a}^a Y_n(y) \frac{\partial \phi^c}{\partial x}(\pm L, y) dy \\ &+ \int_d^h Y_n(y) \frac{\partial \phi^u}{\partial x}(\pm L, y) dy. \end{aligned} \quad (6.63)$$

This time we substitute (6.17)–(6.21) into (6.63) and invoke OR (6.3) to arrive at

$$\begin{aligned} A_m &= \frac{\delta_{m0}}{\sigma_m} + \frac{1}{h\sigma_m\epsilon_m} \sum_{n=0}^{\infty} \{ (B_n e^{i\nu_n L} - C_n e^{-i\nu_n L}) \nu_n Q_{nm} + (D_n e^{is_n L} - E_n e^{-is_n L}) s_n R_{nm} \\ &+ (F_n e^{i\nu_n L} - G_n e^{-i\nu_n L}) \nu_n P_{nm} \}, \end{aligned} \quad (6.64)$$

and

$$\begin{aligned} H_m &= \frac{1}{h\sigma_m\epsilon_m} \sum_{n=0}^{\infty} \{ (B_n e^{-i\nu_n L} - C_n e^{i\nu_n L}) \nu_n Q_{nm} + (D_n e^{-is_n L} - E_n e^{is_n L}) s_n R_{nm} \\ &+ (F_n e^{-i\nu_n L} - G_n e^{i\nu_n L}) \nu_n P_{nm} \}. \end{aligned} \quad (6.65)$$

Therefore, the addition and subtraction of (6.64) and (6.65) furnish

$$\psi_m^\pm = \frac{\delta_{m0}}{\sigma_m} + \frac{2}{h\sigma_m\epsilon_m} \sum_{n=0}^{\infty} \left\{ \Xi_n^\pm Q_{nm} \nu_n \zeta^\mp(\nu_n L) + \chi_n^\pm R_{nm} s_n \zeta^\mp(s_n L) + \varpi_n^\pm P_{nm} \nu_n \zeta^\mp(\nu_n L) \right\}. \quad (6.66)$$

In a nutshell, we get an infinite system of linear algebraic equations given by (6.51), (6.56), (6.61), (6.66) in infinite number of unknowns, $\Xi_n^\pm, \chi_n^\pm, \varpi_n^\pm$, and ψ_m^\pm , as in

the case of porous wall.

6.3 Numerical Results and Discussion

The numerical solution to the model problem is obtained by simultaneously solving the system (6.28), (6.34), (6.39), and (6.47) (in the case of a porous wall) and the system (6.51), (6.56), (6.61), and (6.66) (for the case of a metallic fairing) after truncation.

The numerical results are presented in terms of the transmission loss (TL) which is the usual performance measure of the silencers. We define the TL as

$$TL = -10 \log_{10} (P_{\text{trans}}/P_{\text{inc}}),$$

where

$$P_{\text{trans}} = \frac{1}{2} Re \left[\sum_{n=0}^{\infty} |H_n|^2 \eta_n \epsilon_n \right] \quad \text{and} \quad P_{\text{inc}} = 1,$$

are the transmitted and incident powers, respectively. We also define the reflected power P_{ref} as

$$P_{\text{ref}} = \frac{1}{2} Re \left[\sum_{n=0}^{\infty} |A_n|^2 \eta_n \epsilon_n \right].$$

Notice that the conserved power or energy flux identity, i.e., $P_{\text{ref}} + P_{\text{trans}} = 1$ does not hold here due to the porous wall and metallic fairing of the central region. In fact, some of the power is absorbed in such waveguides whereas the absorbed power is $P_{\text{abs}} := 1 - (P_{\text{trans}} + P_{\text{ref}})$.

The dimensionless propagation constant for the porous material Γ and the corresponding normalized complex density $\beta(\omega)$ are expressed in the forms

$$\Gamma := 1 + ia_1 \xi^{a_2} + a_3 \xi^{a_4} \quad \text{and} \quad \beta := \Gamma(1 + a_5 \xi^{a_6} - ia_7 \xi^{a_8}),$$

where $\xi = f\rho/\sigma$ is the dimensionless frequency, defined in terms of the flow resistivity σ (*Rayls* · m^{-1}). Here, a_1, \dots, a_8 are the parameters related to the bulk

acoustic properties of the porous material, and are found experimentally. We refer the interested readers to [83].

Throughout this section, we consider Steel Wool, A-Glass, E-Glass, and Delany-Bazley as the absorbent materials. The experimental values of a_1, \dots, a_8 corresponding to these absorbent materials are furnished in Table 6.3 (see, [83]).

TABLE 6.1: Parameters a_1, \dots, a_8 related to the bulk acoustic properties of considered absorbent materials.

	A-Glass	E-Glass	Steel Wool	Delany-Bazley
a_1	0.2251	0.2202	0.1540	0.189
a_2	-0.5827	-0.5850	-0.7093	-0.595
a_3	0.1443	0.2010	0.1328	0.0978
a_4	-0.7088	-0.5829	-0.5571	-0.7
a_5	0.0924	0.0954	0.0877	0.0571
a_6	-0.7177	-0.6687	-0.5557	-0.754
a_7	0.1457	0.1689	0.0876	0.087
a_8	-0.5951	-0.5707	-0.7609	-0.732

In the rest of this section, the values of $c = 343ms^{-1}$, $\rho = 1.2043kgm^{-3}$, $\rho_m = 0.2kgm^{-3}$, and flow resistivity $\sigma = 16000Rayls \cdot m^{-1}$ are fixed.

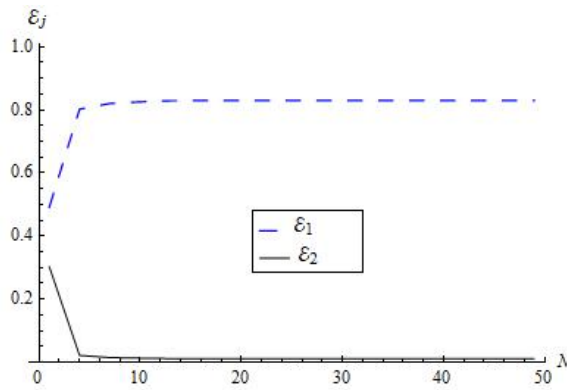
6.3.1 Scheme Validation

The accuracy of the mode-matching (MM) solution is checked through the conservation of energy and the reconstruction of the matching conditions. As the silencer components encompass both orthogonal and non-orthogonal modes, the use of orthogonal characteristics defined in [13, 26] is indispensable. The results for the reflected power in inlet (P_{ref}) and the transmitted power in outlet (P_{trans}) for different values of truncation parameter N are shown in Table 6.3.1. Note that the sum of scattering energies for different values of N remains unity. That validates the accuracy of algebra for the configurations of the expansion chamber.

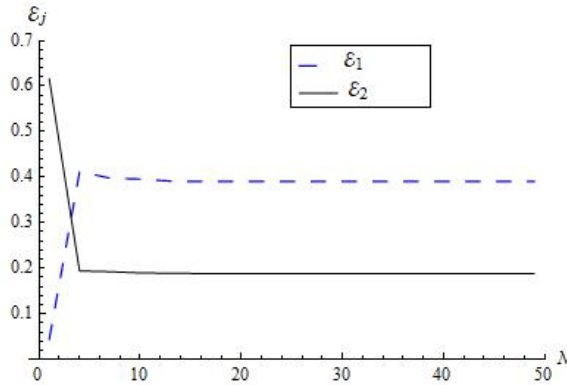
It is clear from Table 6.3.1 that relatively more energy is absorbed by a porous wall than a metallic fairing.

TABLE 6.2: Discontinuous expansion chamber: $\bar{a} = 0.06m$, $\bar{d} = 0.1m$, $\bar{h} = 0.15m$, $\bar{b} = 0.3m$, $\bar{L} = 0.25m$, $T=350N$, $f = 500Hz$.

Cases	N	P_{ref}	P_{trans}	$P_{ref} + P_{trans}$	P_{abs}
Porous Wall	10	0.395782	0.189768	0.58555	0.41445
	15	0.390547	0.188521	0.579069	0.420931
	20	0.390547	0.188521	0.579069	0.420931
	25	0.390547	0.188521	0.579069	0.420931
	30	0.390547	0.188521	0.579069	0.420931
Metallic Fairing Wall	10	0.825114	0.0132823	0.838397	0.161603
	15	0.829004	0.0117569	0.840761	0.159239
	20	0.829004	0.0117569	0.840761	0.159239
	25	0.829004	0.0117569	0.840761	0.159239
	30	0.829004	0.0117569	0.840761	0.159239



(a) Metallic fairing



(b) Porous wall

FIGURE 6.3: Reflected (ϵ_1) power and transmitted power (ϵ_2) versus truncation parameter (N) with $\bar{a} = 0.06m$, $\bar{d} = 0.1m$, $\bar{h} = 0.15m$, $\bar{b} = 0.3m$, $\bar{L} = 0.25m$, $T = 350Nm^{-2}$, and $f = 500Hz$.

In Figures 6.3, we plot the reflected and transmitted powers versus the truncation number, N . It is observed that by increasing N , the scattering components converge adequately even if very few terms are considered when solving the infinite systems by truncation.

Besides validation through energy conservation and power analysis, we reconstruct the matching conditions at interfaces $x = \pm L$ to validate the truncated solution with the truncation parameter $N = 50$. The real and imaginary parts of dimensionless pressures and normal velocities are plotted in Figures 6.4 and 6.5. Specifically, the dimensionless pressure versus duct height are plotted for metallic fairing (Figure 6.4) and the dimensionless velocity versus duct height are plotted for the porous wall (Figure 6.5).

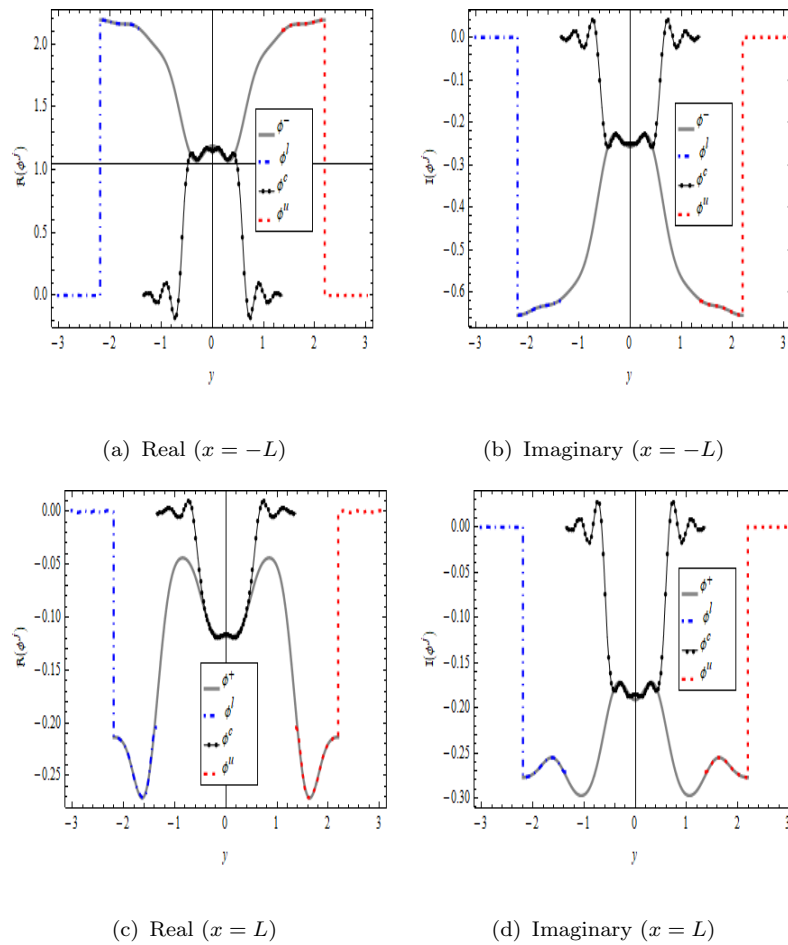


FIGURE 6.4: Real and imaginary parts of pressure vs. duct height (y) for metallic fairing with $N = 50$, $\bar{a} = 0.06m$, $\bar{d} = 0.15m$, $\bar{h} = 0.24m$, $\bar{b} = 0.33m$, and $\bar{L} = 0.25m$.

It is observed that the real and imaginary components of the dimensionless pressures of the inlet and outlet regions, respectively $\phi^-(-L, y)$ and $\phi^+(L, y)$ (for $-h < y < h$), accurately match at the aperture with $\phi^l(\pm L, y)$ (for $-b < y < -d$), $\phi^c(\pm L, y)$ (for $-d < y < d$), and $\phi^u(\pm L, y)$ ($d < y < b$).

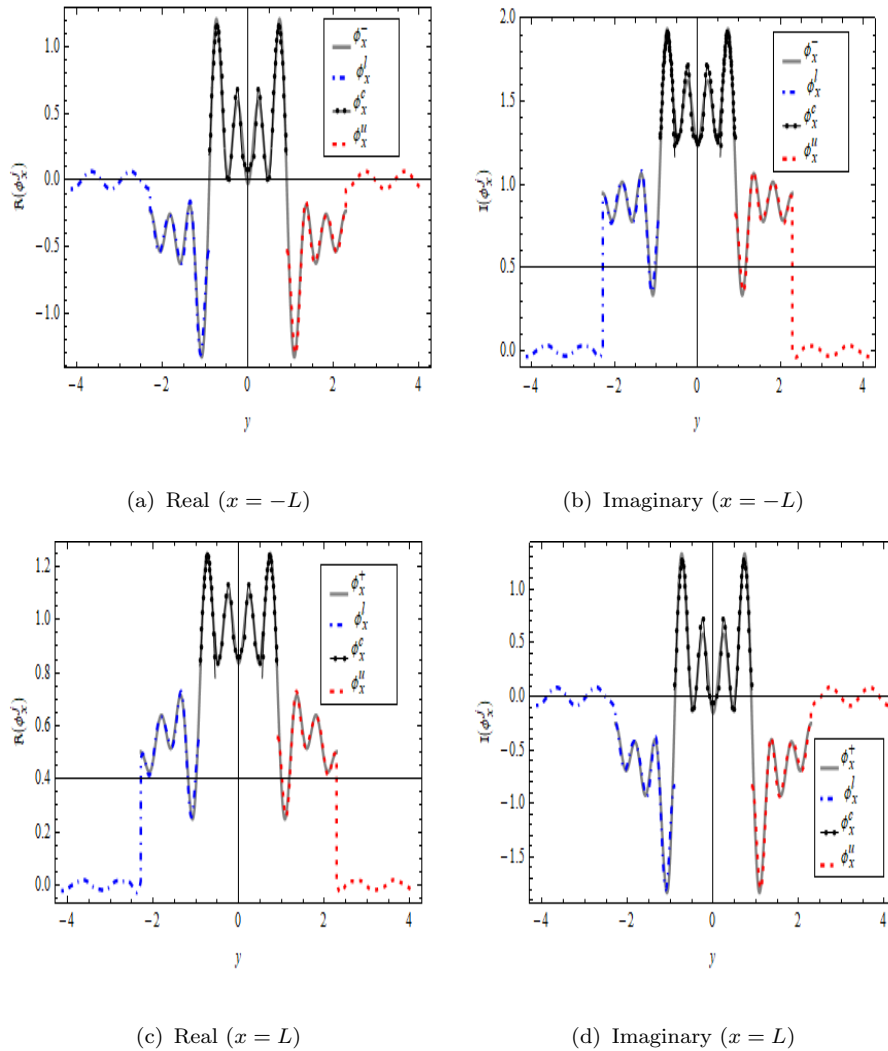


FIGURE 6.5: Real and imaginary parts of velocity vs. duct height (y) for porous wall with $N = 50$, $\bar{a} = 0.06m$, $\bar{d} = 0.1m$, $\bar{h} = 0.25m$, $\bar{b} = 0.45m$, and $\bar{L} = 0.25m$.

Similarly, the real and imaginary components of the dimensionless normal velocities of the inlet and outlet regions, respectively $\phi_x^-(-L, y)$ and $\phi_x^+(L, y)$ for $-h < y < h$ match at the aperture with $\phi_x^l(\pm L, y)$ (for $-b < y < -d$), $\phi_x^c(\pm L, y)$ (for $-d < y < d$), and $\phi_x^u(\pm L, y)$ (for $d < y < b$). Further, the truncated forms of

the acoustic pressures tend to zero along the soft walls in the respective regions as assumed in (6.47), (6.52), and (6.57) (see Figure 6.4). Besides, the truncated form of the normal velocities also tend to zero along the rigid walls in the respective regions conforming to (6.22), (6.35) and (6.62) (see Figures. 6.5). Therefore, the MM scheme successfully reconstructs the matching conditions.

6.3.2 Transmission Loss (TL) Analysis

In order to discuss the performance of the silencer, we analyze its TL. Towards this end, FIGURE 6.6 shows the TL versus frequency for the silencer containing absorbent material (Steel Wool, A-Glass, or E-Glass) with tension $T = 3250N/m^2$. The splitter in the central region of the expansion chamber is terminated at $x = \pm L$ by metallic fairing (Figure 6.6(a)) or by a porous wall (Figure 6.6(b)). Besides, the rest of the dimensional variables and physical parameters are kept invariant. The TL curves in Figure 6.6(a) delineate almost identical behaviors for all three absorbent materials but E-Glass yields relatively higher TL as compared to the Steel Wool and A-Glass. Moreover, in the porous wall case, the TL curves show that Steel Wool yields relatively higher TL as compared to A-Glass and E-Glass (see, Figure 6.6(b)).

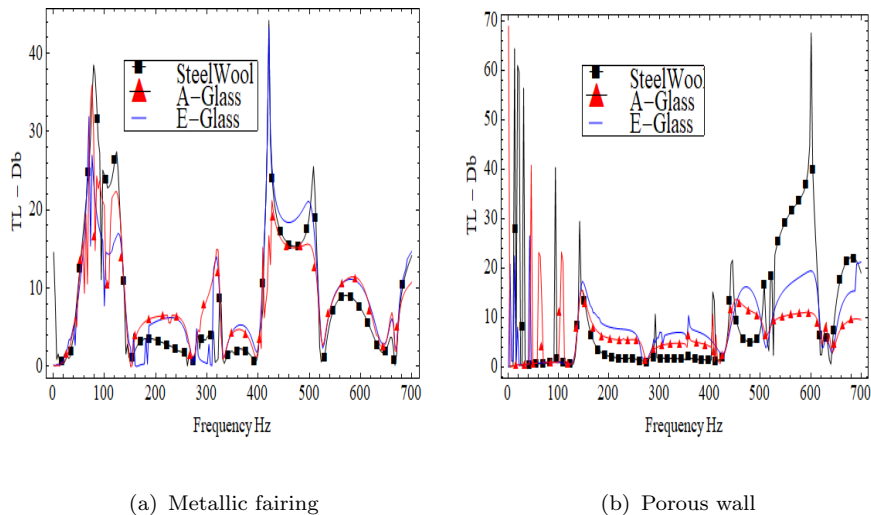


FIGURE 6.6: Transmission loss (Db) vs. frequency (Hz) with $\bar{a} = 0.06m$, $\bar{d} = 0.1m$, $\bar{h} = 0.15m$, $\bar{b} = 0.3m$, $\bar{L} = 0.25m$, and $N = 20$ terms.

By setting tension $T = 3250Nm^{-2}$, the TL versus frequency for the silencer containing Delany-Bazley absorbent material is shown in Figure 6.7 for three different choices of each height \bar{a} and \bar{b} . Clearly, a porous wall yields higher TL as compared to metallic fairing for $0Hz < f < 300Hz$ and $500Hz < f < 700Hz$ frequency bands. In contrast, the metallic fairing yields higher TL than the porous wall at frequencies between 300Hz to 500Hz (see Figures 6.7(a)-6.7(d)).

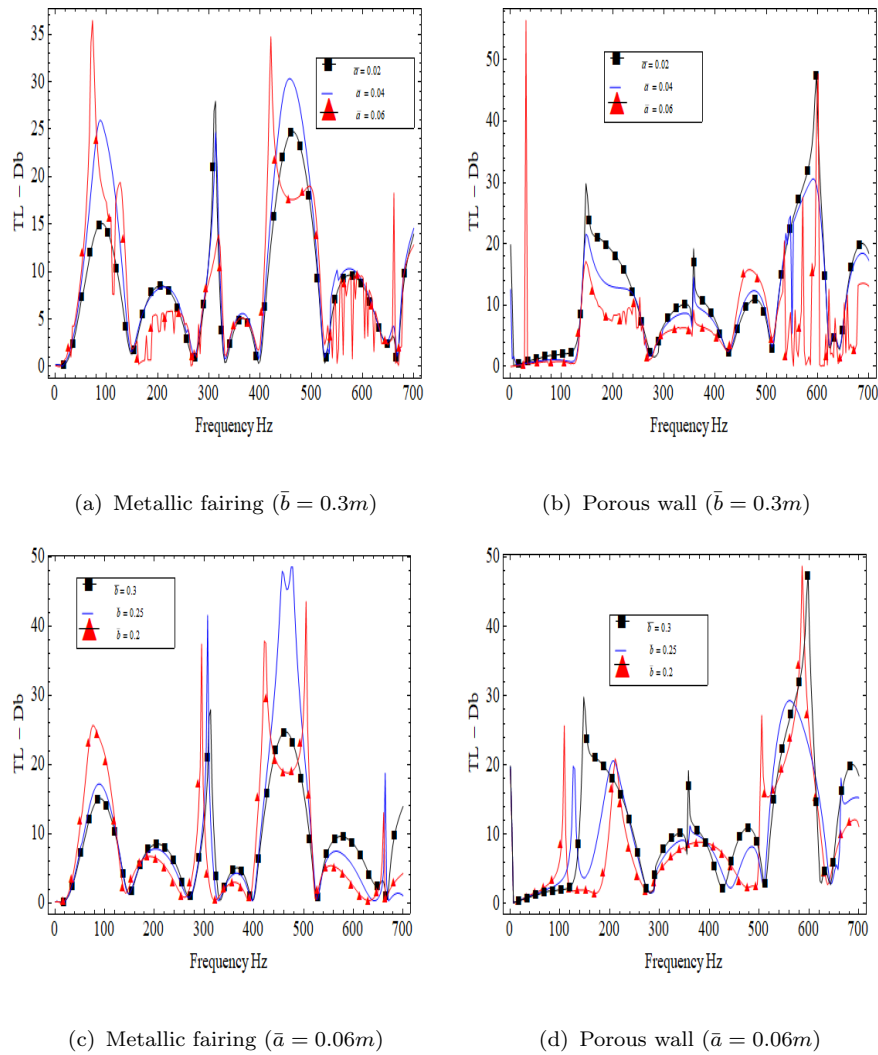
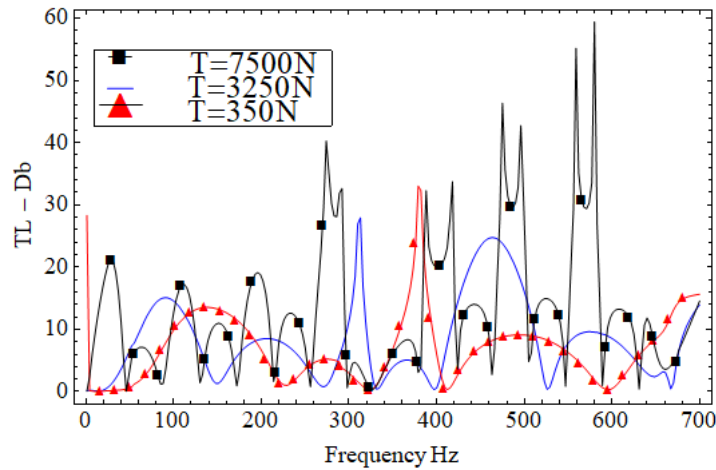


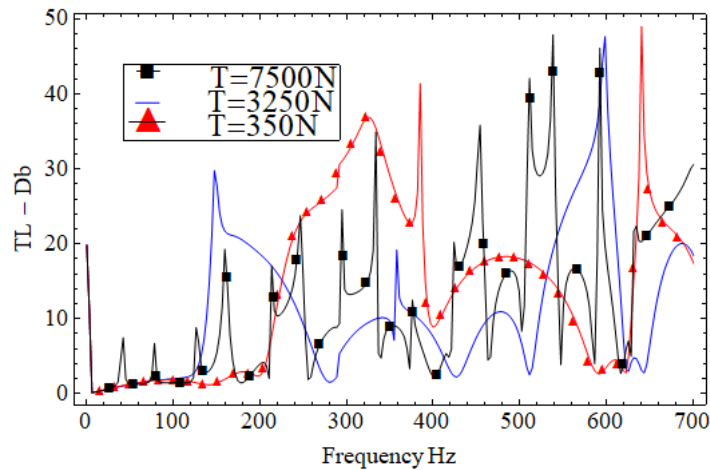
FIGURE 6.7: Transmission loss (Db) vs. frequency (Hz) for different choices of height \bar{a} (top) and \bar{b} (bottom) with $\bar{d} = 0.1m$, $\bar{h} = 0.15m$, $\bar{L} = 0.25m$, and $N = 20$ terms.

The effect of tension on the TL in different frequency bands is delineated in Figure 6.8. We choose three different values of T , specifically, $T = 7500Nm^{-2}$, $T =$

$3250Nm^{-2}$, and $T = 350Nm^{-2}$. The TL versus frequency is displayed in Figure 6.8 for the silencer containing Delany-Bazley as an absorbent material.



(a) Metallic fairing



(b) Porous wall

FIGURE 6.8: Transmission loss (Db) vs. frequency (Hz) for different choices of tension T with $\bar{a} = 0.02m$, $\bar{b} = 0.3m$, $\bar{d} = 0.1m$, $\bar{h} = 0.15m$, $\bar{L} = 0.25m$, and $N = 20$ terms.

Clearly, at values of tension T , Delany-Bazley absorbent material in metallic fairing shows higher TL (up to $100Hz$) as compared to the porous wall (see FIGURE 6.8(a)-6.8(b)). Over this frequency, the process varies inversely. Moreover, Delany-Bazley absorbent material yields higher TL at $T = 7500Nm^{-2}$ than at $T = 3250Nm^{-2}$ and $T = 350Nm^{-2}$.

Chapter 7

Conclusion

The Chapter wise summary and conclusion of the present study are enclosed in this Chapter. Chapter 1 depicts back ground and literature survey relevant to the current study alongwith thesis structure. The inductory details of the class of the problems included in this thesis and a brief overview of the mode-matching (MM) and low frequency approximation (LFA) technique from the perspective of generalized OR have been discussed in Chapter 2. Also the standard and generalized OR have been explored on the basis of physical models in the category of either Sturm Liouville or non-Sturm Liouville systems in this chapter.

In Chapter 3 the model problem highlights the scattering of acoustic radiation in trifurcated waveguide containing rigid/flexible boundaries along with the structural discontinuities. The MM solution has been explored to analyze the energy flux in various duct regions against the dimensions of the waveguide and frequency. It is important to notice that the eigenfunctions for the regions comprising rigid-flexible boundaries yield the non-Sturm Liouville systems wherein the use of recently developed orthogonal characteristics are indispensable [24]. Thus, the use of the generalized OR (3.20) and (3.38) enabled to recast the differential system into the linear algebraic system that has been solved later numerically. It is interesting to note that the conserved power identity not only provide a useful check on the accuracy of algebra but also provide a useful information about the cut-on

modes versus various duct configurations and frequency regime. Unlike to Wiener-Hopf approach [35, 37], the solution scheme discussed here can equally cope the wave scattering in planar and discontinuous waveguide along with different material properties. It is seen that the variation of membrane tension and structural discontinuities greatly affect the scattering energies. The fulfillment of matching conditions and energy balance confirm the accuracy of truncated form of the solution.

Chapter 4 highlights the transmission loss (TL) effects through a waveguide comprising partitioning of the wave-bearing expansion chamber. Two silencer configurations including; vertical step-discontinuities containing expansion chamber ($\bar{b} > \bar{a}$) and the planar expansion chamber ($\bar{b} = \bar{a}$), along with the different bounding properties of the central region have been analyzed. The results for rigid, soft or absorbent lining type conditions of the central region have been presented. The modeled problem has been solved by using MM and LFA. A good agreement in TL results obtained via MM scheme and LFA solutions have been observed. In MM technique case, the non-SL systems in elastic membrane bounded regions appear, for which the use of generalized orthogonality conditions is indispensable [24, 28, 47, 54]. Thus, the use of generalized and/or usual orthogonality conditions, whichever is appropriate, yield two systems of infinite equations. These systems are truncated and solved numerically. It is seen that the truncated systems of equations converge rapidly. Moreover, the truncated solution has reconstructed the matching conditions at interfaces successfully which undoubtedly justifies the accuracy of algebra. From numerical results, it is observed that the scattering energies and the TL is significantly affected by the bounding characteristics as well by the geometrical configurations of the expansion chamber. For instance, the energy absorbed in planar case is greater than discontinuous case and also their is more absorption of energy in perforated case than the fibrous case, (see Table 4.3 and 4.4). Furthermore, as the outer boundaries of the expansion chamber are composed of isotropic elastic membranes and a significant variations in scattering by changing its material properties is observed. Thus, the devise can be opted for both the reactive and passive control measures of sound.

In Chapter 5 sound attenuation by a splitting expansion chamber is investigated. The segments of the chamber contain sandwiched elastic components backed by rigid cavities and the absorbent linings. It is well established that the use of elastic components such as elastic membranes or plates in the an expansion chamber of silencer can reduce significantly the vibration of low-frequency. Also the use of absorbent materials is the most practical way to mitigate the unwanted noise. Nevertheless, it is effective largely to attenuate the noise with higher frequencies. This article has investigated the combined effects of elastic components and absorbent linings for an expansion chamber silencer useful in ducting system. The physical problem is solved by using the MM scheme. The traveling waveforms of eigenmodes determine coupled as well as uncoupled modes formulation, and are non-orthogonal in the segments comprising elastic membranes. The use of generalized orthogonal characteristics developed recently [24], provides the adequate convergence of the solution. The truncated form solution is validated altogether through reconstruction of matching conditions and conservation of energy flux.

Moreover, the numerical results of TL are compared with LFA. A good agreement in both solutions in low frequency range is achieved. From numerical results, it is observed that the position of membranes in cavities and associated tensile force are important to tuned the devise at specific frequencies of interest. Also noticed that when membranes are pinned inside of the cavities the silencer produces narrow stopbands. But when membranes are attached at the apertures of the cavities the bandwidth of stopbands tends to broaden. However, the passbands do exist and cannot be eliminated by altering the position of membranes. Furthermore, the characteristics of porous material remarkably affect the TL; fibrous material yields comparatively greater TL and broaden stopbands than perforated material. Interestingly, the amount of absorbed power due porous linings is linked with properties of the material used as well as the position of membranes in the cavities such as, more power is absorbed with fibrous material than perforated material. Likewise when membranes are pinned inside of the cavities yield greater absorbed power than the case when membranes are attached at the apertures. Thus, by means of envisaged characteristics the device can easily be tuned which make it

useful to be opted as reactive and dissipative control measure of sound.

In Chapter 6, we have analyzed the performance of a two-dimensional silencer with an expansion chamber. The segments of the chamber contained sandwiched elastic membranes and two splitters in its central region. The TL effect was discussed as the performance measure. Two silencer configurations with different bounding properties of the central region and splitters have been analyzed. The results for rigid, soft, or absorbent lining type conditions of the central region were presented. In particular, the effect of splitter fairing and the porous wall on the performance of the silencer was studied. The modeled problem was solved by using the MM scheme. The generalized and/or usual orthogonality conditions yielded an infinite system of linear equations in infinite unknowns. The system was solved numerically after the truncation of terms whereas the truncated system converged rapidly as the truncation parameter $N \rightarrow +\infty$. The MM framework has been validated for the accuracy and appositeness of performed algebra through the reconstruction of the matching conditions at interfaces.

The numerical results highlight that the scattering energies and the TL are significantly affected by the bounding characteristics as well as by the geometrical configurations of the expansion chamber. It is observed that the metallic fairing yields higher TL than the porous wall at frequencies between $300Hz$ to $500Hz$ whereas a porous wall yields higher TL at frequencies between $0Hz$ to $300Hz$ and $500Hz$ to $700Hz$ when Delany-Bazley absorbent material is used. It is also observed that E-Glass performs better than Steel Wool and A-Glass in metallic fairing whereas Steel Wool performs better than A-Glass and E-Glass in porous walls. In the light of these observations, the scattering energy and the TL can be significantly tuned by varying the material properties of the elastic membranes and the bounding wall conditions. Accordingly, the studied configurations are suitable for reactive as well as passive control measures of sound.

Bibliography

- [1] R. A. Scott, “The propagation of sound between walls of porous material”, *Proceedings of Physical Society*, vol. 58, pp. 358-368, 1946.
- [2] S. H. Ko, “Theoretical analyses of sound attenuation in acoustically lined flow ducts separated by porous splitters (rectangular, annular, circular ducts)”, *Journal of Sound and Vibration*, vol. 39, pp. 471-487, 1975.
- [3] R. Kirby and A. Cummings, “The impedance of perforated plates subjected to grazing gas flow and backed by porous media”, *Journal of Sound and Vibration*, vol. 217, pp. 619-636, 1998.
- [4] A. Selamet, I. J. Lee and N. T. Huff, “Acoustic attenuation of hybrid silencers”, *Journal of Sound and Vibration*, vol. 262, pp. 509-527, 2003.
- [5] S. J. Estve and M. E. Johnson, “Development of an adaptive Helmholtz resonator for broadband noise control”, *Proceeding of International Mechanical Engineering Congress and Exposition*, vol. 47152, pp. 47-53, 2004.
- [6] J. F. T. MacLaren, A. B. Tramschek and O. F. Pastrana, “A study of unsteady gas flow in perforated pipes in compressor systems”, *International Compressor Engineering Conference*, vol. 215, pp. 360-367, 1976.
- [7] I. J. Hughes and A. P. Dowling, “The absorption of sound by perforated linings”, *Cambridge University Press*, vol. 218, pp. 299-335, 1990.
- [8] H. Tasli and M. C. Gokgoz, “Does central tympanic membrane perforation affect infrared tympanic thermometer measurements in adults”, *Journal of Otology*, vol. 13, pp. 128-130, 2018.

- [9] S. Laugesen, “Active control of multi-modal propagation of tonal noise in ducts”, *Journal of Sound and Vibration*, vol. 195, pp. 33-56, 1996.
- [10] J. W. Lee and Y. Y. Kim, “Topology optimization of muffler internal partitions for improving acoustical attenuation performance”, *International Journal for Numerical Methods in Engineering*, vol. 80, pp. 455-477, 2008.
- [11] H. Hamakawa, M. Miyazaki, Y. Asai, E. Kurihara, E. Nishida and H. Hayashi, “Prediction of acoustic absorption performance of a perforated plate with air jets”, *Journal of Thermal Science*, vol. 26, pp. 378-384, 2017.
- [12] L. Huang, “Modal analysis of a drumlike silencer”, *Journal of Acoustical Society of America*, vol. 112, pp. 2014-2025, 2002.
- [13] J. B. Lawrie and I. M. M. Guled, “On tuning a reactive silencer by varying the position of an internal membrane”, *Journal of Acoustical Society of America*, vol. 120, pp. 780-790, 2006.
- [14] L. Huang, “Broadband sound reflection by plates covering side-branch cavities in a duct”, *Journal of the Acoustical Society of America*, vol. 119, pp. 2628-2638, 2006.
- [15] M. Ayub, M. H. Tiwana and A. B. Mann, “Wiener-Hopf analysis of an acoustic plane wave in a trifurcated waveguide”, *Archive of Applied Mechanics*, vol. 81, pp. 701-713, 2011.
- [16] A. Cummings and N. Sormaz, “Acoustic attenuation in dissipative silencers containing mean fluid flow”, *Journal of Sound and Vibration*, vol. 168, pp. 209-227, 1993.
- [17] A. Cummings, “Sound attenuation in ducts lined on two opposite walls with porous material with some application to splitters”, *Journal of Sound and Vibration*, vol. 49, pp. 9-35, 1976.
- [18] R. Kirby, “The influence of baffle fairing on the acoustic performance at rectangular splitter silencers”, *Acoustic Society of America*, vol. 118, pp. 2302-2312, 2005.

-
- [19] E. Nolde, A. V. Pichugin and J. Kaplunov, “An asymptotic higher-order theory for rectangular beams”, *Proceedings of the Royal Society A: Mathematical, Physical and Engineering Sciences*, vol. 474, pp. 20180001, 2018.
- [20] O. Sahin, B. Erbas, J. Kaplunov and T. Savsek, “The lowest vibration modes of an elastic beam composed of alternating stiff and soft components”, *Archive of Applied Mechanics*, vol. 90, pp. 339-352, 2020.
- [21] K. S. Peat and K. L. Rathi, “A finite element analysis of the convected acoustic wave motion in dissipative silencers”, *Journal of Sound and Vibration*, vol. 184, pp. 529-545, 1995.
- [22] R. Kirby and J. B. Lawrie, “A point collocation approach to modelling large dissipative silencers”, *Journal of Sound and Vibration*, vol. 286, pp. 313-339, 2005.
- [23] A. Maurel, J. F. Mercier, and S. Flix, “Wave propagation through penetrable scatterers in a waveguide and through a penetrable grating”, *Journal of the Acoustical Society of America*, vol. 135, pp. 165-174, 2014.
- [24] J. B. Lawrie, “On eigenfunction expansions associated with wave propagation along ducts with wave-bearing boundaries”, *IMA Journal of Applied Mathematics*, vol. 72, pp. 376-394, 2007.
- [25] J. B. Lawrie, “Comments on a class of orthogonality relations relevant to fluid-structure interaction”, *Meccanica*, vol. 47, pp. 783-788, 2012.
- [26] M. Afzal, R. Nawaz and A. Ullah, “Attenuation of dissipative device involving coupled wave scattering and change in material properties”, *Applied Mathematics and Computation*, vol. 290, pp. 154-163, 2016.
- [27] S. Shafique, M. Afzal and R. Nawaz, “Mode-Matching analysis of fluid structure coupled wave scattering between two flexible waveguides”, *Canadian Journal of Physics*, vol. 95, pp. 1-25, 2017.

-
- [28] M. Afzal, M. Ayub R. Nawaz and A. Wahab, “Mode-matching solution of a scattering problem in flexible waveguide with abrupt geometric changes”, *American Mathematical Society*, vol. 660, pp. 113-129, 2016.
- [29] A. P. Dowling and J. E. Ffowcs Williams, “Sound and sources of sound”, *Horwood*, 1983.
- [30] R. Nawaz, M. Afzal, and M. Ayub, “Acoustic propagation in two dimensional waveguide for membrane bounded ducts”, *Communication in Nonlinear Science and Numerical Simulation*, vol. 20, pp. 421-435, 2015.
- [31] R. Nawaz and J. B. Lawrie, “Scattering of a fluid-structure coupled wave at a flanged junction between two flexible waveguides”, *Journal of Acoustical Society of America*, vol. 134, pp. 1939-1949, 2014.
- [32] R. B. Lindsay, “The story of acoustics”, *Journal of Acoustical Society of America*, vol. 39, pp. 629-644, 1966.
- [33] L. Rayleigh, “J.W. Strutt: The theory of sound”, *Dover publications, New York*, 1945.
- [34] I. D. Abrahams, “Scattering of sound by two parallel semi-infinite screens”, *Wave Motion*, vol. 9, pp. 289-300, 1987.
- [35] M. Hassan and A. D. Rawlins, “Radiation from a two dimensional duct”, *Canadian Journal of Physics*, vol. 1, pp. 375-384, 1997.
- [36] B. Polat, “Plane wave diffraction by a semi-infinite soft/hard parallel plate waveguide”, *Canadian Journal of Physics*, vol. 76, pp. 771-784, 1998.
- [37] A. D. Rawlins, “Wave propagation in a bifurcated impedance-lined cylindrical waveguide”, *Journal of Engineering Mathematics*, vol. 59, pp. 419-435, 2007.
- [38] M. Hassan, M., H. Meylan, and M. A. Peter, “Water-wave scattering by submerged elastic plates”, *The Quarterly Journal of Mechanics and Applied Mathematics*, vol. 62, pp. 321-344, 2009.

- [39] A. Buyukaksoy and B. Polat, "A bifurcated waveguide problem", *ARI-An International Journal for Physical and Engineering Sciences*, vol. 51, pp. 196-202, 1999.
- [40] J. W. Miles, "The analysis of plane discontinuities in cylindrical tubes", *Journal of Acoustical Society of America*, vol. 17, pp. 259-271, 1946.
- [41] S. Brown, "Acoustic design of broadcasting studio", *Journal of Sound and Vibration*, vol. 3, pp. 239-257, 1964.
- [42] M. Abom, "Derivation of four-pole parameters including higher order mode effects for expansion chamber mufflers with extended inlet and outlet", *Journal of Sound and Vibration*, vol. 137, pp. 403-418, 1990.
- [43] A. Selamet and Z.L. Ji, "Acoustic attenuation performance of circular expansion chambers with extended inlet/outlet", *Journal of Sound and Vibration*, vol. 223, pp. 197-212, 1999.
- [44] L. Huang and Y. S. Choy, "Vibroacoustics of three-dimensional drum silencer", *Journal of the Acoustical Society of America*, vol. 112, pp. 2313-2320, 2005.
- [45] C. Q. Wang, L. Cheng and L. Huang, "Realisation of a broadband low frequency plate silencer using sandwich plates", *Journal of Sound and Vibration*, vol. 318, pp. 792-808, 2008.
- [46] R. J. Astley and A. Cummings, "A finite element scheme for attenuation in ducts lined with porous material comparison with experiment", *Journal of Sound and Vibration*, vol. 116, pp. 239-263, 1987.
- [47] M. Afzal, R. Nawaz and M. Ayub, "Acoustic scattering in flexible waveguide involving step discontinuity", *PloS one*, vol. 9, pp. e103807, 2014.
- [48] A. H. Nayfeh, J. E. Kaiser, and D. P. Telionis, "Acoustics of aircraft engine duct systems", *Aiaa Journal*, vol. 13, pp. 130-153, 1975.

- [49] A. D. Rawlins, "Radiation of sound from an unflanged rigid cylindrical duct with an acoustically absorbing internal surface", *Proceedings of the Royal Society London Series A*, vol. 361, pp. 65-91, 1978.
- [50] M. Hassan and A. D. Rawlins, "Sound radiation in a planar trifurcated lined duct", *Wave Motion*, vol. 29, pp. 157-174, 1999.
- [51] M. Ayub, M. H. Tiwana and A. B. Mann, "Influence of the dominant mode propagation in a trifurcated lined duct with different impedances", *Physica Scripta*, vol. 1, pp. 035402, 2010.
- [52] M. Hassan, "Wave scattering by soft-hard three spaced waveguide", *Applied Mathematical Modelling*, vol. 38, pp. 4528-4537, 2014.
- [53] M. Hassan, M.H. Meylan , A. Bashir and M. Sumbul, "Mode-matching analysis for wave scattering in triple and pentafurcated spaced ducts", *Mathematical Methods in the Applied Sciences*, vol. 39, pp. 3043-3057, 2016.
- [54] J. B. Lawrie and I. D. Abraham, "An orthogonality condition for a class of problem with high order boundary conditions, applications in sound/structure interaction", *The Quarterly Journal of Mechanics and Applied Mathematics*, vol. 52, pp. 161-181, 1999.
- [55] D. P. Warren, J. B. Lawrie and I. M. Mohamed, "Acoustic scattering in waveguides with discontinuities in height and material property", *Wave Motion*, vol. 36, pp. 119-142, 2002.
- [56] J. B. Lawrie and J. Kaplunov, "Edge waves and resonance on elastic structures an overview", *Mathematics and Mechanics of Solids*, vol. 17, pp. 4-16, 2012.
- [57] J. B. Lawrie and M. Afzal, "Acoustic scattering in a waveguide with a height discontinuity bridged by a membrane a tailored Galerkin approach", *Journal of Engineering Mathematics*, vol. 105, pp. 99-115, 2016.
- [58] M. Ayub, M. H. Tiwana and A. B. Mann, "Acoustic diffraction in a trifurcated waveguide with mean flow", *Communications in Nonlinear Science and Numerical Simulation*, vol. 15, pp. 3939-3949, 2010.

- [59] J. M. de Bedout, M. A. Franckek, R. J. Bernhard, and L. Mongeau, “Adaptive-passive noise control with self-tuning Helmholtz resonators”, *Journal of Sound and Vibration*, vol. 202, pp. 109-123, 1997.
- [60] J. D. Wu and M. R. Bai, “Application of feedforward adaptive active noise control for reducing blade passing noise in centrifugal fans”, *Journal of Sound and Vibration*, vol. 239, pp. 1051-1062, 2001.
- [61] J. K. Kruger, “The calculation of actively absorbing silencers in rectangular ducts”, *Journal of Sound and Vibration*, vol. 257, pp. 887-902, 2002.
- [62] A. Selemet, I. J. Lee, and N. T. Huff, “Acoustic attenuation of hybrid silencers”, *Journal of Sound and Vibration*, vol. 262, pp. 509-527, 2003.
- [63] J. W. Lee and G. W. Jang, “Topology design of reactive mufflers for enhancing their acoustic attenuation performance and flow characteristics simultaneously”, *International Journal for Numerical Methods in Engineering*, vol. 91, pp. 552-570, 2012.
- [64] J. M. Middelberg, T. J. Barber, S. S. Leong, K. P. Byrne and E. Leonardi, “Computational fluid dynamics analysis of the acoustic performance of various simple expansion chamber mufflers”, *Proceedings of Acoustics*, pp. 123-127, 2004.
- [65] P. Morse and K. Ingard, “Encyclopedia of Physics”, *Acoustics I. Springer-Verlag, Berlin*, 1961.
- [66] H. Singh, “Laterally loaded reinforced concrete stiffened plates analytical investigations”, *Practice Periodical on Structural Design and Construction*, vol. 17, pp. 21-29, 2012.
- [67] J. Farkas and K. Jarmai, “Optimum design of steel structures”, *Springer*, 2013.

- [68] N. Challamel, H. Zhang, C. M. Wang and J. Kaplunov, "Scale effect and higher-order boundary conditions for generalized lattices, with direct and indirect interactions", *Mechanics Research Communications*, vol. 97, pp. 1-7, 2019.
- [69] A. Cummings and I. J. Chang, "Sound attenuation on a finite length dissipative flow duct silencer with internal mean flow in the absorbent", *Journal of Sound and Vibration*, vol. 127, pp. 1-17, 1998.
- [70] Mechel and FP, "Noise and vibration control Engineering Principles and Applications edited by L.L.Beraneic and I.L.Ver (Wiley, NewYork)", *Wiley, New York*, 1992.
- [71] R. Kirby, "Simplified techniques for predicting the transmission loss of a circular dissipation silencer", *Journal of Sound and Vibration*, vol. 243, pp. 403-426, 2001.
- [72] S. N. Panigrahi and M. L. Munjal, "Comparison of various methods for analysing lined circular ducts", *Journal of Sound and Vibration*, vol. 285, pp. 905-923, 2005.
- [73] R. Kirby, "The acoustic modelling of dissipative elements in automotive exhausts", *University of Hull*, 1996.
- [74] R. Kirby and F. D. Denia, "Analytic mode matching for a circular dissipative silencer containing mean flow and a perforated pipe", *Journal of Acoustical Society of America*, vol. 122, pp. 3471-3482, 2007.
- [75] D. A. Bies, C. H. Hansen and G. E. Bridges, "Sound attenuation in rectangular and circular cross-section ducts with flow and bulk-reacting liner", *Journal of Sound and Vibration*, vol. 116, pp. 239-263, 1987.
- [76] R. Ramakrishnan and W. R. Watson, "Design curves for rectangular splitter silencers", *Applied Acoustics*, vol. 35, pp. 1-24, 1992.

-
- [77] J. F. Allard and Y. Champoux, “New empirical equation for sound propagation in rigid frame fibrous materials”, *Journal of Acoustic Society of America*, vol. 91, pp. 3346-3353, 1992.
- [78] D. V. Evans and C. M. Linton, “Trapped Modes in Open Channels”, *Journal of Fluid Mechanics*, vol. 225, pp. 153-175, 1991.
- [79] N. N. Lebedev, I. P. Skalskaya and Y. S. Uflyand, “Worked Problems in Applied Mathematics”, *Dover New York*, 1979.
- [80] P. G. Drazin and W. H. Reid, “Hydrodynamic Stability. Cambridge, Cambridge University Press”, 1981.
- [81] Tyn Myint-U and Lokenath Debnath, “Linear Partial Differential Equations for Scientist and Engineers”, *Springer*, 2007.
- [82] Rao, Singiresu S, “Vibration of Conitnuous Systems”, *Wiley Online Library*, 2007.
- [83] R. Kirby and A. Cummings, “Prediction of bulk acoustic properties of fibrous materials at low frequencies”, *Journal of Applied Acoustics*, vol. 56, pp. 101-125, 1999.